Spring 2019

# Bioinspired Glycopolymers: Models to Investigate the Effect of Saccharide Structure and Concentration on Amyloid Beta Aggregation

Pradipta Kumar Das
*University of Southern Mississippi*

# BIOINSPIRED GLYCOPOLYMERS: MODELS TO INVESTIGATE THE EFFECT OF SACCHARIDE STRUCTURE AND CONCENTRATION ON AMYLOID BETA AGGREGATION

by

Pradipta Kumar Das

A Dissertation
Submitted to the Graduate School,
the College of Arts and Sciences
and the School of Polymer Science and Engineering
at The University of Southern Mississippi
in Partial Fulfillment of the Requirements
for the Degree of Doctor of Philosophy

Approved by:

Dr. Sarah E. Morgan, Committee Chair
Dr. Robert L. Lochhead
Dr. Sergei Nazarenko
Dr. Derek L. Patton
Dr. Vijayaraghavan Rangachari

| | | |
|---|---|---|
| _____ | _____ | _____ |
| Dr. Sarah E. Morgan | Dr. Jeffrey S. Wiggins | Dr. Karen S. Coats |
| Committee Chair | Director of School | Dean of the Graduate School |

May 2019

***Published by the Graduate School***

ABSTRACT

Aggregation and subsequent deposition of amyloid-β (Aβ) peptide on neuronal cell membranes have been implicated as a cause of Alzheimer's disease. Gangliosides in their clustered form seed and promote the Aβ aggregation process. However, the effects of the structure and the concentration of ganglioside saccharides on Aβ aggregation are not well understood. We investigated how the specific structure of saccharides (β-D-galactose and β-D-glucose) affect the aggregation pathways, kinetics, and the aggregated structures of Aβ via in vitro experiments. The effects of the local concentration of saccharides on the Aβ aggregation were also investigated.

To mimic the multivalent effect of the ganglioside saccharides, we designed and synthesized stereospecific bio-relevant saccharide containing model polymers, known as glycopolymers in solution and from surfaces. Acrylamide based glycopolymers of desired molecular weights were synthesized in solution via reversible addition-fragmentation chain transfer (RAFT) polymerization. Using thioflavin T fluorescence (ThT) and polyacrylamide gel electrophoresis (PAGE), we found that the Aβ formed small aggregates in the presence of high molecular weight (DP 350) glucose containing polymers, but large aggregates were formed in the presence of low (DP 35) molecular weight glucose containing polymers, low and high molecular weight galactose containing polymers, and non-saccharide control polymers.

Glycopolymer films of high and low thickness were synthesized from silicon surfaces via photopolymerization and surface-initiated RAFT polymerization and the effect of the saccharides of grafted glycopolymers on Aβ aggregation were investigated. Quartz crystal microbalance (QCM)experiments established that the Aβ bound more

strongly with the glucose polymer grafted surfaces than the galactose polymer grafted surfaces. AFM imaging revealed that the Aβ aggregated to form fibrils when incubated with the thin films of glucose or galactose polymers and control surfaces.

These results suggest that the high molecular weight glucose-containing polymers strongly affect and alter the Aβ aggregation pathway and promote the formation of Aβ oligomers while other polymers do not affect the aggregation process.

ACKNOWLEDGMENTS

I would like to thank my advisor Prof. Sarah E Morgan for being a wonderful mentor who helped me to develop as a researcher. I could not have completed my PhD research at USM without her constant support and guidance. I am sincerely thankful to my supportive committee members, Dr. Robert L Lochhead, Dr. Sergei Nazarenko, Dr. Derek L Patton, and Dr. Vijayaraghavan Rangachari for their immense help and guidance. I would also like to thank Dr. Lisa Kemp for helping me shape my scientific writing skills and for the intellectual discussions we had over the years.

There are many others who have played very important roles during this journey. I thank past group members of the Morgan Research Group, Dr. Qi Wu, Dr. Mithun Bhattacharya, Dr. Sarah Exley, Dr. Katrina Knauer, Dr. Levi Moore, and Dr. April Fogel who were some of the best mentors and friends. I also thank present Morgan Group members Ashleigh Bristol, Kelli Stockmal, Mitchell Woellner, Rahul Shankar, Anthony Benasco, Garrett Abrahamsen, and Kyle Mehringer and the undergraduate students for their constant encouragement and support.

My undergraduate students whom I have mentored and taught during this period, Bernardo Lopez, Fayth Stewart, LeDarius Whitley, and Jacob Von Harman and all the undergraduate and graduate students who took lab classes under my guidance and the numerous high school students for whom I demonstrated many scientific experiments, I thank you all for helping me become a better mentor, communicator, and a researcher.

I also thank Dr. Wei Guo, Dr. Brooks Abel, and Dr. Dexter Dean, former Ph.D. students of The University of Mississippi, and Dr. Fei Liu of the University of Alabama, Birmingham for their help and useful discussions.

I would like to thank the National Science Foundation's Experimental Program to Stimulate Competitive Research (EPSCoR) under Cooperative Agreement No. IIA1430364 and NSF OIA-1632825 for the financial support throughout this research. I would also like to thank Mississippi INBRE for allowing me to use their facilities.

Finally, my journey would not have been completed without the endless support and encouragement of my family. I especially thank my wife, Haimanti, for being with me during this testing time.

TABLE OF CONTENTS

LIST OF TABLES

LIST OF ILLUSTRATIONS

LIST OF SCHEMES

LIST OF ABBREVIATIONS

| | |
|---|---|
| AcGalEAm | 2′-acrylamidoethyl-2,3,4,6-tetra-O-acetyl-*β*-D-galactopyranoside |
| AcGlcEAm | 2′-acrylamidoethyl-2,3,4,6-tetra-O-acetyl-β-D-galactopyranoside |
| GalEAm | 2′-acrylamidoethyl-β-D-galactopyranoside |
| GlcEAm | 2′-acrylamidoethyl-*β*-D-glucopyranoside |
| DP | Degree of polymerization |
| PGalEAm35 | Poly[2′-acrylamidoethyl-*β*-D-galactopyranoside] of DP of 35 |
| PGalEAm350 | Poly[2′-acrylamidoethyl-*β*-D-galactopyranoside] of DP of 350 |
| PGlcEAm35 | Poly[2′-acrylamidoethyl-*β*-D-glucopyranoside] of DP of 35 |
| PGlcEAm350 | Poly[2′-acrylamidoethyl-*β*-D-glucopyranoside] of DP of 350 |
| PDMA35 | Poly(N,N-dimethyl acrylamide) of DP of 35 |
| PDMA350 | Poly(N,N-dimethyl acrylamide) of DP of 350 |
| CTA | Chain transfer agent |
| CEP | 4-cyano-4-(ethylsulfanylthiocarbonyl) sulfanylpentanoic acid |
| V-501 | 4,4′-azobis(4-cyanopentanoic acid) |

| | |
|---|---|
| Irgacure 2959 | 2-Hydroxy-1-[4-(2-hydroxyethoxy) phenyl]-2-methyl-1-propanone |
| aRAFT | Aqueous reversible addition fragmentation chain transfer |
| NMR | Nuclear magnetic resonance |
| GPC | Gel permeation chromatography |
| ESI-MS | Electrospray ionization mass spectrometry |
| ThT | Thioflavin T Fluorescein |
| PAGE | Polyacrylamide gel electrophoresis |
| AFM | Atomic force microscopy |
| QCM-D | Quartz crystal microbalance with dissipation monitoring |

# CHAPTER I - INTRODUCTION

## 1.1 Understanding the role of saccharides in amyloid-β aggregation

Alzheimer's disease (AD) is a neurodegenerative disease which accounts for 60-80% of all reported dementia cases. According to a recent report, more than 5.5 million Americans of all ages were suffering from Alzheimer's disease in 2018, and this figure may cross 16 million by 2050.[1, 2] Currently there is no cure, no method of prevention, no absolute diagnostic test, and only partially effective treatments available to slow the progression of the disease. To adequately prevent or treat the disease, it is important to first understand the factors which are responsible for the disease and how the factors affect the disease progression.

Aggregation of amyloid-β (Aβ) peptide is believed to be one of the contributing factors in Alzheimer's disease.[3-5] Aβ can aggregate to form toxic oligomers and plaques which deposit on neuronal cell membranes obstructing the normal functions of neurons.[6-8] Precise mechanisms of formation of toxic Aβ species from non-toxic Aβ peptides, their deposition, and the factors responsible for their aggregation are not yet entirely understood despite years of intensive research. GM1 gangliosides, which are present at elevated concentrations in the plasma membranes of an aged brain and consists of a hydrophobic tail and a saccharide-containing hydrophilic head group, have been reported to seed Aβ aggregation.[3, 6 9, 10 11] It has been reported by Matsuzaki et al. and others that the clustering of GM1, known as a glyco-cluster, plays an important role in the seeding and promotion of Aβ aggregation.[3, 6, 11-13] Greater understanding of the role of the structure and concentration of ganglioside saccharides on the assembly of Aβ peptide is needed. Glycopolymers, or synthetic polysaccharides, provide an in vitro platform for the

investigation of the effects of saccharide structure and concentration on the kinetics of Aβ aggregation and the size and morphology of the aggregates.

The goal of this project was to design, synthesize, and utilize glycopolymer platforms as biologically-relevant models for the determination of saccharide/protein interactions in vitro. Specifically, glycopolymers with β-D-glucose and β-D-galactose as pendant groups were synthesized in solution and from well-characterized surfaces to model the saccharides of gangliosides found in the brain. The model polymers were then utilized to investigate the effects of the saccharide structure and concentration on the Aβ peptide assembly processes.

We hypothesized that the Aβ aggregation pathways, size and structures of the aggregates, and the kinetics of the aggregation are dependent on the structure of the pendant saccharides and the molecular weight (saccharide concentration) of the model glycopolymers studied.

The hypotheses were tested via three main research objectives:

1. Synthesis of glycomonomers with stereospecific saccharides as pendant groups and preparation of glycopolymers with target degrees of polymerization (DP) of 35 and 350 via aqueous reversible addition fragmentation chain transfer (RAFT) polymerization.
2. Synthesis of glycopolymer brushes with desired stereochemistry of saccharides and target thickness to correspond to the degrees of polymerization of 35 and 350 from well characterized surfaces via UV-photopolymerization and surface-initiated RAFT polymerization techniques.

3. Determination of Aβ assembly processes and dynamics of aggregation in the presence of glycopolymers in solution and glycopolymer brushes via in vitro biochemical experiments (ThT fluorescence and polyacrylamide gel electrophoresis (PAGE)) and utilizing advance analytical techniques such as quartz crystal microbalance (QCM) and atomic force microscopy (AFM).

This research provides a platform for the investigation of many other biomedical phenomena involving protein/peptide and saccharide interactions, such as virus or cancer research where the surface-immobilized glycopolymers can act as cell markers.[14, 15]

### 1.2 Amyloid-β (Aβ) peptides and their relation to AD

Abnormal accumulation of amyloid-β peptide in the brain has been widely accepted as the central cause of neurodegeneration and cognitive decline in AD.[6, 16] Aβ is a natural peptide, found in the brain's extracellular space, formed through the heterogeneous cleavage of the amyloid precursor protein (APP) by the enzyme γ-secretase.[17] Among several isoforms of Aβ formed during the cleavage, the 40-amino acid residue, Aβ40, is found to be the most abundant (~90%), while the 42-amino acid variant, Aβ42, is less abundant (~5-10%) but is the most aggregation prone.[18-20] Aβ42 has been abundantly found in both the diffuse (prefibrillar oligomeric) and senile (mature fibrillar) plaque of AD patients but Aβ40 has only been detected in the senile plaques.[21] The concentration of Aβ in biological fluid is very low (~2.5 ng/mL in healthy human (13-50 years) cerebrospinal fluid (CSF) i.e. $<10^{-8}$ M).[3, 22] The monomers of Aβ are soluble, unordered, and non-toxic but exhibit neurotoxicity once they aggregate under certain pathological conditions.[3, 23] Aβ peptides are amphiphilic species that self-assemble to form aggregated structures of different sizes, including dimers, trimers,

oligomers, protofibrils, and fibrils.[24] Soluble oligomers of Aβ have been reported to be the most toxic among all of the aggregated forms.[23, 24,25] While the soluble aggregates of both the Aβ40 and Aβ42 are found to be toxic, the latter is much more toxic, by a factor of 100.[26] Growing literature evidence suggests that the prefibrillar oligomeric aggregates are the primary pathological species in AD.[18, 25, 27] The primary difference between Aβ40 and Aβ42 is that the Aβ42 has two additional hydrophobic amino acid residues, isoleucine, and alanine.[18] These additional hydrophobic amino acid residues make the Aβ42 more prone towards the formation of toxic oligomers and fibrils.[18, 28] Most of the early research involving amyloid-β aggregation utilized Aβ40 because of its lower cost and easier synthesis and purification as compared to the Aβ42.[26] Our research focused on understanding the aggregation and conformational changes of Aβ42 in the presence of glucose and galactose containing glycopolymers in solution or bound to a surface. Aβ henceforth in this document will refer to Aβ42.

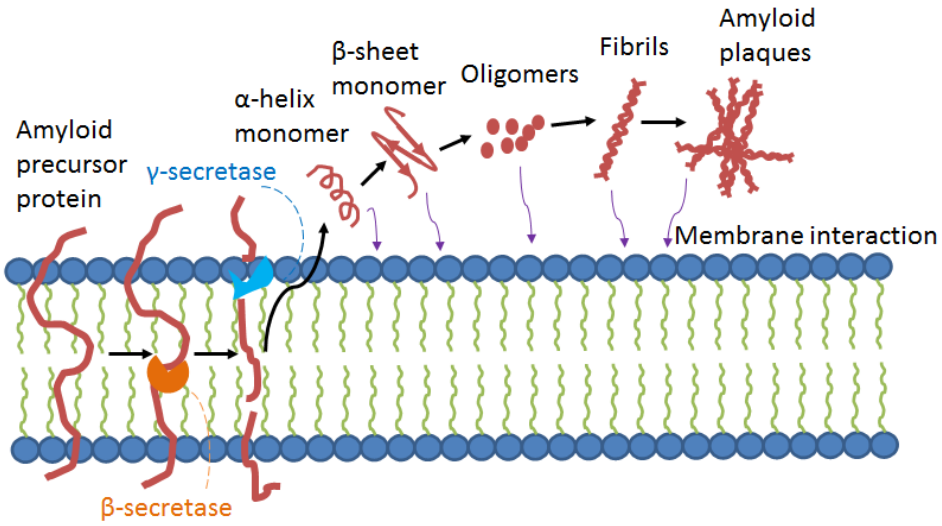


Figure 1.1 Schematic of the formation of Aβ and then aggregation into different structures. Adapted from Drolle et al.[29]

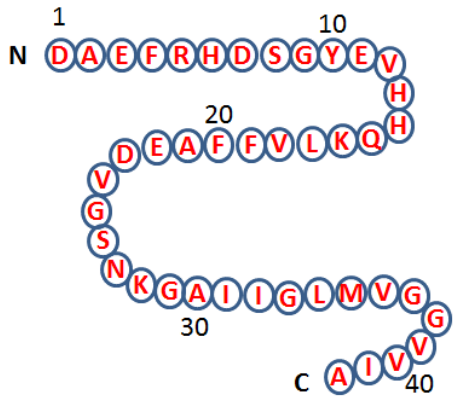


Figure 1.2 The primary amino acid sequence of the 42 amino acid Aβ isoform, Aβ42. Adapted from Figure 3, Chen et al.[30]

Aβ monomers remain as random coils in solution, but they aggregate to form oligomers or fibrils in the presence of modulators, for example, SDS or fatty acids.[31, 32] The mechanism of formation of oligomers and fibrils of Aβ and whether one type of aggregate leads to the formation of other types are still being debated. Gellermann et al.[32] reported that the formation of oligomers follows a pathway which is completely different from the fibrillation pathway. It was found that the oligomers and fibrils remained stable for a long time under incubation conditions.[32] Kumar et al. also reported the presence of two pathways leading to the formation of oligomers and fibrils but found that some of the oligomers, under certain conditions, can lead to fibril formation.[31] Using medium chain (C9-C12) saturated non-esterified fatty acids, Kumar et al. established that the oligomers of certain size (12-18 mers) slowly associated to form larger aggregates and eventually fibrils, and the process depended on the concentration of the fatty acids.[31] In the absence of fatty acids or at a very low concentration of fatty acids (much lower than the critical micelle concentration (CMC)), Aβ formed fibrils via a nucleation dependent 'on pathway' mechanism. Regardless of the kind of fatty acids used, when the concentrations

of the fatty acids were approximately equal to their CMCs, kinetically trapped 'off pathway' oligomers (12-18 mers) were formed which ultimately produced fibrils. When the concentrations of the fatty acids were much higher than their CMCs, stable oligomers (4-5 mers) were formed which did not lead to the formation of fibrils.[31] This was referred to as an 'off pathway' mechanism.[31, 33] In the presence of specific modulators, such as the GM1 ganglioside, aggregation and conformational changes of Aβ peptides from disordered aggregates to ordered β-sheet structures were found to accelerate, leading to the formation of either plaques or soluble oligomers.[25]

Conformation and toxicity of the Aβ aggregates depend on the concentration of Aβ and the modulator; for example, when the ratio of Aβ/GM1 ganglioside is between 0.013 - 0.044, Aβ forms a mixture β-sheets (of ~15 molecules) and α-helix rich structures, but when the concentration of Aβ is high and the ratio of Aβ/GM1 is > 0.044, fibrils with anti-parallel β-sheet rich structure form.[3] It was also reported that the GM1 clusters not only accelerate the Aβ aggregation but also impart higher cytotoxicity to the Aβ aggregates by forming anti-parallel β-sheets. On the other hand, the aggregates formed in solution without GM1 gangliosides contain parallel β-sheets and are less toxic.[3, 6, 34]

### 1.3 Role of saccharides of GM1 ganglioside in Aβ aggregation

A ganglioside is composed of a hydrophobic lipid tail made of ceramide and a hydrophilic head group made of saccharide moieties.[35-37] Gangliosides are positioned at the cell surface, with the hydrophobic fatty ceramide embedded in the cell membrane and the hydrophilic saccharide moieties extended well into the extracellular space where they function as cell-type specific markers, receptors, and mediators of cell adhesion.[37]

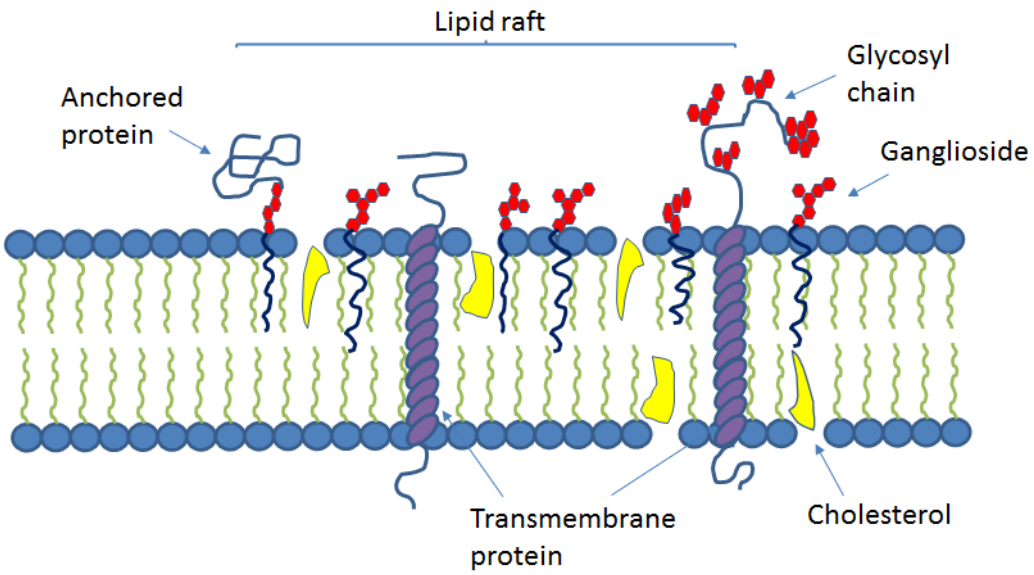


Figure 1.3 Schematic of a cell membrane which shows the clustering of the gangliosides in a raft-like (high concentration of cholesterol) membrane

GM1 ganglioside has been reported to promote Aβ aggregation by acting as a seed for nucleation.[6, 38] However, it is not clear what role each individual unit of GM1 ganglioside plays in Aβ aggregation. Kumar et al[31] investigated the effects of fatty acids of different chain lengths and concentrations on Aβ aggregation. It was reported that the size of the aggregates and the aggregation pathways depend on the concentration of the fatty acids as described in the previous section. However, the fatty acid (ceramide) portion of the GM1 ganglioside remains embedded in the cell membrane and the saccharide head groups extend into the extracellular space making them more accessible by Aβ molecules. Therefore, it is expected that the saccharide head groups strongly affect Aβ aggregation.

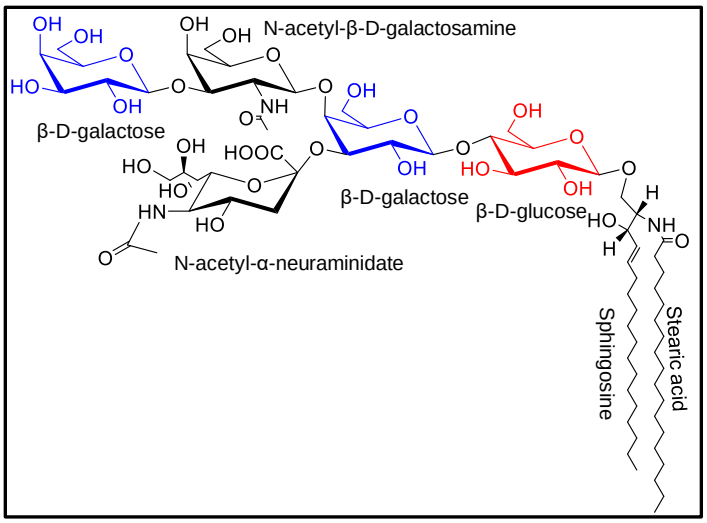


Figure 1.4 Structure of GM1 ganglioside

Fung et al. investigated the effect of free-floating simple saccharides on Aβ aggregation. Monomeric glucose has been found to promote the formation of short and flexible proto-fibrils of Aβ whereas monomeric galactose promoted the formation of mature fibrils.[39] This difference in Aβ aggregation has been attributed to the H-bonding pattern between the Aβ and the saccharides. Glucose has been reported to form stronger H-bonds with Aβ, thus forming a larger number of nucleating seeds which leads to the formation of the smaller aggregates or oligomers. Galactose, on the other hand, forms weaker H-bonds with Aβ resulting in fewer nucleating seeds and larger aggregates of Aβ, known as fibrils.[39, 40] The structure of the saccharides also affects the amount of the β-structures formed. Aβ random to β-sheet structure formation was found to increase with increasing concentration of glucose, while galactose induced no such effect.[39]

Saccharide-peptide interactions using surface immobilized saccharides have previously been investigated by Matsumoto et al.[41] Several monosaccharides including β-galactose and β-glucose were immobilized on the surfaces of silicon, glass, and quartz crystals via click chemistry and then the saccharide immobilized surfaces were utilized

for Aβ aggregation studies. It was found that the β-galactose promoted formation of Aβ fibrils with β-sheet structures, while β-glucose promoted the formation of smaller aggregates with no apparent β-sheet structure.[41] The observation of Matsumoto et al.[41] that galactose promoted β-sheet structure formation while glucose did not contradicts the findings of Fung et al,[39] who reported that glucose rather than galactose promoted concentration dependent β-sheet formation. This apparent contradiction may be explained by the fact that the Matsumoto group utilized saccharides grafted onto surfaces, while the Fung group utilized free floating saccharides in solution, indicating that bound and free-floating saccharides could affect aggregation and conformational changes differently. This might also be the reason for the observed difference in toxicity of the Aβ aggregates formed in presence of GM1 attached with a membrane vs GM1 in solution as reported by Matsuzaki et al.[3]

It has been reported that the Aβ binds with only those GM1 gangliosides which remain as clusters, called glyco-clusters, not with the uniformly distributed GM1 gangliosides.[3] For animals, including human beings, GM1 clustering depends on cholesterol content with clustering increasing with higher cholesterol.[42] For in vitro experiments, the clustering effect of GM1 saccharides can be synthetically mimicked by synthesizing polymers containing pendant saccharide units, known as glycopolymers.

### 1.4 Glycopolymers as in vitro models to mimic glyco-cluster effect

Glycopolymers are synthetic polymers which contain hydrophilic pendant saccharide groups.[43, 44] They are attracting increased attention due to their applicability to a wide range of fields, including biochemical and biomedical research,[45] drug delivery, affinity chromatography, and cell culture.[43] The most commonly used method for

glycopolymer synthesis involves polymerizable saccharide derivatives.[43, 46] Although less frequently employed, the method of post polymerization glycosylation is also reported.[47] A range of glycopolymers have been reported, including those based on polyacrylamides,[48] polyacrylates,[49] and polymethacrylamides.[50] Acrylamide-based glycopolymers offer the advantage of biocompatibility, water solubility, and hydrolytic stability over a wide range of salt concentration and pH.[44]

The affinity between proteins and simple monovalent carbohydrate residues is often weak ($K_a = 10^3$-$10^4$ L mol$^{-1}$).[51-53] In an in vitro setting, physiologically relevant levels of association and affinities between saccharides and proteins generally require a multivalent presentation of ligands.[51] Glycopolymers can mimic the multivalent 'glyco-cluster' effect of saccharides of gangliosides[41, 51, 54] and provide a model for determining the effects of the individual saccharide components on Aβ aggregation.

In their natural environment, gangliosides are attached to cell membranes via the ceramide tail.[37] These phospholipid membranes are semi-solid in nature, more like liquid cooking oil than solid shortening.[55] Due to the physical nature of the membrane, the movement of the gangliosides is not completely free but rather restricted.[56] Previous reports suggested that the structures and the toxicity of Aβ aggregates vary based on the mobility of the structures studied (solution vs surface-anchored).[3] Therefore, in vitro experiments of Aβ aggregation in this work were performed with model glycopolymers dissolved in aqueous solution and attached to surfaces. We synthesized high (DP of 350) and low (DP of 35) molecular weight acrylamide based glycopolymers with β-D-glucose and β-D-galactose as pendant groups maintaining the same stereospecificity of

saccharides of the GM1 ganglioside. These polymers were expected to mimic the glyco-clustering effect of the saccharides of ganglioside.

Glycopolymers of target molecular weight and thickness were synthesized in solution and on surfaces via addition fragmentation chain transfer polymerization (RAFT) and photo polymerization techniques. The effect of the structure of saccharides (i.e. glucose vs galactose) and their concentration on Aβ aggregation using appropriate and relevant model systems has not previously been reported in the literature. Here we report the design, synthesis and characterization of model glycomonomers and polymers with controlled structures and molecular weights and utilized them for the investigation of Aβ aggregation via advanced in vitro experiments.

### 1.5 References

(1) Hebert, L. E.; Weuve, J.; Scherr, P. A.; Evans, D. A. Alzheimer disease in the United States (2010-2050) estimated using the 2010 census. Neurology, **2013**, *80*(19), 1778-83.

(2) Alzheimer'sAssociation. 2018 Alzheimer's disease facts and figures. Alzheimer's & Dementia, **2018**, *14*(3), 367-429.

(3) Matsuzaki, K. How Do Membranes Initiate Alzheimer's Disease? Formation of Toxic Amyloid Fibrils by the Amyloid β-Protein on Ganglioside Clusters. Accounts of Chemical Research, **2014**, *47*(8), 2397-2404.

(4) Selkoe, D. J. Alzheimer's disease: genes, proteins, and therapy. Physiological reviews, **2001**, *81*(2), 741-66.

(5) Citron, M. Alzheimer's disease: treatments in discovery and development. Nature neuroscience, **2002**.

(6) Matsuzaki, K.; Kato, K.; Yanagisawa, K. Aβ polymerization through interaction with membrane gangliosides. Biochimica et Biophysica Acta (BBA) - Molecular and Cell Biology of Lipids, **2010**, *1801*(8), 868-877.

(7) Levy, E.; Carman, M. D.; Fernandez-Madrid, I. J.; Power, M. D.; Lieberburg, I.; van Duinen, S. G.; Bots, G. T.; Luyendijk, W.; Frangione, B. Mutation of the Alzheimer's disease amyloid gene in hereditary cerebral hemorrhage, Dutch type. Science, **1990**, *248*(4959), 1124-6.

(8) Nilsberth, C.; Westlind-Danielsson, A.; Eckman, C. B.; Condron, M. M.; Axelman, K.; Forsell, C.; Stenh, C.; Luthman, J.; Teplow, D. B.; Younkin, S. G.; Naslund, J.; Lannfelt, L. The 'Arctic' APP mutation (E693G) causes Alzheimer's disease by enhanced Abeta protofibril formation. Nature neuroscience, **2001**, *4*(9), 887-93.

(9) Yu, R. K.; Tsai, Y.-T.; Ariga, T.; Yanagisawa, M. Structures, biosynthesis, and functions of gangliosides--an overview. Journal of oleo science, **2011**, *60*(10), 537-544.

(10) Yu, R. K.; Tsai, Y. T.; Ariga, T.; Yanagisawa, M. Structures, biosynthesis, and functions of gangliosides--an overview. J Oleo Sci, **2011**, *60*(10), 537-44.

(11) Ariga, T.; Kobayashi, K.; Hasegawa, A.; Kiso, M.; Ishida, H.; Miyatake, T. Characterization of high-affinity binding between gangliosides and amyloid beta-protein. Arch Biochem Biophys, **2001**, *388*(2), 225-30.

(12) McLaurin, J.; Franklin, T.; Fraser, P. E.; Chakrabartty, A. Structural transitions associated with the interaction of Alzheimer beta-amyloid peptides with gangliosides. J Biol Chem, **1998**, *273*(8), 4506-15.

(13) Thompson, J. P.; Schengrund, C.-L. Inhibition of the adherence of cholera toxin and the heat-labile enterotoxin of Escherichia coli to cell-surface GM1 by oligosaccharide-derivatized dendrimers. Biochemical Pharmacology, **1998**, *56*(5), 591-597.

(14) Van Breedam, W.; Pöhlmann, S.; Favoreel, H. W.; de Groot, R. J.; Nauwynck, H. J. Bitter-sweet symphony: glycan–lectin interactions in virus biology. FEMS Microbiology Reviews, **2014**, *38*(4), 598-632.

(15) Nangia-Makker, P.; Conklin, J.; Hogan, V.; Raz, A. Carbohydrate-binding proteins in cancer, and their ligands as therapeutic agents. Trends Mol Med, **2002**, *8*(4), 187-92.

(16) Hardy, J.; Allsop, D. Amyloid deposition as the central event in the aetiology of Alzheimer's disease. Trends in Pharmacological Sciences, **1991**, *12*, 383-388.

(17) Gilbert, B. J. The role of amyloid beta in the pathogenesis of Alzheimer's disease. Journal of clinical pathology, **2013**, *66*(5), 362-6.

(18) Haass, C.; Selkoe, D. J. Soluble protein oligomers in neurodegeneration: lessons from the Alzheimer's amyloid [beta]-peptide. Nat Rev Mol Cell Biol, **2007**, *8*(2), 101-112.

(19) Winklhofer, K. F.; Tatzelt, J.; Haass, C. The two faces of protein misfolding: gain- and loss-of-function in neurodegenerative diseases. The EMBO Journal, **2008**, *27*(2), 336-349.

(20) Younkin, S. G. The role of A beta 42 in Alzheimer's disease. Journal of physiology, Paris, **1998**, *92*(3-4), 289-92.

(21) Cummings, B. J.; Satou, T.; Head, E.; Milgram, N. W.; Cole, G. M.; Savage, M. J.; Podlisny, M. B.; Selkoe, D. J.; Siman, R.; Greenberg, B. D.; Cotman, C. W. Diffuse

plaques contain C-terminal Aβ42 and not Aβ40: Evidence from cats and dogs. Neurobiology of aging, **1996**, *17*(4), 653-659.

(22) Seubert, P.; Vigo-Pelfrey, C.; Esch, F.; Lee, M.; Dovey, H.; Davis, D.; Sinha, S.; Schiossmacher, M.; Whaley, J.; Swindlehurst, C.; McCormack, R.; Wolfert, R.; Selkoe, D.; Lieberburg, I.; Schenk, D. Isolation and quantification of soluble Alzheimer's [beta]-peptide from biological fluids. Nature, **1992**, *359*(6393), 325-327.

(23) Dahlgren, K. N.; Manelli, A. M.; Stine, W. B., Jr.; Baker, L. K.; Krafft, G. A.; LaDu, M. J. Oligomeric and fibrillar species of amyloid-beta peptides differentially affect neuronal viability. J Biol Chem, **2002**, *277*(35), 32046-53.

(24) Lin, M.-S.; Chen, L.-Y.; Tsai, H.-T.; Wang, S. S. S.; Chang, Y.; Higuchi, A.; Chen, W.-Y. Investigation of the Mechanism of β-Amyloid Fibril Formation by Kinetic and Thermodynamic Analyses. Langmuir, **2008**, *24*(11), 5802-5808.

(25) Ahmed, M.; Davis, J.; Aucoin, D.; Sato, T.; Ahuja, S.; Aimoto, S.; Elliott, J. I.; Van Nostrand, W. E.; Smith, S. O. Structural conversion of neurotoxic amyloid-[beta]1-42 oligomers to fibrils. Nat Struct Mol Biol, **2010**, *17*(5), 561-567.

(26) Findeis, M. A. The role of amyloid beta peptide 42 in Alzheimer's disease. Pharmacology & therapeutics, **2007**, *116*(2), 266-86.

(27) Glabe, C. G. Common mechanisms of amyloid oligomer pathogenesis in degenerative disease. Neurobiology of aging, **2006**, *27*(4), 570-5.

(28) Hung, L. W.; Ciccotosto, G. D.; Giannakis, E.; Tew, D. J.; Perez, K.; Masters, C. L.; Cappai, R.; Wade, J. D.; Barnham, K. J. Amyloid-beta peptide (Abeta) neurotoxicity is modulated by the rate of peptide aggregation: Abeta dimers and trimers correlate with

neurotoxicity. The Journal of neuroscience : the official journal of the Society for Neuroscience, **2008**, *28*(46), 11950-8.

(29) Drolle, E.; Hane, F.; Lee, B.; Leonenko, Z. (2014). Atomic force microscopy to study molecular mechanisms of amyloid fibril formation and toxicity in Alzheimer's disease.

(30) Chen, G.-f.; Xu, T.-h.; Yan, Y.; Zhou, Y.-r.; Jiang, Y.; Melcher, K.; Xu, H. E. Amyloid beta: structure, biology and structure-based therapeutic development. Acta Pharmacologica Sinica, **2017**, *38*, 1205.

(31) Kumar, A.; Bullard, R. L.; Patel, P.; Paslay, L. C.; Singh, D.; Bienkiewicz, E. A.; Morgan, S. E.; Rangachari, V. Non-Esterified Fatty Acids Generate Distinct Low-Molecular Weight Amyloid-β (Aβ42) Oligomers along Pathway Different from Fibril Formation. PLoS ONE, **2011**, *6*(4), e18759.

(32) Gellermann, G. P.; Byrnes, H.; Striebinger, A.; Ullrich, K.; Mueller, R.; Hillen, H.; Barghorn, S. Abeta-globulomers are formed independently of the fibril pathway. Neurobiology of disease, **2008**, *30*(2), 212-20.

(33) Kumar, A.; Paslay, L. C.; Lyons, D.; Morgan, S. E.; Correia, J. J.; Rangachari, V. Specific Soluble Oligomers of Amyloid-β Peptide Undergo Replication and Form Non-fibrillar Aggregates in Interfacial Environments. The Journal of Biological Chemistry, **2012**, *287*(25), 21253-21264.

(34) Okada, T.; Ikeda, K.; Wakabayashi, M.; Ogawa, M.; Matsuzaki, K. Formation of Toxic Aβ(1–40) Fibrils on GM1 Ganglioside-Containing Membranes Mimicking Lipid Rafts: Polymorphisms in Aβ(1–40) Fibrils. Journal of molecular biology, **2008**, *382*(4), 1066-1074.

(35) Acquotti, D.; Poppe, L.; Dabrowski, J.; Von der Lieth, C. W.; Sonnino, S.; Tettamanti, G. Three-dimensional structure of the oligosaccharide chain of GM1 ganglioside revealed by a distance-mapping procedure: a rotating and laboratory frame nuclear overhauser enhancement investigation of native glycolipid in dimethyl sulfoxide and in water-dodecylphosphocholine solutions. Journal of the American Chemical Society, **1990**, *112*(21), 7772-7778.

(36) Moghimi, S. M.; Hunter, A. C.; Murray, J. C. Long-Circulating and Target-Specific Nanoparticles: Theory to Practice. Pharmacological Reviews, **2001**, *53*(2), 283-318.

(37) Sonnino, S.; Mauri, L.; Chigorno, V.; Prinetti, A. Gangliosides as components of lipid membrane domains. Glycobiology, **2007**, *17*(1), 1R-13R.

(38) Yanagisawa, K. Role of gangliosides in Alzheimer's disease. Biochimica et Biophysica Acta (BBA) - Biomembranes, **2007**, *1768*(8), 1943-1951.

(39) Fung, J.; Darabie, A. A.; McLaurin, J. Contribution of simple saccharides to the stabilization of amyloid structure. Biochemical and Biophysical Research Communications, **2005**, *328*(4), 1067-1072.

(40) Allison, S. D.; Chang, B.; Randolph, T. W.; Carpenter, J. F. Hydrogen Bonding between Sugar and Protein Is Responsible for Inhibition of Dehydration-Induced Protein Unfolding. Archives of Biochemistry and Biophysics, **1999**, *365*(2), 289-298.

(41) Matsumoto, E.; Yamauchi, T.; Fukuda, T.; Miura, Y. Sugar microarray via click chemistry: molecular recognition with lectins and amyloid β (1–42). Science and Technology of Advanced Materials, **2009**, *10*(3), 034605.

(42) Kakio, A.; Nishimoto, S. I.; Yanagisawa, K.; Kozutsumi, Y.; Matsuzaki, K. Cholesterol-dependent formation of GM1 ganglioside-bound amyloid beta-protein, an endogenous seed for Alzheimer amyloid. J Biol Chem, **2001**, *276*(27), 24985-90.

(43) Ambrosi, M.; Batsanov, A. S.; Cameron, N. R.; Davis, B. G.; Howard, J. A. K.; Hunter, R. Influence of preparation procedure on polymer composition: synthesis and characterisation of polymethacrylates bearing [small beta]-D-glucopyranoside and [small beta]-D-galactopyranoside residues. Journal of the Chemical Society, Perkin Transactions 1, **2002**, (1), 45-52.

(44) Ladmiral, V.; Melia, E.; Haddleton, D. M. Synthetic glycopolymers: an overview. European Polymer Journal, **2004**, *40*(3), 431-449.

(45) Miura, Y. Synthesis and biological application of glycopolymers. Journal of Polymer Science Part A: Polymer Chemistry, **2007**, *45*(22), 5031-5036.

(46) Gruber, H.; Knaus, S. Synthetic polymers based on carbohydrates: preparation, properties and applications. Macromolecular Symposia, **2000**, *152*(1), 95-105.

(47) Nukada, T.; Berces, A.; Zgierski, M. Z.; Whitfield, D. M. Exploring the Mechanism of Neighboring Group Assisted Glycosylation Reactions. Journal of the American Chemical Society, **1998**, *120*(51), 13291-13295.

(48) Bahulekar, R.; Tokiwa, T.; Kano, J.; Matsumura, T.; Kojima, I.; Kodama, M. Polyacrylamide containing sugar residues: synthesis, characterization and cell compatibility studies. Carbohydrate Polymers, **1998**, *37*(1), 71-78.

(49) Li, Z.-C.; Liang, Y.-Z.; Chen, G.-Q.; Li, F.-M. Synthesis of amphiphilic block copolymers with well-defined glycopolymer segment by atom transfer radical polymerization. Macromolecular Rapid Communications, **2000**, *21*(7), 375-380.

(50) Nakaya, T.; Nishio, K.; Memita, M.; Imoto, M. Polymeric glycolipid analogues, 3. Polymethacrylates containing glucose moieties attached to the polymer backbones via n-alkyl chains of various length. Die Makromolekulare Chemie, Rapid Communications, **1993**, *14*(2), 77-83.

(51) Yu, K.; Kizhakkedathu, J. N. Synthesis of Functional Polymer Brushes Containing Carbohydrate Residues in the Pyranose Form and Their Specific and Nonspecific Interactions with Proteins. Biomacromolecules, **2010**, *11*(11), 3073-3085.

(52) Mandal, D. K.; Kishore, N.; Brewer, C. F. Thermodynamics of Lectin-Carbohydrate Interactions. Titration Microcalorimetry Measurements of the Binding of N-Linked Carbohydrates and Ovalbumin to Concanavalin A. Biochemistry, **1994**, *33*(5), 1149-1156.

(53) Schwarz, F. P.; Puri, K. D.; Bhat, R. G.; Surolia, A. Thermodynamics of monosaccharide binding to concanavalin A, pea (Pisum sativum) lectin, and lentil (Lens culinaris) lectin. Journal of Biological Chemistry, **1993**, *268*(11), 7668-7677.

(54) Mammen, M.; Choi, S.-K.; Whitesides, G. M. Polyvalent Interactions in Biological Systems: Implications for Design and Use of Multivalent Ligands and Inhibitors. Angewandte Chemie International Edition, **1998**, *37*(20), 2754-2794.

(55) Sherwood, L. (2011). Fundamentals of Human Physiology, Cengage Learning.

(56) Dzikovski, B.; Freed, J. H.; Begley, T. P. (2007). Membrane Fluidity. Wiley Encyclopedia of Chemical Biology, John Wiley & Sons, Inc.

# CHAPTER II - AQUEOUS RAFT SYNTHESIS OF GLYCOPOLYMERS FOR DETERMINATION OF SACCHARIDE STRUCTURE AND CONCENTRATION EFFECTS ON AMYLOID-β AGGREGATION

This chapter and the images of the appendix A were published in Biomacromolecules, 2017, 18(10), 3359-3366.

## 2.1 Introduction

The clustered saccharides of the GM1 ganglioside have been reported to seed Aβ aggregation.[1, 2] The aggregation mechanism of Aβ in the presence of the GM1 ganglioside and the specific functions of the individual saccharide groups in the aggregation process are not yet fully understood. The observation that among the gangliosides, which differ primarily in their saccharides, GM1 strongly promotes Aβ aggregation indicates that the glycoform distribution plays an important role in the aggregation process. [3-7]

Glycosaminoglycans (GAGs), which are polyanionic polysaccharides, have also been reported to exhibit a strong effect on amyloid aggregation.[8-13] The aggregation depends on several factors, such as the length of the polysaccharides,[9, 11] the nature and the degree of functionalization (eg. sulfation),[8] and the ratio of the GAGs to the amyloid.[14] Short polysaccharides (DP < 5) show a very minimal effect on the rate of amyloid fibrillation, which increases with increasing chain length and ultimately reaches a maximum at high chain lengths (DP >> 18).[11, 15] Fung et al.[16] reported the effect of free floating simple carbohydrates on Aβ42 aggregation and conformational changes. Glucose promoted nucleation, resulting in the formation of short and flexible protofibrils; whereas galactose promoted mature fiber formation.[16] The level of β-sheet conformation increased

with increasing glucose concentration, while galactose showed no such influence, indicating that the H-bonding pattern of saccharides is an important factor in determining the aggregation behavior of Aβ42.[16]

Matsuzaki et al. reported that gangliosides can mediate Aβ aggregation only when they remain as clusters and not when present as uniformly distributed moieties.[1] It is also reported that the in vitro interactions between proteins and saccharides are substantially weaker than those observed in vivo.[17, 18] A physiologically relevant level of association and affinities between saccharides and proteins requires the multivalent effect of saccharides, known as the 'glyco-cluster' effect.[19-21] To model the glyco-cluster effect, we employed aqueous reversible addition fragmentation chain transfer (aRAFT) polymerization to achieve high molecular weight acrylamide-based glycopolymers of desired structure and molecular weight. Pendant groups of galactose or glucose with β-stereochemistry were synthesized to model the saccharides of GM1. Acrylamide was chosen as the backbone due to its excellent water solubility, hydrolytic stability, and its stability over a wide range of pH and salt concentrations.[22] These model glycopolymers were studied to investigate physiological scenarios to determine how saccharide type (galactose vs glucose) of GM1 ganglioside influences Aβ aggregation.[23]

## 2.2 Materials and methods

### 2.2.1 Materials

All reagents and solvents were obtained from Sigma-Aldrich Corporation (USA) or ThermoFisher Scientific (USA) in their highest purity available. The chemicals were used without further purification unless otherwise stated. Lyophilized stocks of synthetic, wild-type Aβ42, herein referred to as Aβ (obtained from the Mayo Clinic, Rochester,

MN) were stored at -20 °C. The chain transfer agent, 4-cyano-4-(ethylsulfanylthiocarbonyl) sulfanylpentanoic acid (CEP) was synthesized by adapting previously reported procedures.[24, 25]

### 2.2.2 Characterization

Nuclear Magnetic Resonance (NMR) spectroscopy was performed with a Varian MercuryPLUS (300 MHz) spectrometer by taking an average of 128 scans (delay 5 s) using appropriate solvents ($CDCl_3$ or $D_2O$). Gel Permeation Chromatography (GPC) was performed on a Waters system with Waters 1525 Binary Pump and Waters 2414 differential refractive index detector utilizing two highly efficient PolySep GFC columns (elution range 3 k to 400 kDa). An aqueous solution containing 0.1 M $NaNO_3$ and 0.01% (w/v) $NaN_3$ was filtered and used as the eluent at a flow rate of 1 mL/min at 25 ºC. The molecular weight calibration was performed with monodisperse linear polyethylene oxide (Polymer Standard Service). For molecular weights, the entire signal of a major peak including its shoulder at a lower retention volume was integrated. Mass spectrometry was done on a ThermoFinnigan TSQ 7000 triple-quadrapole instrument that was equipped with an electrospray ionization (ESI) source. Glycomonomer samples (1 mg/mL) in a 1:1 (v/v) methanol/water solution containing sodium chloride (1 mg/mL) were injected into the ESI source at a rate of 10 µL/s. All data were analyzed using Xcalibur (FisherScientific, Inc.) software.

### 2.2.3 In vitro glycopolymer-Aβ interactions

Freshly purified Aβ monomer (25 µM) was coincubated with 75 µM of either poly(N,N-dimethyl acrylamide) (PDMA), galactose-containing glycopolymers (PGalEAm), or glucose-containing glycopolymers (PGlcEAm). Note that the solution

molarity is determined based on the polymer theoretical number average molecular weight. Thus, concentration of pendant saccharide groups is ten-fold higher in the high molecular weight glycopolymer solutions than in the low molecular weight analogues. For all samples, 0.1 M $NaNO_3$ was added for polymer stability and 0.01% (w/v) $NaN_3$ was added to prevent bacterial growth. All reactions were buffered in 20 mM Tris at pH 8.0 and were carried out at 37 °C under quiescent conditions with periodic monitoring by thioflavin-T (ThT) fluorescence and immunoblotting.

### 2.2.4 Thioflavin T (ThT) fluorescence

Measurements were collected by mixing 70 μL of ThT (10 μM) with 5 μL of each sample. After a 1 min equilibration period, fluorescence kinetics were measured in a microcuvette with a Cary Eclipse spectrometer (Varian, Inc.) by exciting at 452 nm while monitoring emission at 482 nm over a 1 min period. Excitation and emission slits were kept constant at 10 nm.

### 2.2.5 Polyacrylamide gel electrophoresis

Samples were diluted into 1X Laemmli loading buffer either with (denaturing) or without (non-denaturing) 1% SDS and then loaded without heating onto either NuPAGE 4-12% Bis-Tris gels resolved in 1X MES running buffer containing 0.1% SDS (Life Technologies) for SDS-PAGE or 4-20% BioRad gels resolved in 1X Laemmli buffer for native PAGE. For SDS-PAGE, pre-stained molecular weight (MW) markers (Novex Sharp Protein Standard, Life Technologies) were run in parallel for MW determination. Proteins were transferred to a 0.2 μm nitrocellulose membrane (BioRad) and boiled for 1 min in a microwave oven in 1X PBS followed by blocking for 1.5 h in 1X PBS containing 5% nonfat dry milk with 1% Tween 20. Blots were then probed overnight at

4°C with a 1:6000 dilution of Ab5 monoclonal antibody, which detects amino acids 1-16 of Aβ. Blots were then incubated with a 1:6000 dilution of anti-mouse, horseradish peroxidase conjugated secondary antibody and developed with ECL reagent (Thermo Scientific).

### 2.2.6 Amyloid-β (Aβ) monomer purification and isolation

Before the use of Aβ in any reaction, the peptide was purified by size exclusion chromatography (SEC) to remove any preformed aggregates. Briefly, 1.5–2 mg of peptide was dissolved in 0.5 mL of 10 mM aqueous NaOH and allowed to stand for 15 min at room temperature prior to SEC using a 1X30-cm Superdex-75 HR 10/30 column (GE Healthcare) attached to an ÄKTA FPLC system (GE Healthcare).[26] The column was pre-equilibrated with 20 mM Tris-HCl (pH 8.0) at 25°C, and the protein was eluted at a flow rate of 0.5 mL/min. Fractions of 500 μL were collected and the concentration of Aβ was determined by UV-visible spectrometry on a Cary 50 spectrophotometer (Varian Inc.) using a molar extinction coefficient of 1450 $cm^{-1}$ $M^{-1}$ at 276 nm (ExPASy) corresponding to the single tyrosine residue. Peptide integrity after SEC was periodically confirmed via MALDI-ToF mass spectrometry, which showed a monoisotopic molecular mass of 4515 Da. Monomeric Aβ42 fractions were stored at 4 °C and used within 48 h of SEC purification to eliminate any possibilities of preformed aggregates in the reactions.

### 2.2.7 Glycomonomer synthesis

The acetyl protected glycomonomers, 2′-acrylamidoethyl-2,3,4,6-tetra-O-acetyl-*β*-D-galactopyranoside (AcGalEAm) and 2′-acrylamidoethyl-2,3,4,6-tetra-O-acetyl-*β*-D-glucopyranoside (AcGlcEAm) were synthesized by adapting the procedures reported by Ambrosi et al.[27] for the synthesis of 2′-(2,3,4,6–tetra-O-acetyl-β-D-galactosyloxy)ethyl

methacrylate and 2′-(2,3,4,6–tetra-O-acetyl-β-D-glucosyloxy)ethyl methacrylate. In short, either 2,3,4,6-tetra-O-acetyl-α-D-galactopyranosyl bromide (15 g, 36.5 mmol) or 2,3,4,6-tetra-O-acetyl-α-D-glucopyranosyl bromide (15 g, 36.5 mmol) was reacted with an excess amount of N-hydroxyethyl acrylamide (HEAm) (21 g, 182.4 mmol) in anhydrous dichloromethane (400 mL) using excess silver trifluoromethanesulfonate (AgOTf) (14 g, 54.5 mmol) as a catalyst. Dry molecular sieves (20 g, 3 Å size) were added to the reaction mixture before the addition of silver trifluoromethanesulfonate to ensure that the reaction medium was completely dry. The reaction mixture was stirred for 48 h at 0°C in an $N_2$ atmosphere. Then the reaction mixture was filtered, and the filtrate was washed three times with 1M HCl and dried over sodium sulphate. A yellow colored and highly viscous product was obtained after solvent removal via rotary evaporation. Flash chromatography was performed with the crude products using silica gel as the stationary phase and a mixture of 10:1 ethyl acetate:hexane as the eluent. The eluent fractions with retardation factor ($R_f$) = 0.45 were collected and the solvent was evaporated by rotary evaporation to obtain a white crystalline pure product (9.1 g, 20.43 mmol).

**AcGalEAm** , $^1$H NMR (300 MHz, $CDCl_3$): δ [ppm] 1.99, 2.02, 2.16 (s, s, s, 12H-13,14,15,16), 3.57 (m, 2H-5), 3.72 (m, 1H-9), 3.90 (m, 2H-4), 4.13 (m, 2H-11,12), 4.46 (m, 1H-6), 5.01 (d of d, 1H-10), 5.16 (m, 1H-7), 5.37 (t, 1H-8), 5.66 (d of d, 1H-1), 6.10 (m, 1H-2), 6.31 (m, 1H-3). [$^1$H NMR spectra, Supporting information, Appendix A, A.1] [**ESI** m/z: 445 + 23 ($Na^+$), Supporting information, Appendix A, Figure A.5]

**AcGlcEAm** , $^1$H NMR (300 MHz, $CDCl_3$): δ [ppm] 1.97, 2.03, 2.14 (s, s, s, 12H-13,14,15,16), 3.57 (m, 2H-5), 3.70 (m, 1H-9), 3.91 (m, 2H-4), 4.14 (m, 2H-11,12), 4.48

(m, 1H-6), 5.02 (d of d, 1H-10), 5.16 (m, 1H-7), 5.38 (t, 1H-8), 5.66 (d of d, 1H-1), 6.05 (m, 1H-2), 6.31 (m, 1H-3). [$^1$H NMR spectra, Supporting information, Appendix A, Figure A.3] [**ESI** m/z: 445 + 23 ($Na^+$)]

### 2.2.8 Glycomonomer deprotection

Acetyl protected monomer, AcGalEAm (9.1 g) or AcGlcEAm (9.1 g), was dissolved in anhydrous methanol (46 mL) in a round bottom flask equipped with a stir bar. The flask was sealed with rubber septum and purged with $N_2$ for 15 min before the dropwise addition of 25% (w/v) sodium methoxide solution in methanol (4.55 mL), and the reaction was stirred for another 45 min in an $N_2$ atmosphere. Acetic acid was added dropwise until a neutral or a slightly acidic pH (pH≈6) was achieved. The solvent was removed by rotary evaporation to obtain a highly viscous, colorless liquid which became a strongly hygroscopic, colorless solid after freeze drying. The complete deprotection of the glycomonomers was confirmed via $^1$H-NMR and ESI-MS.

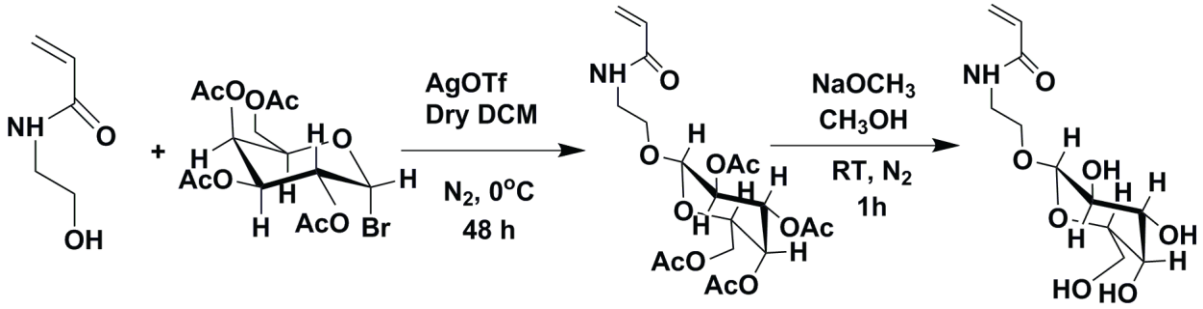


Scheme 2.1 Reaction scheme for the synthesis of glycomonomer AcGalEAm and its deprotection to GalEAm. (Same scheme applies for GlcEAm monomer synthesis)

**GalEAm,** $^1$H-NMR (300 MHz, $D_2O$): δ [ppm] 3.31-4.09 (m, 10H-4, 5, 7, 8, 9, 10, 11, 12), 4.39 (d, 1H-6), 5.72 (d of d, 1H-1), 6.07-6.36 (m, 1H-3, 1H-2). [**ESI-MS** m/z: 277+ 23 ($Na^+$) Supporting information, Appendix A, Figure A.2]

**GlcEAm,** $^{1}$H-NMR (300 MHz, $D_2O$): δ [ppm] 3.49-4.11 (m, 10H-4, 5, 7, 8, 9, 10, 11, 12), 4.39 (d, 1H-6), 5.75 (d of d, 1H-1), 6.19 (m, 1H-3, 1H-2). [$^{1}$H NMR spectra, Supporting information, Appendix A, Figure A.4] [**ESI-MS** m/z: 277+ 23 ($Na^+$)]

### 2.2.9 General procedure for aRAFT polymerization of glycomonomer

Glycopolymers with a target degree of polymerization (DP) of 35 (molecular weight= 9951 g/mol) and 350 (molecular weight = 97206 g/mol) were synthesized by aRAFT polymerization. The reaction conditions for the RAFT polymerizations were selected based on previous reports for acrylate or acrylamide based polymers.[28-32] The initial concentration of the monomer to chain transfer agent and the chain transfer agent to initiator were maintained at 500:1 and 5:1 respectively for a target DP of 35 achievable at 7% conversion and a target DP of 350 achievable at 70% conversion. The initial glycomonomer concentration in the reaction mixture was kept at 1M. 4-cyano-4-(ethylsulfanylthiocarbonyl) sulfanylpentanoic acid (CEP) was used as a chain transfer agent (CTA) and 4,4′-azobis(4-cyanopentanoic acid), V-501, was used as a free radical initiator for the polymerization reaction. Benzenesulfonic acid (BSA) was used as an internal standard to monitor the progress of the reactions, which were performed in a 0.1M sodium acetate buffer solution of pH 5.0 at 70 °C. A typical procedure for glycopolymer synthesis is as follows: 7.97 mL of monomer solution (GalEAm or GlcEAm) in acetate buffer from a stock solution of 0.348 g/mL was transferred to a 10 mL graduated cylinder, and 113.5 μL of CEP solution in methanol from a 46.4 mg/mL of stock solution and 22.8 μL of V-501 solution in methanol from a stock solution of 49.1 mg/mL was added to the cylinder, followed by addition of 527 μL BSA solution in buffer from a stock solution of 150.2 mg/mL. The mixture was diluted to a total volume of 10

mL with acetate buffer. The reaction mixture was then transferred to a 25 mL round bottom flask equipped with a stir bar. The flask was sealed with a rubber septum and parafilm and purged with high purity nitrogen gas for 40 min while stirring. An initial aliquot was taken, and the flask was placed in an oil bath heated to 70°C. Aliquots were taken at 30 minute intervals and rapidly quenched with liquid nitrogen. $^{1}$H NMR spectroscopy was performed with the quenched aliquots to determine the monomer conversion to polymer. Monomer conversion was determined by comparing relative integral areas of the vinyl proton peak of the monomers (5.73 ppm, 1H) to the aromatic proton peak of the BSA standard (7.77 ppm, 2H) at different reaction times. Molecular weight of the polymers formed at different time points was calculated from the NMR spectroscopy conversion data. The quenched solutions were transferred to dialysis tubes of molecular weight cut off 3500 Dalton (Spectra/Por) and dialysed for a period of five days (24h X 5) in distilled water. The dialysed samples were freeze dried at -50°C in high vacuum (0.05 torr) for two days. The samples corresponding to ~7% and ~70% conversion (~35DP and ~350DP respectively) were tested for their molecular weight and dispersity via gel permeation chromatography (GPC). These samples with two different molecular weights (35 and 350DP) and two different saccharide units (gal and glc) were used to further investigate their effect on Aβ aggregation.

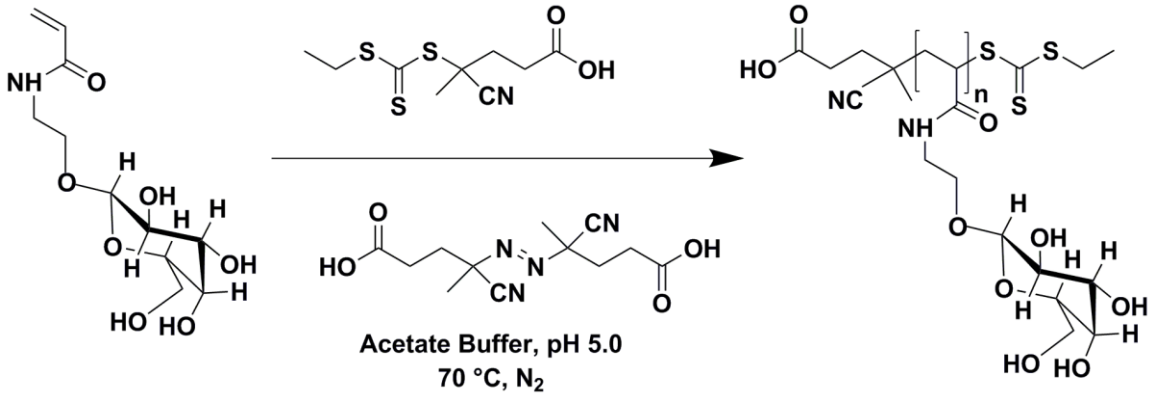


Scheme 2.2 Synthetic scheme for the aqueous RAFT polymerization of GalEAm. (same scheme applies for the glucose containing glycomonomer GlcEAm).

### 2.2.10 RAFT polymerization of dimethyl acrylamide

Dimethyl acrylamide (DMA) monomers were purified to remove inhibitor by passing through a column filled with basic aluminium oxide. Polymerization of DMA monomers was carried out via an aqueous RAFT polymerization technique to produce polymers with a degree of polymerization of 35 and 350, following the procedure outlined for the glycopolymer synthesis.

## 2.3 Results and discussion

### 2.3.1 Glycomonomer synthesis

The acetyl protected glycomonomers were synthesized as described in the experimental section and characterized via $^{1}$H NMR spectroscopy (Supporting information, Appendix A, Figure A.1 and A.3). The debromination reaction between the glycosyl donor, acetobromo-α-D-galactose, and the glycosyl acceptor, N-hydroxyethyl acrylamide, is evidenced by the shift in the C1 proton NMR peak from 6.69 ppm in the galactose precursor to 4.5 ppm in AcGalEAm. Complete conversion of the limiting reactant, acetobromo saccharide, was confirmed via TLC by the absence of the spot representing unreacted saccharides.

Pre-polymerization deprotection of the glycomonomers was chosen over post-polymerization deprotection to minimize incomplete removal of the acetyl protecting groups, which can affect the biological properties of the sugars and their protein interactions.[21, 33] Complete deprotection of the protected glycomonomers was confirmed by the disappearance of the characteristic $^{1}$H NMR peak for the acetyl groups at 1.99-2.16 ppm, and by ESI-MS [m/z: 445 + 23 ($Na^{+}$) for AcGlcEAm and AcGalEAm, and m/z: 277 + 23 ($Na^{+}$) for GlcEAm and GalEAm].

To model the GM1 ganglioside, where saccharides are of β-stereo conformation, it is desirable to have the same stereochemistry in our glycomonomers and polymers. The stereochemistry was determined via $^{1}$H NMR spectroscopy, and the percentage of β-anomers in monomers was estimated by comparing the proton peak area at 4.5 ppm (β-anomers) to that at 5.2 ppm (α-anomers). Excellent stereospecificity was obtained (>98% β-anomers), which is attributed to neighboring group participation involving the acetate group as reported by Ambrosi et al.[27] The stereospecificity of the saccharides was retained during glycomonomer deprotection and polymerization reactions as evidenced by the unchanged $^{1}$H NMR spectra [Supporting information, Appendix A, Figure A.7]. Yu et al. reported the synthesis of the same monomers via a different reaction pathway which produced only 84% of β-anomers.[21] We adapted the procedures reported by Ambrosi et al.[27] for synthesis of methacrylate glycopolymers to achieve acrylamide-based glycopolymers in high yield (~60%) and almost complete conversion to β-anomers (~98%).

### 2.3.2 Aqueous RAFT homopolymerization of glycomonomers

Monomer conversion was monitored via $^{1}H$ NMR spectroscopy by comparing the relative integral areas of the vinyl proton peak of the glycomonomers (5.73 ppm, 1H) with the aromatic proton peak of benzenesulfonic acid (7.77 ppm, 2H), the internal standard used in the reactions. A linear increase of $\ln([M]_0/[M])$ as a function of time is observed for the polymerization reactions (Figure 2.1), where $[M]_0$ is the initial molar concentration of the deprotected glycomonomer (GlcEAm or GalEAm) and [M] is the molar concentration of the monomer at any given time point, indicating pseudo first order kinetics.

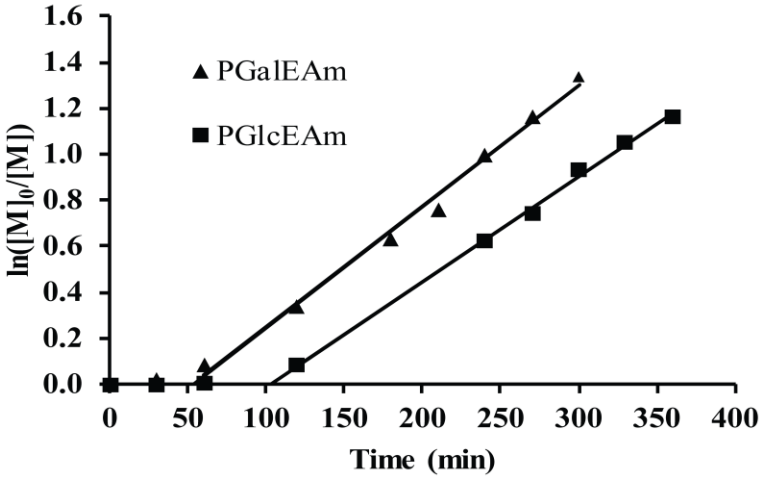


Figure 2.1 Plots of $\ln([M]_0/[M])$ vs reaction time for the aqueous RAFT polymerization of glycomonomers (GalEAm and GlcEAm) at 70 ºC using CEP as chain transfer agent indicating pseudo first order polymerization kinetics.

The aRAFT polymerization of PGalEAm exhibits an initialization period of 50 min while that of PGlcEAm is 100 min. Similar initialization periods in aqueous RAFT polymerizations have been reported previously by our team, including Alidedeoglu et al.[28] for 2-aminoethyl methacrylate monomers and McCormick et al.[32] for acrylamido monomers. McLeary et al.[34] investigated the initialization period observed in the RAFT polymerization of styrene with the chain transfer agent cyanoisopropyl dithiobenzoate via

in situ $^{1}$H NMR. It was found that the time taken by the chain transfer agents to react with a single monomer unit is the reason for the observed delay of polymerization. Chain growth did not start until all of the CTAs were consumed. This observation was attributed to the much faster propagation rate of the CTA radicals than the radicals of the propagating chains containing a single monomer unit.[34] Monomer conversions of ~7% and ~70% were achieved in 60 min and 270 min respectively for the GalEAm reaction, whereas it took 120 min and 360 min to achieve the same conversions for the GlcEAm reaction. The longer inhibition time for GlcEAm may be the result of stabilization of the macro CTA through hydrogen bonding with the pendant group, which occurs to a greater extent with the glucose derivative than with the galactose.

Aliquots were taken from the reaction mixture at 30 minute intervals, and the monomer conversion was calculated via $^{1}$H NMR spectroscopy. The theoretical number average molecular weight ($M_{nth}$) was calculated from $^{1}$H NMR spectroscopy according to equation 1, where ρ is the fractional monomer conversion, $MW_{mon}$ is the molecular weight of the monomer, $[M]_0$ is the initial concentration of monomer, $[CTA]_0$ is the initial concentration of the chain transfer agent, and $MW_{CTA}$ is the molecular weight of the chain transfer agent.[31] The degree of polymerization was calculated from the $M_{nth}$ using equation 2.

$$M_{\mathrm{nth}} = (\rho \mathrm{MW}_{\mathrm{mon}}[M]_0/[\mathrm{CTA}]_0) + \mathrm{MW}_{\mathrm{CTA}} \quad (1)$$

$$DP_{th} = (M_{nth} - MW_{CTA})/MW_{mon} \quad (2)$$

The monomer conversion, molecular weight, and degree of polymerization data are summarized in Table 2.1.

Table 2.1 Conversion and molecular weight data for glycopolymers and PDMA as determined via NMR and GPC.

| Sample | Target DP | % Conversion | $DP_{th}$ | $M_{nth}$ (g/mol) | $M_{n(GPC)}$[a] (g/mol) | $M_w/M_n$[b] |
|---|---|---|---|---|---|---|
| PGalEAm35 | 35 | 8.4 | 42 | 11800 | 2740 | 1.13 |
| PGalEAm350 | 350 | 69 | 344 | 95500 | 39100 | 3.82 |
| PGlcEAm35 | 35 | 7.8 | 39 | 11000 | 4640 | 1.16 |
| PGlcEAm350 | 350 | 69 | 344 | 95500 | 39600 | 3.82 |
| PDMA35 | 35 | 7.9 | 40 | 4220 | 3760 | 1.17 |
| PDMA350 | 350 | 69 | 346 | 34500 | 32800 | 1.24 |

[a]Relative to PEO standards, [b]As determined by GPC (aqueous solution, 0.1 M $NaNO_3$ and 0.01% (w/v) $NaN_{3)}$.

Figure 2.2 shows GPC traces for the four glycopolymers. The low molecular weight glycopolymers exhibit narrow unimodal peaks and low dispersities (PGalEAm35 $Đ_M$ = 1.13 and PGlcEAm35 $Đ_M$ = 1.16), while the high molecular weight glycopolymers show broad peaks with extended shoulders at shorter retention times. The peak broadening is attributed to aggregation, which is observed only for the high molecular weight glycopolymers. Similar association was reported by Liang et al.[35] for poly[2-(β-D-glucosyloxy)ethyl acrylate in water. They reported the critical aggregation concentration (cac) to be inversely related to the glycopolymer molecular weight. They

noted that while the side chains are highly hydrophilic, the backbone is hydrophobic, and fluorescence studies indicated that the interior of the aggregates was hydrophobic. Thus, aggregation may be attributed in part to hydrophobic interactions. Other reports have attributed polysaccharide aggregation to intermolecular hydrogen bonding.[36, 37] It is likely that similar associations occur in our glycopolymers. Note that in Table 2.1, both theoretical $M_n$ ($M_{nth}$, determined by NMR) and relative $M_n$ (determined by GPC) are reported. The relative $M_n$ was calculated with respect to PEO standards, and these values are lower by a factor of approximately 2.4 in comparison to those calculated from the NMR monomer conversion data. Molecular weight trends are similar for the two sets of data, and both show a factor of ten increase in molecular weight for the high DP glycopolymers.

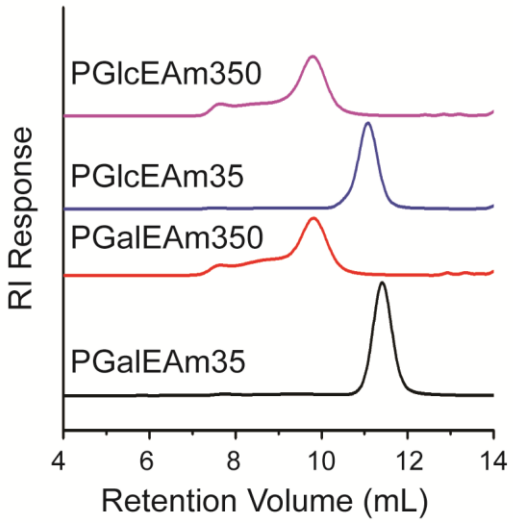


Figure 2.2 GPC traces for PGalEAm35, PGalEAm350, PGlcEAm35, and PGlcEAm350. Low molecular weight polymers yield narrow dispersities, while high molecular weight systems show apparent aggregation.

### 2.3.3 RAFT polymerization of N, N′-dimethyl acrylamide

To clearly establish the effects of the backbone structure and saccharide moieties of a glycopolymer on Aβ aggregation, polymers having similar backbone structures without saccharide units were synthesized. Poly(N,N-dimethyl acrylamide) (PDMA) with controlled molecular weights (~35DP and ~350DP) and low dispersities were synthesized for the Aβ aggregation studies and utilized separately from the glycopolymers. GPC and NMR data are shown in Table 1, and the dispersities are 1.17 and 1.24 for PDMA35 and PDMA350, respectively. (GPC traces, Supporting information, Appendix A, Figure A.12)

### 2.3.4 Investigation of Aβ42 aggregation in the presence of glycopolymers

The effects of saccharide pendant group and molecular weight on Aβ aggregation were determined using ThT fluorescence by monitoring solutions of glycopolymers and the PDMA standard co-incubated with Aβ42 monomer. ThT is a fluorescent dye which preferentially binds to β-sheet rich amyloid aggregates, yielding an increase in fluorescence intensity.[38, 39] Three-fold molar excess (75 μM) of polymer was incubated with Aβ (25 μM) in 20 mM Tris at pH 8.0 with 0.1 M $NaNO_3$ and 0.01% $NaN_3$. Samples were kept at 37 °C and ThT fluorescence was measured periodically (Figure 2.3. A-C). Aβ in the absence of polymer displays a short lag phase (2 h) before association (growth phase) and saturation as fibrils at 24 h of incubation (where plateau is reached) (Figure 2.3. A, ■). Aβ in the presence of PDMA alone (negative control) shows a small decrease in aggregation rate (increase in the lag phase), however the saturation level is reached at 48 h (within standard experimental error) for solutions of both molecular weight polymers (Figure 2.3. A, ○ and ▲). Samples containing PGalEAm show a marginally

decreased aggregation rate in comparison to the Aβ control, particularly for the low molecular weight polymer, but the plateau region is reached at 72 h. (Figure 2.3. B, ○ and ▲). For the PGlcEAm35 solution, Aβ aggregation rate is initially reduced (Figure 2.3. C, ○), but saturation occurs at similar intensities within 36 hours. This suggests that the Aβ aggregation rate is influenced by the polymers PDMA, PGalEAm, and PGlcEAm35, but these polymers do not influence the final product of Aβ aggregation (fibrils). Fung et al.[16] reported a decrease of lag phase of Aβ42 aggregation in the presence of glucose and galactose monosaccharides, whereas Rajaram et al.[40] reported a concentration dependent increase in lag phase for Aβ40 aggregation in the presence of glycoclusters made of six units of either glucose or galactose. We observed a minor decrease in lag phase for Aβ42 aggregation in the presence of PDMA, PGalEAm and PGlcEAm35 (Figure 2.3 A, B, and C).

Aβ aggregation in the presence of PGlcEAm350, however, displays a very distinct aggregation profile (Figure 2.3. C, ▲). The ThT intensity rapidly increases and plateaus within the first three hours of incubation (Figure 2.3. D, ▲). The decreased fluorescence intensity as compared to other samples indicates that the size of the aggregates and/or the structure of the aggregates is different from that of the other samples. This unique aggregation profile suggests that Aβ rapidly forms smaller oligomers, but not fibrils, in the presence of PGlcEAm350. The initial rapid increase in fluorescence intensity can be attributed to the fast nucleation of Aβ in presence of PGlcEAm350 and formation of a large number of nucleation seeds at the beginning of the interaction. Because the number of nucleation sites is higher, the number of Aβ per site is low and thus small aggregates are formed.

Fung et al. reported the formation of small aggregates of Aβ in the presence of glucose while galactose promoted mature fibril formation.[16] Glycoclusters of glucose and galactose have been reported to promote the formation of fibrils of Aβ40.[40] In contrast, our ThT experiments showed that the low molecular weight glucose containing glycopolymer, PGlcEAm35, promotes Aβ fibril formation whereas the high molecular weight PGlcEAM350 promotes formation of small aggregates (oligomers) (Figure 2.3 C). Both low (PGalEAm35) and high (PGalEAm350) molecular weight galactose containing polymers promote formation of Aβ fibrils (Figure 2.3 B).

To determine if this was indeed the case, polyacrylamide gel electrophoresis (PAGE) in conjunction with immunoblotting was utilized. Samples were electrophoresed under denaturing conditions (sodium dodecyl sulphate, SDS-PAGE) at 6 h and 72 h of incubation (Figure 2.3. E). At 6h of incubation, all samples contained a band at 4.5 kDa corresponding to monomeric Aβ as well as a low molecular weight (LMW) oligomeric species (~15 kDa). High molecular weight (HMW) fibrils, which do not enter the gel, were observed in all samples with the exception of Aβ incubated with PGlcEAm350. The same analysis at 72 h revealed a small amount of Aβ monomers along with a significant concentration of HMW soluble oligomers, which is likely due to dissociation of the insoluble fibrils in denaturing conditions. However, no insoluble fibrils were observed for Aβ incubated with PGlcEAm350, and the monomer content appears to be larger than in other samples. Together with the ThT data, this analysis confirms that PDMA, PGalEAm, and PGlcEAm35 polymers marginally affect the rate in which Aβ aggregation occurs, but the polymers do not affect the formation of the final product of fibrils. However, Aβ in the presence of PGlcEAm350 differs from the others in that oligomeric species are

formed. To gain better perspective of this, non-denaturing (native) PAGE was employed at both 6 h and 72 h of incubation (Figure 2.3 F). It is important to note that the MW makers used for SDS-PAGE in panel E do not correspond to panel F, as these samples were electrophoresed under native conditions, and therefore size estimations cannot be determined. Regardless, similar to that observed in the denaturing gel, all samples contained monomeric Aβ which had not undergone aggregation. Also, HMW fibrils were observed in all samples, except Aβ with PGlcEAm350, which exclusively formed an intermediate soluble oligomer. By 72 h of incubation, all samples (except Aβ incubated with PGlcEAm350) formed HMW fibrils with no discernible monomers or oligomers. However, the Aβ incubated with PGlcEAm350 displayed disperse soluble oligomer formation, with minimal fibril formation. From this data, it is clear that the HMW glucose containing glycopolymers show distinctly different behaviour from that of other glycopolymers towards Aβ aggregation. This specific interaction produces soluble oligomers, which are reported to be the primary cause of toxicity in AD.

The difference in Aβ aggregation behaviour in the presence of glycopolymers of different structures can be related to H-bonding patterns.[16, 41] Glucose forms stronger H-bonds with Aβ whereas galactose forms weaker bonds.[16] Because the bonding between PGalEAm and Aβ is weak, more H-bonding sites are available within Aβ, which promotes self-association of Aβ and ultimately produces mature fibrils.[16] Glucose has been reported to promote formation of oligomers of Aβ by forming stronger H-bonds with Aβ.[16] These strong H-bonds lead to formation of more nucleating seeds and fewer H-bonding sites available within Aβ. From our ThT and PAGE experiments, it is clear

that glucose-containing glycopolymers with two different molecular weights, low and high, behave differently towards Aβ aggregation. Aβ forms fibrils in the presence of PGlcEAm35 whereas it forms small aggregates or oligomers in the presence of PGlcEAm350. This suggests that H-bonding alone is not sufficient to significantly change the aggregation behavior of Aβ, and there is a concentration dependence of the glucose units (clustering effect).

It has been reported that saccharide clusters exhibit stronger H-bonding tendencies than their monosaccharide counterparts.[42, 43] We believe that the glucose units in the high molecular weight PGlcEAm350 form intramolecular/intermolecular clusters due to the presence of the large number of glucose units in close proximity, as reported for similar systems by others.[35-37] The concentration of saccharide pendant groups is ten-fold lower in the solutions of low molecular weight PGlcEAm35, and as reported in reference Liang et al.,[35] critical aggregation concentration (cac) is inversely related to molecular weight. Thus, cluster formation is not observed in the low molecular weight system because of the lower concentration of saccharide units and lower H-bonding propensity. It is possible, therefore, that stronger H-bonding due to the clustering glucose is responsible for oligomer formation by Aβ in the presence of PGlcEAm350.

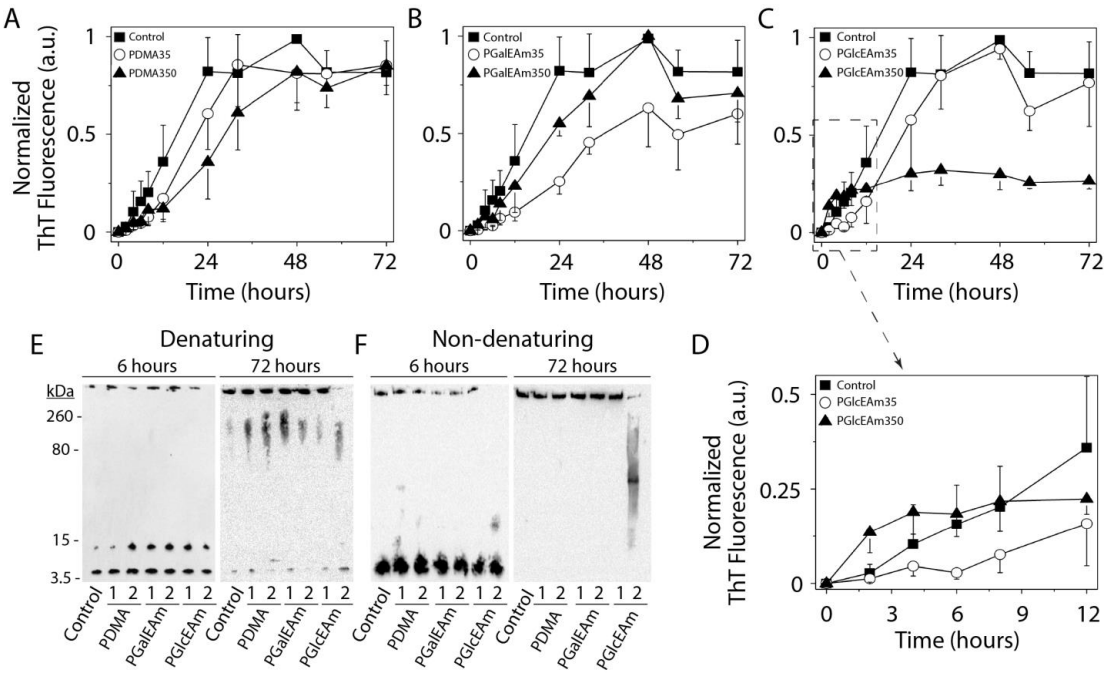


Figure 2.3 Glycopolymer-Aβ aggregation studies using ThT-fluorescent (A), (B), (C), and (D). Polyacrylamide gel electrophoresis in denaturing condition (E) and in non-denaturing condition (F). Control sample refers to Aβ alone without any polymer. In the images (E) and (F), 1 stands for polymer with a DP of 35 and 2 stands for DP of 350. PGlcEAm350 promotes formation of oligomers with minimal fibril production.

## 2.4 Conclusions

Acrylamide based glycopolymers with β-D-glucose and β-D-galactose pendant moieties were synthesized to high (DP 350) and low (DP 35) molecular weights via aqueous RAFT polymerization for determination of the effects of saccharide structure and concentration on Aβ aggregation. Dimethylacrylamide with no pendant saccharide was polymerized to similar molecular weights as a negative control. The high molecular weight glucose containing glycopolymers exhibited a large effect on the Aβ aggregation process, inducing the formation of toxic soluble oligomers while limiting fibril formation. The other glycopolymers and PDMA caused a minor reduction in the rate of Aβ aggregation but had no effect on the ultimate extent of fibril formation. The unusual Aβ

aggregation behaviour in the presence of the high molecular weight glucose containing polymers may be the result of hydrogen bonding of Aβ with the glucose pendant groups and the polysaccharide cluster effect, which does not occur with the low molecular weight polymer because of its reduced concentration of saccharide. These model systems provide information about the behaviour of Aβ in the presence of polysaccharides, and more importantly, demonstrate the specificity in generating low molecular weight, toxic oligomers. The report also demonstrates the potential of utilizing glycopolymer systems of controlled composition and molecular weight in determining the mechanisms of toxic oligomer and fibril formation.

## 2.5 Acknowledgements

ThT and PAGE experiments were performed by Dr. Dexter Dean under the supervision of Dr. Vijayaraghavan Rangachari of the University of Southern Mississippi. GPC was performed by Dr. Fei Liu and Dr. V. Kozlovskaya of the University of Alabama at Birmingham.

## 2.6 References

(1) Matsuzaki, K. How Do Membranes Initiate Alzheimer's Disease? Formation of Toxic Amyloid Fibrils by the Amyloid β-Protein on Ganglioside Clusters. Accounts of Chemical Research, **2014**, *47*(8), 2397-2404.

(2) Matsuzaki, K.; Kato, K.; Yanagisawa, K. Aβ polymerization through interaction with membrane gangliosides. Biochimica et Biophysica Acta (BBA) - Molecular and Cell Biology of Lipids, **2010**, *1801*(8), 868-877.

(3) Matsuzaki, K.; Kato, K.; Yanagisawa, K. Aβ polymerization through interaction with membrane gangliosides. Biochim. Biophys. Acta, Mol. Cell. Biol. Lipids, **2010**, *1801*(8), 868-877.

(4) Yanagisawa, K. Role of gangliosides in Alzheimer's disease. Biochimica et Biophysica Acta (BBA) - Biomembranes, **2007**, *1768*(8), 1943-1951.

(5) McLaurin, J.; Franklin, T.; Fraser, P. E.; Chakrabartty, A. Structural transitions associated with the interaction of Alzheimer beta-amyloid peptides with gangliosides. J Biol Chem, **1998**, *273*(8), 4506-15.

(6) Ariga, T.; Kobayashi, K.; Hasegawa, A.; Kiso, M.; Ishida, H.; Miyatake, T. Characterization of high-affinity binding between gangliosides and amyloid beta-protein. Arch Biochem Biophys, **2001**, *388*(2), 225-30.

(7) Cebecauer, M.; Hof, M.; Amaro, M. Impact of GM1 on Membrane-mediated Aggregation/Oligomerization of β-amyloid: Unifying View. Biophys. J., **DOI: 10.1016/j.bpj.2017.03.009**.

(8) Bourgault, S.; Solomon, J. P.; Reixach, N.; Kelly, J. W. Sulfated Glycosaminoglycans Accelerate Transthyretin Amyloidogenesis by Quaternary Structural Conversion. Biochemistry, **2011**, *50*(6), 1001-1015.

(9) Anoop, A.; Ranganathan, S.; Dhaked, B. D.; Jha, N. N.; Pratihar, S.; Ghosh, S.; Sahay, S.; Kumar, S.; Das, S.; Kombrabail, M.; Agarwal, K.; Jacob, R. S.; Singru, P.; Bhaumik, P.; Padinhateeri, R.; Kumar, A.; Maji, S. K. Elucidating the Role of Disulfide Bond on Amyloid Formation and Fibril Reversibility of Somatostatin-14: RELEVANCE TO ITS STORAGE AND SECRETION. Journal of Biological Chemistry, **2014**, *289*(24), 16884-16903.

(10) Stewart, K. L.; Hughes, E.; Yates, E. A.; Akien, G. R.; Huang, T.-Y.; Lima, M. A.; Rudd, T. R.; Guerrini, M.; Hung, S.-C.; Radford, S. E.; Middleton, D. A. Atomic Details of the Interactions of Glycosaminoglycans with Amyloid-β Fibrils. Journal of the American Chemical Society, **2016**, *138*(27), 8328-8331.

(11) Takase, H.; Tanaka, M.; Yamamoto, A.; Watanabe, S.; Takahashi, S.; Nadanaka, S.; Kitagawa, H.; Yamada, T.; Mukai, T. Structural requirements of glycosaminoglycans for facilitating amyloid fibril formation of human serum amyloid A. Amyloid : the international journal of experimental and clinical investigation : the official journal of the International Society of Amyloidosis, **2016**, *23*(2), 67-75.

(12) Maji, S. K.; Perrin, M. H.; Sawaya, M. R.; Jessberger, S.; Vadodaria, K.; Rissman, R. A.; Singru, P. S.; Nilsson, K. P.; Simon, R.; Schubert, D.; Eisenberg, D.; Rivier, J.; Sawchenko, P.; Vale, W.; Riek, R. Functional amyloids as natural storage of peptide hormones in pituitary secretory granules. Science, **2009**, *325*(5938), 328-32.

(13) Quittot, N.; Sebastiao, M.; Bourgault, S. Modulation of amyloid assembly by glycosaminoglycans: from mechanism to biological significance. Biochemistry and cell biology = Biochimie et biologie cellulaire, **2017**.

(14) Bazar, E.; Jelinek, R. Divergent heparin-induced fibrillation pathways of a prion amyloidogenic determinant. Chembiochem, **2010**, *11*(14), 1997-2002.

(15) Jha, S.; Patil, S. M.; Gibson, J.; Nelson, C. E.; Alder, N. N.; Alexandrescu, A. T. Mechanism of Amylin Fibrillization Enhancement by Heparin. Journal of Biological Chemistry, **2011**, *286*(26), 22894-22904.

(16) Fung, J.; Darabie, A. A.; McLaurin, J. Contribution of simple saccharides to the stabilization of amyloid structure. Biochemical and Biophysical Research Communications, **2005**, *328*(4), 1067-1072.

(17) Lindhorst, T. (2002). Artificial Multivalent Sugar Ligands to Understand and Manipulate Carbohydrate-Protein Interactions. Host-Guest Chemistry. S. Penadés, Springer Berlin Heidelberg. **218:** 201-235.

(18) Lundquist, J. J.; Toone, E. J. The cluster glycoside effect. Chem Rev, **2002**, *102*(2), 555-78.

(19) Mammen, M.; Choi, S.-K.; Whitesides, G. M. Polyvalent Interactions in Biological Systems: Implications for Design and Use of Multivalent Ligands and Inhibitors. Angewandte Chemie International Edition, **1998**, *37*(20), 2754-2794.

(20) Matsumoto, E.; Yamauchi, T.; Fukuda, T.; Miura, Y. Sugar microarray via click chemistry: molecular recognition with lectins and amyloid β (1–42). Science and Technology of Advanced Materials, **2009**, *10*(3), 034605.

(21) Yu, K.; Kizhakkedathu, J. N. Synthesis of Functional Polymer Brushes Containing Carbohydrate Residues in the Pyranose Form and Their Specific and Nonspecific Interactions with Proteins. Biomacromolecules, **2010**, *11*(11), 3073-3085.

(22) Ladmiral, V.; Melia, E.; Haddleton, D. M. Synthetic glycopolymers: an overview. European Polymer Journal, **2004**, *40*(3), 431-449.

(23) Das, P. K.; Dean, D. N.; Fogel, A. L.; Liu, F.; Abel, B. A.; McCormick, C. L.; Kharlampieva, E.; Rangachari, V.; Morgan, S. E. Aqueous RAFT Synthesis of Glycopolymers for Determination of Saccharide Structure and Concentration Effects on Amyloid β Aggregation. Biomacromolecules, **2017**, *18*(10), 3359-3366.

(24) Convertine, A. J.; Benoit, D. S. W.; Duvall, C. L.; Hoffman, A. S.; Stayton, P. S. Development of a novel endosomolytic diblock copolymer for siRNA delivery. Journal of Controlled Release, **2009**, *133*(3), 221-229.

(25) Le, T. P.; Moad, G.; Rizzardo, E.; Thang, S. H. (May11, 2010). Polymerization with living characteristics, US7714075 B1.

(26) Kumar, A.; Paslay, L. C.; Lyons, D.; Morgan, S. E.; Correia, J. J.; Rangachari, V. Specific Soluble Oligomers of Amyloid-β Peptide Undergo Replication and Form Non-fibrillar Aggregates in Interfacial Environments. J. Biol. Chem., **2012**, *287*(25), 21253-21264.

(27) Ambrosi, M.; Batsanov, A. S.; Cameron, N. R.; Davis, B. G.; Howard, J. A. K.; Hunter, R. Influence of preparation procedure on polymer composition: synthesis and characterisation of polymethacrylates bearing [small beta]-D-glucopyranoside and [small beta]-D-galactopyranoside residues. Journal of the Chemical Society, Perkin Transactions 1, **2002**, (1), 45-52.

(28) Alidedeoglu, A. H.; York, A. W.; McCormick, C. L.; Morgan, S. E. Aqueous RAFT polymerization of 2-aminoethyl methacrylate to produce well-defined, primary amine functional homo- and copolymers. Journal of Polymer Science Part A: Polymer Chemistry, **2009**, *47*(20), 5405-5415.

(29) Lowe, A. B.; Sumerlin, B. S.; McCormick, C. L. The direct polymerization of 2-methacryloxyethyl glucoside via aqueous reversible addition-fragmentation chain transfer (RAFT) polymerization. Polymer, **2003**, *44*(22), 6761-6765.

(30) Bernard, J.; Hao, X.; Davis, T. P.; Barner-Kowollik, C.; Stenzel, M. H. Synthesis of Various Glycopolymer Architectures via RAFT Polymerization: From Block Copolymers to Stars. Biomacromolecules, **2006**, *7*(1), 232-238.

(31) Abel, B. A.; Sims, M. B.; McCormick, C. L. Tunable pH- and CO2-Responsive Sulfonamide-Containing Polymers by RAFT Polymerization. Macromolecules, **2015**, *48*(16), 5487-5495.

(32) McCormick, C. L.; Lowe, A. B. Aqueous RAFT Polymerization: Recent Developments in Synthesis of Functional Water-Soluble (Co)polymers with Controlled Structures. Accounts of Chemical Research, **2004**, *37*(5), 312-325.

(33) Gruber, H.; Knaus, S. Synthetic polymers based on carbohydrates: preparation, properties and applications. Macromolecular Symposia, **2000**, *152*(1), 95-105.

(34) McLeary, J. B.; Calitz, F. M.; McKenzie, J. M.; Tonge, M. P.; Sanderson, R. D.; Klumperman, B. Beyond Inhibition: A 1H NMR Investigation of the Early Kinetics of RAFT-Mediated Polymerization with the Same Initiating and Leaving Groups. Macromolecules, **2004**, *37*(7), 2383-2394.

(35) Liang, Y.-Z.; Li, Z.-C.; Li, F.-M. Self-Association of Poly[2-(β-D-glucosyloxy)ethyl Acrylate] in Water. Journal of Colloid and Interface Science, **2000**, *224*(1), 84-90.

(36) Balasubramanian, D.; Raman, B.; Sundari, C. S. Polysaccharides as amphiphiles. Journal of the American Chemical Society, **1993**, *115*(1), 74-77.

(37) Winnik, F. M. Association of hydrophobic polymers in water: fluorescence studies with labeled (hydroxypropyl)celluloses. Macromolecules, **1989**, *22*(2), 734-742.

(38) LeVine, H., 3rd. Thioflavine T interaction with synthetic Alzheimer's disease beta-amyloid peptides: detection of amyloid aggregation in solution. Protein Sci, **1993**, *2*(3), 404-10.

(39) Lindberg, D. J.; Wranne, M. S.; Gilbert Gatty, M.; Westerlund, F.; Esbjörner, E. K. Steady-state and time-resolved Thioflavin-T fluorescence can report on morphological differences in amyloid fibrils formed by Aβ(1-40) and Aβ(1-42). Biochemical and Biophysical Research Communications, **2015**, *458*(2), 418-423.

(40) Rajaram, H.; Palanivelu, M. K.; Arumugam, T. V.; Rao, V. M.; Shaw, P. N.; McGeary, R. P.; Ross, B. P. 'Click' assembly of glycoclusters and discovery of a trehalose analogue that retards Abeta40 aggregation and inhibits Abeta40-induced neurotoxicity. Bioorganic & medicinal chemistry letters, **2014**, *24*(18), 4523-8.

(41) Allison, S. D.; Chang, B.; Randolph, T. W.; Carpenter, J. F. Hydrogen Bonding between Sugar and Protein Is Responsible for Inhibition of Dehydration-Induced Protein Unfolding. Archives of Biochemistry and Biophysics, **1999**, *365*(2), 289-298.

(42) Hayashida, O.; Mizuki, K.; Akagi, K.; Matsuo, A.; Kanamori, T.; Nakai, T.; Sando, S.; Aoyama, Y. Macrocyclic Glycoclusters. Self-Aggregation and Phosphate-Induced Agglutination Behaviors of Calix[4]resorcarene-Based Quadruple-Chain Amphiphiles with a Huge Oligosaccharide Pool. Journal of the American Chemical Society, **2003**, *125*(2), 594-601.

(43) Aoyama, Y. Macrocyclic Glycoclusters: From Amphiphiles through Nanoparticles to Glycoviruses. Chemistry – A European Journal, **2004**, *10*(3), 588-593.

# CHAPTER III - MODEL GLYCOPOLYMER BRUSH: LONG CHAIN BRUSH SYNTHESIS VIA PHOTOPOLYMERIZATION AND BRUSH CHARACTERIZATION

## 3.1 Introduction

We have reported that high molecular weight glucose containing glycopolymers in aqueous solution induced the formation of smaller aggregates or oligomers of Aβ, whereas galactose containing polymers of similar molecular weight promoted fibril formation.[1] The kinetics of Aβ aggregation was also found to be significantly different for the two systems.[1] As mentioned in Chapter I, gangliosides in their natural environment are embedded in phospholipid cell membranes via their ceramide tail.[2] These phospholipid membranes are semi-solid in nature, more like a liquid cooking oil than a solid shortening.[3] Therefore, due to their attachment within the membranes, the movement of the gangliosides and hence the movement of the saccharides of gangliosides is restricted.[4] It has been reported that the morphology and the toxicity of the peptide aggregates depends on the aggregation conditions, such as bulk solution versus surface or the physiological condition of the interface.[5-10] Therefore, evaluation of a surface-immobilized glycopolymer model was necessary for an improved understanding of the effect of the saccharides of gangliosides on Aβ aggregation.

There are two general ways to immobilize polymer chains on a surface: self-assembled monolayer (SAM) formation, and covalent attachment. The SAM is a relatively simple and straightforward process. However, due to the weak interactions between the polymers and the surface, thermal and solvolytic instabilities might occur.[11] This drawback can be avoided by tethering polymers via covalent attachment.

There are several routes by which covalently attached glycopolymers can be synthesized on a surface, and Figure 3.1 shows some of the common routes.

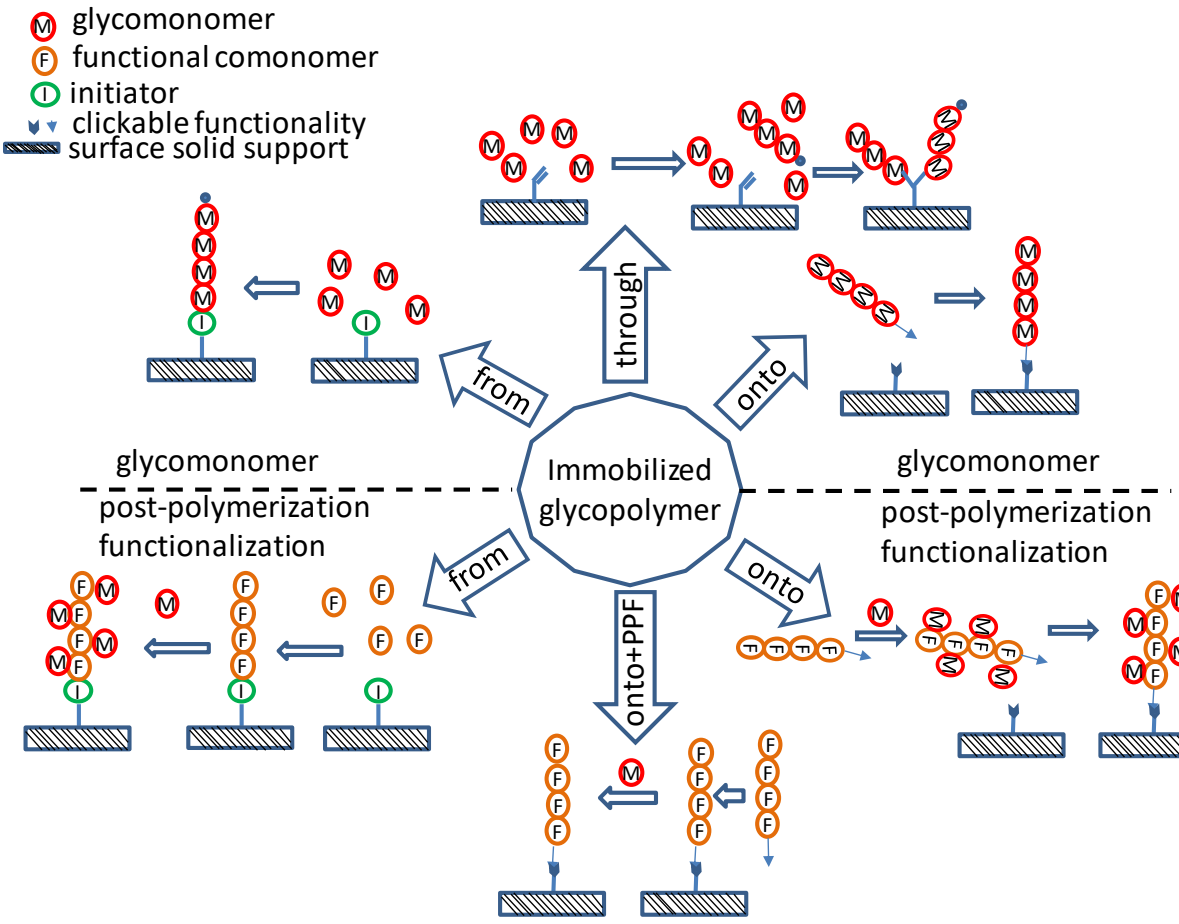


Figure 3.1 Schematic overview of different techniques for glycopolymer immobilization on a surface. Adapted from Ehe et al[12].

Surface polymerization can be achieved through grafting-from, grafting-to/onto, or grafting-through techniques.[13] The grafting-to and grafting-through methods involve the attachment of large prefabricated glycopolymers to a surface.[14] These techniques generally result in a low graft density due to the steric hindrance of the bulky saccharide side groups.[13] The 'grafting from' method involves the growth of the glycopolymers from

a surface.[15] In this technique, polymer formation is less sterically hindered because monomers gradually add to the growing chains.[16]

Pfaff et al.[17] reported synthesis of galactose and mannose containing glycopolymers grafted on poly(divinylbenzene) via grafting from, grafting-to, and grafting through techniques and found that the grafting from approach yielded much higher grafting density (0.35 chains/nm$^2$) than the grafting-to (0.20 chains/nm$^2$) or grafting-through (0.22 chains/nm$^2$) techniques.[17] Because the grafting-from technique produces brushes with high graft density, it is generally preferred.[12, 14, 16]

Active sites for polymerization can be created directly on the appropriate surfaces by plasma[18] or UV irradiation or a photo or thermal initiator can be immobilized on surfaces and then activated by applying heat,[19] UV irradiation,[20] or microwave energy.[21] Controlled radical polymerizations, such as atom transfer radical polymerization (ATRP)[13, 14, 22-24] or reversible addition chain transfer (RAFT) polymerization[25-28] have been widely used due to the controlled nature of the polymerization which allows production of brushes with targeted molecular weight and low dispersity. However, controlled radical polymerization techniques are highly sensitive to reaction conditions and have slow reaction rates.[29, 30] In contrast, conventional or uncontrolled free radical polymerization has the advantages of robust reaction conditions, faster reaction rates, and suitability for a wide range of vinyl monomers.[29, 31, 32] While precise control over the thickness or the molecular weight of the brush cannot be achieved via conventional free radical polymerization,[12] we utilized this method to synthesize glycopolymer brushes of high grafting density and high thickness from silicon wafers and silicon dioxide coated quartz crystal surfaces.

Conventional free radical polymerization for the synthesis of glycopolymer brushes can be initiated by plasma, heat (thermal), or UV irradiation.[12, 18, 19, 33, 34] Deng et al. synthesized a poly(α-allyl glucoside) brush on a hollow microfiltration membrane of polypropylene (PP) by plasma-induced free radical polymerization.[18] In this case, a PP membrane was dipped in the monomer solution for a certain time and then the solvent was evaporated under reduced pressure, followed by plasma irradiation to yield a bulk polymer layer on the membrane surface.[18] Guo et al[19] synthesized lactose-containing glycopolymers on a silica gel surface using AIBN as the initiator. Ulbricht and co-workers grafted poly(2-lactobionamidoethyl methacrylate)[34] and poly(D-gluconamidoethyl methacrylate) [33] on a polypropylene (PP) microfiltration membrane surface by UV-induced graft copolymerization. Here, the photo-initiator benzophenone (BP) was entrapped into the PP membrane by immersing the membrane in the initiator solution.[33, 34] The grafting density of the brushes was controlled by varying the monomer concentration, UV irradiation time, or photo-initiator concentration.[18, 34]

We synthesized glycopolymer brushes of high grafting density and a target thickness of 90 nm which corresponds to a target theoretical degree of polymerization (DP) of 350 via a surface-initiated free radical UV photopolymerization technique (DP calculation : Appendix B, Supporting information for chapter III). The DP of 350 was chosen for comparison with our solution experiments involving glycopolymers of DP 350 described in Chapter II. We hypothesized that the brushes with high grafting density and higher thickness would have more pendant saccharide groups available for interactions with the Aβ. For an effective polymer-Aβ interaction, the concentration of the saccharides and peptide Aβ needs to be higher than a threshold value.[35, 36]

The glycopolymer brushes were fully characterized and then utilized for in vitro Aβ interaction studies utilizing QCM-D and AFM techniques (described in Chapter IV).

## 3.2 Materials and methods

### 3.2.1 Materials

Irgacure 2959 (2-hydroxy-1-[4-(2-hydroxyethoxy) phenyl]-2-methyl-1-propanone) was obtained from Ciba Speciality Chemicals. All other reagents and solvents used in this research were obtained from Sigma-Aldrich Corporation (USA) or ThermoFisher Scientific (USA) in their highest purity available and were used without further purification unless otherwise stated. Silicon wafers and $SiO_2$ coated crystals (QSX 303) were obtained from Sigma Aldrich (USA) and Biolin Scientific AB (Sweden), respectively. The acrylamide-based stereospecific glucose and galactose containing glycomonomers, GlcEAm, and GalEAm respectively, were synthesized and characterized by following the procedures described in Chapter II.

### 3.2.2 Characterization

Nuclear magnetic resonance (NMR) spectroscopy was performed with a Varian MercuryPLUS (300 MHz) spectrometer by taking an average of 128 scans (delay 5 s) using appropriate solvents ($CDCl_3$ or $D_2O$).

Grazing angle total reflection-Fourier transform infrared (GATR-FTIR) spectra of surface grafted polymers were collected via a Nicolet 8700 FTIR spectrometer (Thermo Scientific) attached with a VariGATR grazing angle ATR accessory (Harrick Scientific) using OMNIC software. A bare silicon wafer was used as the background. Spectra were taken with a resolution of 4 $cm^{-1}$ by accumulating a minimum of 100 scans per run.

Nitrogen was constantly purged through the attachment to reduce interference of carbon dioxide and water.

Water contact angles on the surfaces of the unmodified and modified wafers and $SiO_2$ coated quartz crystals were measured after each step during the initiator immobilization and the glycopolymer synthesis. The contact angle was measured by a Rame-Hart 200-00 Std. Tilting B goniometer. A 6 μL water droplet was dropped onto the surface and the average of three measurements is reported.

Ellipsometric measurements were carried out using a Gaertner Scientific Corporation LSE Stokes ellipsometer with a 632.8 nm laser at 70° incident angle. Refractive indices of 3.85 were used for wafers and silicon dioxide coated quartz surfaces and 1.46 were used for initiator and glycopolymer films.

Atomic force microscopy (AFM) imaging was performed with a Dimension Icon (Bruker) instrument in tapping mode. Silicon nitride probes (RTESP from Bruker) with a typical resonance frequency of 324-358 kHz, spring constant of 20-80 N/m, length of 115-135 μm, and tip radius of 8 nm were utilized for the imaging. The AFM images were captured at a scan rate of 1 Hz and 256 X 256 pixels of data points were collected. Images were taken at different locations (at least three) across the surface. Nanoscope 5.30r2 software was used to capture the images, and then the images were flattened for 3$^{rd}$ order fit and analyzed via NanoScope Analysis 1.5 (Bruker) image processing software.

### 3.2.3 Synthesis of glycopolymer brushes on silica surfaces

Glycopolymer brushes on silicon wafers and silicon dioxide coated quartz crystals were synthesized via a two-stage process: first, modification and immobilization of a UV

photoinitiator on the silica surfaces and then glycopolymer synthesis from the initiator-modified surfaces.

### 3.2.4 Initiator modification

The photoinitiator, 2-hydroxy-1-[4-(2-hydroxyethoxy) phenyl]-2-methyl-1-propanone) [Irgacure 2959], was modified to protect the photo-active hydroxyl group and to introduce an anchoring trichlorosilane group which can covalently bind with a silanol-functional surface. Initiator modification was performed by following the procedure reported by Hensarling et al.[37] Scheme 3.2. shows the reaction scheme followed for the initiator modification reactions. Products obtained in each step were characterized and confirmed via $^{1}$H NMR Spectroscopy [Supporting information, Appendix B, Figure B.1 and B.2].

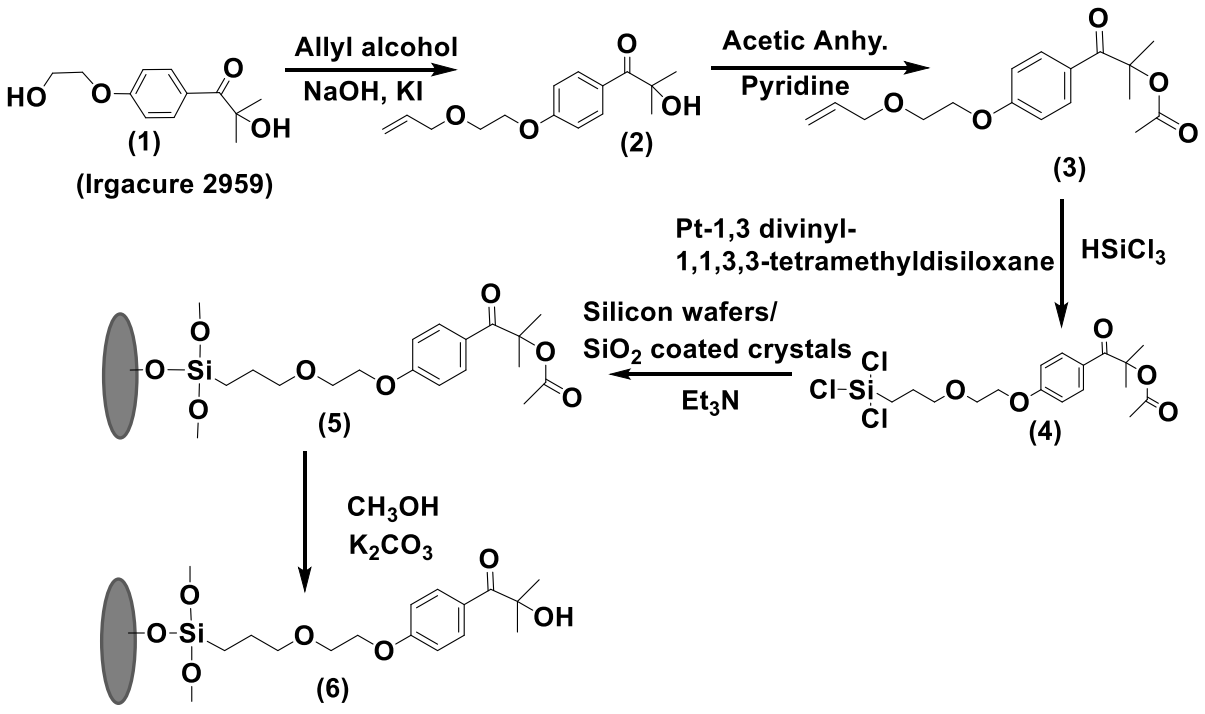


Scheme 3.1 Reaction scheme for the modification of Irgacure 2959 and immobilization on surfaces

### 3.2.5 Initiator immobilization on silicon wafers and quartz crystal surfaces

Silicon wafers were utilized to determine the optimum reaction conditions to achieve a target thickness of 90 nm which corresponds to a theoretical degree of polymerization of 350 for the glycopolymer brush. Once the optimum conditions were determined with silicon wafers, the same reaction conditions were utilized to synthesize glycopolymer brushes on silicon dioxide coated quartz crystals (QSX 303) for QCM-D. Silicon wafers (1 cm X 1 cm) were cleaned ultrasonically in DI water, acetone, and ethanol for 15 min in each of the solvents and dried under a stream of nitrogen. Surfaces were activated by exposing them to plasma for 5 minutes in a nitrogen atmosphere immediately before use for the initiator immobilization reaction. Activated wafers were immersed in a 4 mM solution of the silane modified initiator (4) in dry toluene for 2 h in the presence of triethylamine as a catalyst and acid scavenger. The reaction was performed under anhydrous conditions inside a glove box filled with dry nitrogen gas. After functionalization, the surfaces were washed with toluene and dried under a stream of nitrogen gas. Surfaces were characterized via GATR-FTIR, ellipsometry, and contact angle measurements. The initiator immobilized wafers were stored in toluene in a refrigerator until they were used.

### 3.2.6 Polymerization of glycomonomers on initiator modified surfaces

The acetyl-protected initiator surfaces (5) were deprotected by reacting with potassium carbonate in methanol for a period of 2 h. The surfaces were washed with methanol and water and dried in nitrogen before they were used for the synthesis of glycopolymer brushes. The silicon wafers with deprotected surfaces (6) were immersed into 0.5 M aqueous solutions of the glycomonomers (GalEAm or GlcEAm) in a test tube.

Each test tube was sealed with a rubber septum and purged with nitrogen for 30 min. The wafers immersed in the monomer solutions were irradiated with UV light of intensity 60 mW/cm$^2$ for 20 minutes. The polymer grafted wafers were taken out of the test tubes, immersed in distilled water for a day, and rinsed with a copious amount of distilled water to remove any unreacted monomer and loosely adsorbed polymer. The surfaces were dried with a slow stream of nitrogen and characterized via GATR-FTIR, AFM, ellipsometry, and contact angle measurements. The glycopolymer brush grafted surfaces appeared blue on visual inspection which was clearly different from the initiator modified wafer surface. The dry thickness of the polymer brush was measured via AFM scratch test and ellipsometry, and the results are reported in Table 3.1.

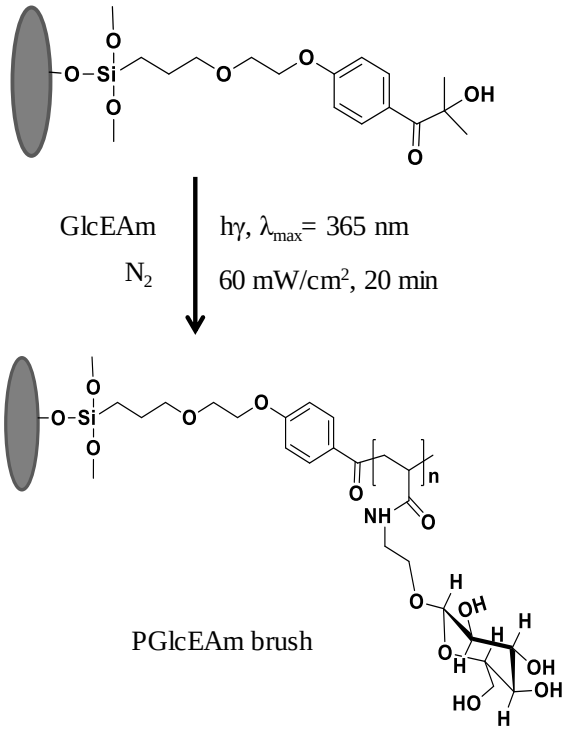


Scheme 3.2 Synthesis of the glycopolymer brushes (PGlcEAm) on the initiator immobilized surface. (same scheme applies for PGalEAm brush synthesis).

Once the reaction conditions were optimized using the silicon wafers, the same conditions and procedures were used for silicon dioxide coated quartz crystal surfaces (QSX 303) for initiator immobilization and brush synthesis. The thickness of the initiator and brush layers on silicon dioxide coated quartz crystal surfaces were measured via ellipsometry. Note that the AFM scratch test for thickness measurement could not be performed on silicon dioxide coated quartz crystal surfaces due to the apparent removal of silicon dioxide during scratching, thus making the thickness measurement via the scratch test erroneous.

### 3.3 Results and discussion

#### 3.3.1 Photoinitiator immobilization on silicon surfaces

The silicon wafer surfaces before and after the immobilization of the photoinitiator were investigated via GATR-FTIR spectroscopy. Observation of the alkane C-H (stretching) peak at 2925 $cm^{-1}$, C=O peak at 1733 $cm^{-1}$ (Ar-CO-iPr), and C-O peak at 1216 and 1112 $cm^{-1}$ for alkyl-aryl ether and aliphatic ethers, respectively, confirmed the immobilization of the modified initiator (5) on the silicon wafer surfaces [detailed peak assignment is in the Supporting information, Appendix B, Table B.1]. Presence of a thin film of the thickness of 3.6 nm (via ellipsometry) on the silicon wafer surface reaffirmed the initiator immobilization. The thickness of the acetyl protected initiator film (5) decreased to 1.6 nm after the deprotection reaction (6). Similarly, initiator immobilization on the silicon dioxide coated quartz crystals (QSX 303) was confirmed via GATR-FTIR and ellipsometry.

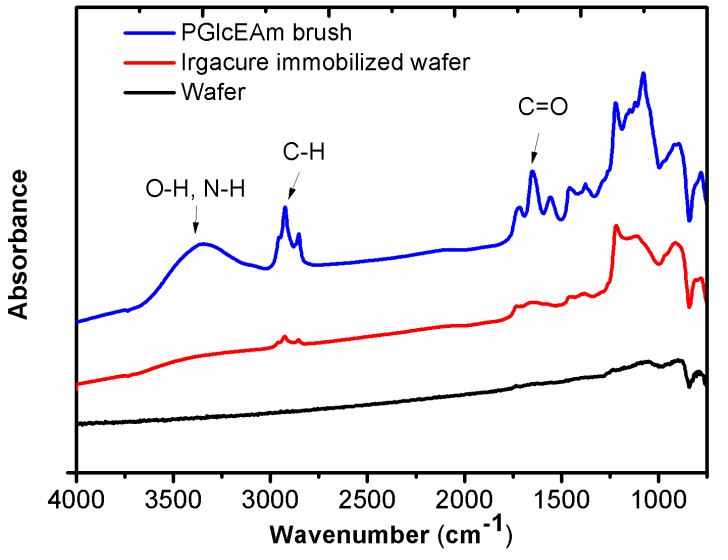


Figure 3.2 GATR-FTIR of silicon wafers, initiator immobilized wafers. and glycopolymer brushes (PGlcEAm).

Water contact angles were measured after each step of the surface modification process of the silicon wafer and $SiO_2$ modified quartz crystal (Figure 3.3). A decrease in water contact angle (increase in hydrophilicity) is observed after plasma treatment. A dramatic increase in water contact angle is apparent after the acetate protected initiator (4) was immobilized on the surfaces. On deprotection of the acetate group of the initiator, the surfaces became hydrophilic and the water contact angles were found to decrease. Hydrophobicity of the protected-initiator modified wafer surfaces was higher than that of the modified crystal surfaces, and after deprotection, the contact angles of the wafer surfaces were lower. We attribute these differences to greater initiator deposition on the wafer surface than on the crystal surface.

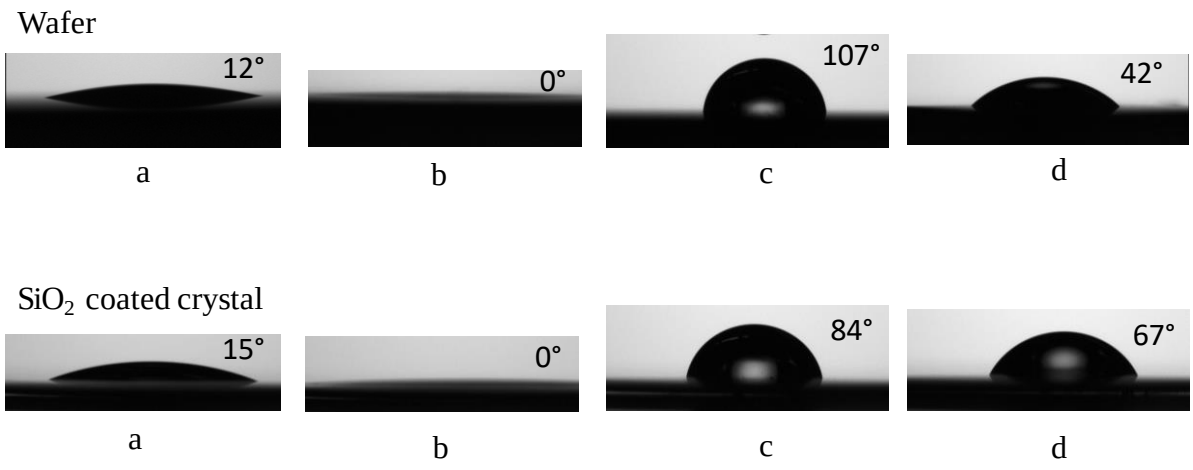


Figure 3.3 Water contact angles at different stages of surface modification. (a) neat, (b) plasma treated, (c) protected initiator, and (d) deprotected surface. Increase in water contact angle indicates effective modification of the surface (c). Removal of the protecting group yields hydroxyl groups; therefore, greater hydrophilicity and reduced water contact angle of the surface (d).

### 3.3.2 Polymerization of glycomonomers on the initiator modified surfaces

Glycomonomers were polymerized from the initiator-modified silicon wafer and QCM crystal surfaces via UV-photoinitiated free radical polymerization and were characterized via GATR-FTIR, contact angle measurement, ellipsometry, and atomic force microscopy (AFM).

Characteristic IR peaks (Figure 3.2) are observed via GATR-FTIR that confirm the presence of the glycopolymers. The broad peak at 3700-3000 $cm^{-1}$ is attributed to the overlap of the amide N-H (stretching) and the saccharide O-H (stretching), and the sharp peak at 1649 $cm^{-1}$ is attributed to the amide C=O (stretching) of the repeat unit GlcEAm.

Glycopolymer brush modified surfaces display increased hydrophilicity as evidenced by a decrease in contact angle (Figure 3.4) from that of the initiator modified surfaces (Figure 3.3). Water contact angles of the glucose containing polymer brush surfaces are lower than those of the galactose containing brush surfaces. This is attributed

to higher roughness of the galactose-polymer surfaces (Figure 3.5) [38, 39] and to the more hydrophilic nature of the glucose than the galactose.[40] Similarly, the contact angle variation between a glycopolymer grafted wafer vs crystal (Figure 3.6 a vs b for glc brush or c vs d for gal brush) can be correlated to the formation of smoother brush surfaces on crystals than on the wafers (Supporting information, Appendix B, Figure B.4).

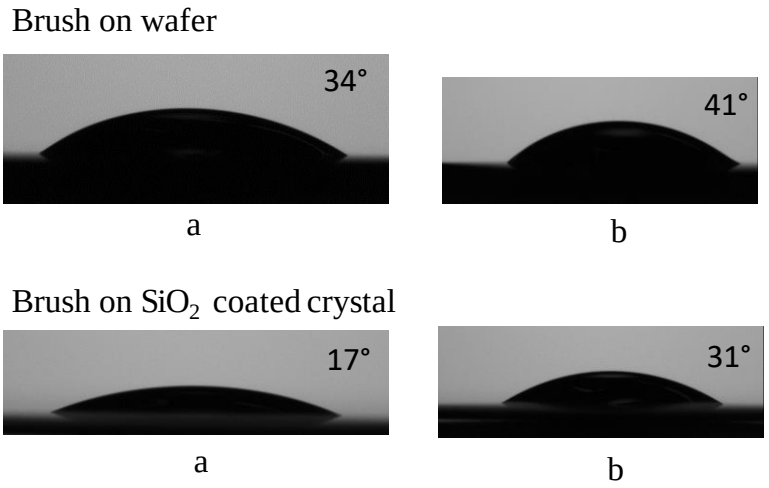


Figure 3.4 Water contact angle of the glycopolymer brushes. (a) glucose brush and (b) galactose brush.

Brush surfaces, on visual inspection, appear smooth and uniform (supporting information, Appendix B, Figure B.3). AFM imaging (Figure 3.5) was performed for a more detailed investigation of the surfaces. For the glucose brush of thickness 76 nm and the galactose brush of thickness 81 nm, a maximum roughness of 4.5 nm and 9.4 nm, respectively, was observed via AFM imaging (Figure 3.5). The surface roughness was less than 15% of the total thickness of the brushes, indicating that the brushes formed uniformly across the surfaces, the grafting density is high, and the structures are representative of brushes and not mushrooms.

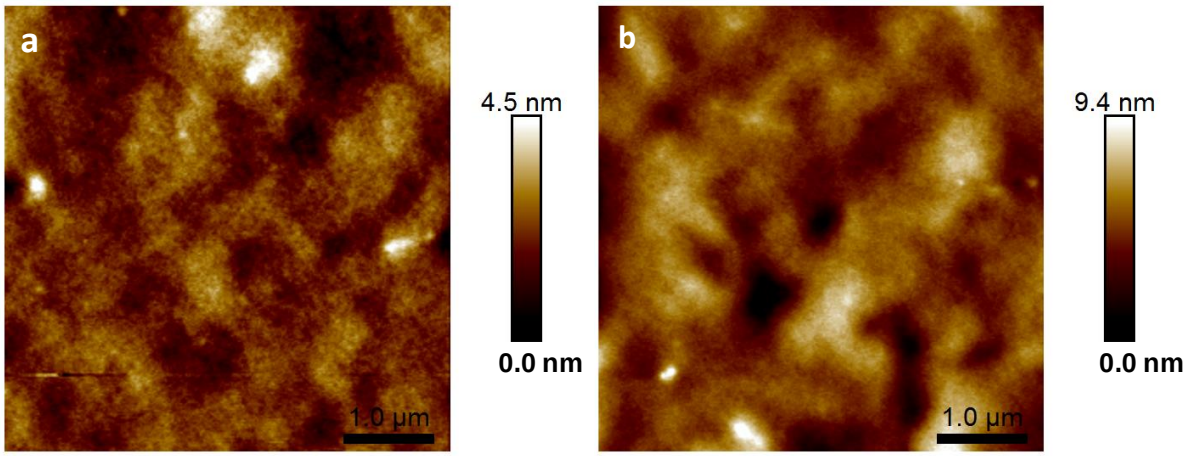


Figure 3.5 AFM height images of (a) GlcEAm brush (RMS roughness 0.58 nm) and (b) GalEAm brush (RMS roughness = 1.22 nm) on silicon dioxide coated quartz crystal surfaces. Scan size = 5.0 µm and scale = 1.0 µm

To further investigate whether the surface grafted polymers were in the brush form, the surfaces were soaked with water for 24, 48, and 72 h. It was expected that if the grafting density was high (e.g. 0.6-0.8 chains/nm$^2$), then there would not be a significant change in the wet thickness of the brushes when soaked in a good or a poor solvent.[41-43] We found that the thickness of the glycopolymer brushes on silicon wafers measured after 24 h of soaking in water (good solvent) and methanol (bad or poor solvent) did not change significantly from that of the dry brush thickness (Table 3.1) implying a high grafting density of the glycopolymers on the surfaces and the glycopolymers indeed formed brushes where chains were stretched and not in a mushroom-like conformation.

Table 3.1 Thickness of the glycopolymer brushes on silicon wafers and silicon dioxide coated quartz crystals of QCM as determined via ellipsometry and AFM scratch test.

| **Brush type** | **Brush on silicon wafers** | | | **Brush on crystals*** | | **Thickness of brush after soaking#** | |
|---|---|---|---|---|---|---|---|
| | Thickness via Ellipsometry (nm) | Thickness via AFM scratch test (nm) | $DP_{theo}$‡ | Thickness via Ellipsometry (nm) | $DP_{theo}$ | 24 h soaked in water | 24 h soaked in $CH_3OH$ |
| **PGlcEAm** | 97 (2.9) | 96 | 382 | 76 (4.7) | 303 | 103 (3.4) | 95 (2.1) |
| **PGalEAm** | 102 (4.7) | 99 | 394 | 81 (10) | 323 | 103 (6.9) | 99 (3.9) |

‡Theoretical degree of polymerization DPth = thickness/ length of a repeat unit, ellipsometric thickness and the length of a repeat unit of 0.251 nm (considering C-C bond length of 0.154 nm) was used for the calculation. #Thickness was determined via AFM scratch tests. *Dry thickness of the brushes on $SiO_2$ coated quartz crystals of QCM could not be determined via AFM scratch test due to the removal of $SiO_2$ layer on scratching. The numbers in parentheses represent standard deviation.

### 3.4 Conclusions

Glycopolymer brushes with a target thickness of 90 nm were synthesized on silicon wafers and $SiO_2$ coated quartz crystal surfaces via a surface-initiated photopolymerization technique and were fully characterized. The brushes were found to be smooth and uniformly distributed across the surfaces and suitable for Aβ interaction experiments via QCM-D.

### 3.5 References

(1) Das, P. K.; Dean, D. N.; Fogel, A. L.; Liu, F.; Abel, B. A.; McCormick, C. L.; Kharlampieva, E.; Rangachari, V.; Morgan, S. E. Aqueous RAFT Synthesis of Glycopolymers for Determination of Saccharide Structure and Concentration Effects on Amyloid β Aggregation. Biomacromolecules, **2017**, *18*(10), 3359-3366.

(2) Sonnino, S.; Mauri, L.; Chigorno, V.; Prinetti, A. Gangliosides as components of lipid membrane domains. Glycobiology, **2007**, *17*(1), 1R-13R.

(3) Sherwood, L. (2011). Fundamentals of Human Physiology, Cengage Learning.

(4) Dzikovski, B.; Freed, J. H.; Begley, T. P. (2007). Membrane Fluidity. Wiley Encyclopedia of Chemical Biology, John Wiley & Sons, Inc.

(5) Kowalewski, T.; Holtzman, D. M. In situ atomic force microscopy study of Alzheimer's β-amyloid peptide on different substrates: New insights into mechanism of β-sheet formation. Proceedings of the National Academy of Sciences of the United States of America, **1999**, *96*(7), 3688-3693.

(6) Sharp, J. S.; Forrest, J. A.; Jones, R. A. L. Surface Denaturation and Amyloid Fibril Formation of Insulin at Model Lipid−Water Interfaces. Biochemistry, **2002**, *41*(52), 15810-15819.

(7) Goldsbury, C.; Kistler, J.; Aebi, U.; Arvinte, T.; Cooper, G. J. Watching amyloid fibrils grow by time-lapse atomic force microscopy. J. Mol. Biol., **1999**, *285*(1), 33-9.

(8) Zhu, M.; Souillac, P. O.; Ionescu-Zanetti, C.; Carter, S. A.; Fink, A. L. Surface-catalyzed Amyloid Fibril Formation. J. Biol. Chem., **2002**, *277*(52), 50914-50922.

(9) Hedegaard, S. F.; Cárdenas, M.; Barker, R.; Jorgensen, L.; van de Weert, M. Lipidation Effect on Surface Adsorption and Associated Fibrillation of the Model Protein Insulin. Langmuir, **2016**, *32*(28), 7241-7249.

(10) Matsuzaki, K. How Do Membranes Initiate Alzheimer's Disease? Formation of Toxic Amyloid Fibrils by the Amyloid β-Protein on Ganglioside Clusters. Accounts of Chemical Research, **2014**, *47*(8), 2397-2404.

(11) Gregory, J. Polymers at interfaces, by G. J. Fleer, M. A. Cohen Stuart, J. M. H. M. Scheutjens, T. Cosgrove and B. Vincent. Chapman and Hall, London, 1993. Pp. xv + 502, price £65.00. ISBN 0-412-58160-4. Polymer International, **1995**, *36*(1), 102-102.

(12) von der Ehe, C.; Weber, C.; Gottschaldt, M.; Schubert, U. S. Immobilized glycopolymers: Synthesis, methods and applications. Progress in Polymer Science, **2016**, *57*, 64-102.

(13) Inoue, Y.; Ishihara, K. Reduction of protein adsorption on well-characterized polymer brush layers with varying chemical structures. Colloids and Surfaces B: Biointerfaces, **2010**, *81*(1), 350-357.

(14) Fu, Z.; Zhang, N.; Liu, J.; Li, T.; Xu, W.; Wang, F.; Wang, T.; Zhai, Z.; Liu, L.; Mao, L.; Wu, Y. N-hydroxymethyl acrylamide polymer brush and its application in catalyzing coupling reaction. Journal of Colloid and Interface Science, **2013**, *394*(0), 409-418.

(15) Yu, K.; Lai, B. F. L.; Kizhakkedathu, J. N. Carbohydrate Structure Dependent Hemocompatibility of Biomimetic Functional Polymer Brushes on Surfaces. Advanced Healthcare Materials, **2012**, *1*(2), 199-213.

(16) Pyun, J.; Kowalewski, T.; Matyjaszewski, K. Synthesis of Polymer Brushes Using Atom Transfer Radical Polymerization. Macromolecular Rapid Communications, **2003**, *24*(18), 1043-1059.

(17) Pfaff, A.; Barner, L.; Müller, A. H. E.; Granville, A. M. Surface modification of polymeric microspheres using glycopolymers for biorecognition. European Polymer Journal, **2011**, *47*(4), 805-815.

(18) Deng, H.-T.; Xu, Z.-K.; Dai, Z.-W.; Wu, J.; Seta, P. Immobilization of Candida rugosa lipase on polypropylene microfiltration membrane modified by glycopolymer: hydrolysis of olive oil in biphasic bioreactor. Enzyme and Microbial Technology, **2005**, *36*(7), 996-1002.

(19) Guo, T.-Y.; Liu, P.; Xia, Y.-Q.; Song, M.-D. Synthesis of lactose-containing glycopolymer-grafted silica gel particles. Journal of Applied Polymer Science, **2010**, *116*(3), 1611-1616.

(20) Yang, Q.; Hu, M.-X.; Dai, Z.-W.; Tian, J.; Xu, Z.-K. Fabrication of Glycosylated Surface on Polymer Membrane by UV-Induced Graft Polymerization for Lectin Recognition. Langmuir, **2006**, *22*(22), 9345-9349.

(21) Guo, W.; Hensarling, R. M.; LeBlanc, A. L.; Hoff, E. A.; Baranek, A. D.; Patton, D. L. Rapid Synthesis of Polymer Brush Surfaces via Microwave-Assisted Surface-Initiated Radical Polymerization. Macromolecular Rapid Communications, **2012**, *33*(9), 863-868.

(22) Yu, K.; Kizhakkedathu, J. N. Synthesis of Functional Polymer Brushes Containing Carbohydrate Residues in the Pyranose Form and Their Specific and Nonspecific Interactions with Proteins. Biomacromolecules, **2010**, *11*(11), 3073-3085.

(23) Park, H.; Rosencrantz, R. R.; Elling, L.; Böker, A. Glycopolymer Brushes for Specific Lectin Binding by Controlled Multivalent Presentation of N-Acetyllactosamine Glycan Oligomers. Macromolecular Rapid Communications, **2015**, *36*(1), 45-54.

(24) Yutaro, O.; Hirokazu, S.; Tatsuya, M.; Yu, H.; Yoshiko, M. Affinity Separation of Lectins Using Porous Membranes Immobilized with Glycopolymer Brushes Containing Mannose or N-Acetyl-D-Glucosamine. Membranes, **2013**, *3*(3), 169-181.

(25) Sugnaux, C.; Klok, H. A. Glucose-Sensitive QCM-Sensors Via Direct Surface RAFT Polymerization. Macromolecular Rapid Communications, **2014**, *35*(16), 1402-1407.

(26) H., S. M.; Ling, Z.; S., H. W. T. Temperature-Responsive Glycopolymer Brushes Synthesized via RAFT Polymerization Using the Z-group Approach. Macromolecular Rapid Communications, **2006**, *27*(14), 1121-1126.

(27) Hee, M. E.; Simon, T. S. R.; Laurent, B.; H., S. M. Thermo-responsive glycopolymer chains grafted onto honeycomb structured porous films via RAFT polymerization as a thermo-dependent switcher for lectin Concanavalin a conjugation. Journal of Polymer Science Part A: Polymer Chemistry, **2010**, *48*(15), 3440-3455.

(28) Housni, A.; Cai, H.; Liu, S.; Pun, S. H.; Narain, R. Facile Preparation of Glyconanoparticles and Their Bioconjugation to Streptavidin. Langmuir, **2007**, *23*(9), 5056-5061.

(29) Matyjaszewski, K.; Spanswick, J. Controlled/living radical polymerization. Materials Today, **2005**, *8*(3), 26-33.

(30) Matyjaszewski, K. (2000). Comparison and Classification of Controlled/Living Radical Polymerizations. Controlled/Living Radical Polymerization, American Chemical Society. **768:** 2-26.

(31) Bordegé, V.; Muñoz-Bonilla, A.; León, O.; Cuervo-Rodríguez, R.; Sánchez-Chaves, M.; Fernández-García, M. Statistical Glycopolymers Based on 2-Hydroxyethyl Methacrylate: Copolymerization, Thermal Properties, and Lectin Interaction Studies. Macromolecular Chemistry and Physics, **2011**, *212*(12), 1294-1304.

(32) Ladmiral, V.; Melia, E.; Haddleton, D. M. Synthetic glycopolymers: an overview. European Polymer Journal, **2004**, *40*(3), 431-449.

(33) Yang, Q.; Xu, Z.-K.; Dai, Z.-W.; Wang, J.-L.; Ulbricht, M. Surface Modification of Polypropylene Microporous Membranes with a Novel Glycopolymer. Chemistry of Materials, **2005**, *17*(11), 3050-3058.

(34) Yang, Q.; Strathmann, M.; Rumpf, A.; Schaule, G.; Ulbricht, M. Grafted Glycopolymer-Based Receptor Mimics on Polymer Support for Selective Adhesion of Bacteria. ACS Applied Materials & Interfaces, **2010**, *2*(12), 3555-3562.

(35) Matsuzaki, K.; Horikiri, C. Interactions of Amyloid β-Peptide (1−40) with Ganglioside-Containing Membranes. Biochemistry, **1999**, *38*(13), 4137-4142.

(36) Matsuzaki, K.; Kato, K.; Yanagisawa, K. Aβ polymerization through interaction with membrane gangliosides. Biochimica et Biophysica Acta (BBA) - Molecular and Cell Biology of Lipids, **2010**, *1801*(8), 868-877.

(37) Hensarling, R. M.; Doughty, V. A.; Chan, J. W.; Patton, D. L. "Clicking" polymer brushes with thiol-yne chemistry: indoors and out. J Am Chem Soc, **2009**, *131*(41), 14673-5.

(38) Malijevský, A. Does surface roughness amplify wetting? The Journal of Chemical Physics, **2014**, *141*(18), 184703.

(39) Svoboda, M.; Malijevský, A.; Lísal, M. Wetting properties of molecularly rough surfaces. The Journal of Chemical Physics, **2015**, *143*(10), 104701.

(40) Miyajima, K.; Machida, K.; Nakagaki, M. Hydrophobic Indexes for Various Monosaccharides. Bulletin of the Chemical Society of Japan, **1985**, *58*(9), 2595-2599.

(41) Moh, L. C. H.; Losego, M. D.; Braun, P. V. Solvent Quality Effects on Scaling Behavior of Poly(methyl methacrylate) Brushes in the Moderate- and High-Density Regimes. Langmuir, **2011**, *27*(7), 3698-3702.

(42) Malham, I. B.; Bureau, L. Density Effects on Collapse, Compression, and Adhesion of Thermoresponsive Polymer Brushes. Langmuir, **2010**, *26*(7), 4762-4768.

(43) Naji, A.; Seidel, C.; Netz, R. R. (2006). Theoretical Approaches to Neutral and Charged Polymer Brushes. Surface-Initiated Polymerization II. R. Jordan. Berlin, Heidelberg, Springer Berlin Heidelberg**:** 149-183.

# CHAPTER IV – INVESTIGATION OF LECTIN AND Aβ INTERACTION WITH SURFACE GRAFTED GLYCOPOLYMERS USING QCM-D

## 4.1 Introduction

Surface grafted glycopolymers have been utilized for sensing, recognition, and interaction studies between saccharides and proteins (lectins),[1-4] bacteria,[5] or fatty acids[6].. The binding ability of a saccharide with a protein depends on the specific structure of the saccharide and the protein. For example, Pfaff et al. reported a strong binding interaction between a galactose grafted poly(divinylbenzene) microsphere and the lectin Ricinus communis agglutinin (RCA120); whereas, mannose-containing grafted glycopolymers lack lectin binding ability.[4] This difference in lectin recognition was attributed to the structural differences of galactose and mannose.[4] Matsumoto et al. demonstrated that β-galactose has a stronger binding affinity towards Aβ than glucose. [7] The structures and size of the Aβ aggregates were found to be dependent on the structure of the saccharides; for example, Aβ formed larger aggregates and showed more β-sheet content (strong negative Cotton effect in circular dichroism) in the presence of a β-galactose immobilized onto a surface in comparison to that formed by glucose modified surfaces. [7]

It has been reported that saccharides of the cell membrane gangliosides in their clustered form seed Aβ aggregation.[8] We have reported (Chapter II) that high molecular weight glycopolymers of glucose affect Aβ aggregation differently than low molecular weight glycopolymers, presumably due to the higher concentration of saccharides in the high molecular weight polymer.[9] Here we investigated the effect of surface immobilized β-D-glucose and β-D-galactose containing glycopolymers on Aβ aggregation using

quartz crystal microbalance with dissipation monitoring (QCM-D) and atomic force microscopy (AFM).

Model studies were first performed utilizing glucose and galactose containing glycopolymers immobilized or deposited onto surfaces and their interactions with a well-known β-galactose specific lectin, Ricinus communis agglutinin (RCA).[10, 11] The interaction of the RCA with the glycopolymer deposited surfaces was monitored via quartz crystal microbalance with dissipation monitoring (QCM-D). Once it was established that the glycopolymer deposited surfaces showed selective interactions with RCA, the glycopolymers were grafted to the surfaces for evaluation of Aβ interaction interactions.

## 4.2 Materials and methods

### 4.2.1 Materials

Gold coated (QSX 301) and $SiO_2$ coated (QSX 303) quartz crystals were obtained from Biolin Scientific AB (Stockholm, Sweden). The glycopolymer grafting to the $SiO_2$ coated crystals and characterization were described in Chapter III. Fluorescein-labelled RCA was obtained from Vector Laboratories (CA, USA), and all other chemicals were obtained from Sigma Aldrich at their highest available purity and used without further purification. The Aβ42 was purified following the procedure reported in Chapter II.

### 4.2.2 Experimental

#### 4.2.2.1 RCA and Aβ interaction with glycopolymers via quartz crystal microbalance with dissipation monitoring (QCM-D)

To investigate the lectin RCA120 interaction/deposition on glycopolymer surfaces, a gold crystal was mounted on the QCM-D flow cell of Q-sense E4 instrument

(Biolin Scientific AB, Stockholm, Sweden). Resonance frequencies of the crystal at different overtones (n = 1, 3, 5, 7, 9, 11, and 13 where the fundamental frequency, $f_0$ = 4.95 MHz) were first determined. A stable baseline was obtained with PBS buffer (10 mM, pH 7.4, saturated with $Ca^{++}$, $Mg^{++}$, and $Mn^{++}$ salts, flow rate = 50 µL/min) followed by a 5 mg/mL solution of either PGlcEAm350 or PGalEAm350. Finally, the RCA solution of 0.2 mg/mL was pumped through the cell followed by a rinsing step using the PBS buffer. Fluorescein-tagged RCA and non-fluorescent RCA were utilized for this investigation and the fluorescein-tagged RCA deposited onto the surfaces of neat and glycopolymer modified QCM crystals after their final buffer wash were imaged via fluorescent microscopy.

For glycopolymer brush-Aβ interaction studies, a glycopolymer grafted QCM crystal was mounted on the flow cell, and Tris buffer (10 mM, pH 8.0, 0.01 % w/v of sodium azide) was pumped through the cells for 10 min followed by Aβ peptide (10 µM) for 8 min. Then the flow was stopped keeping the Aβ inside the cell and in contact with the brush for 24 h, and, finally, a Tris buffer wash was performed.

Note that a constant flow rate of 50 µL/min was maintained for all the QCM-D experiments whenever a solution was pumped through the flow cells (modules) using a peristaltic pump (ISMATEC) and the temperature of the flow cell was kept constant at 25 °C during the experiments. The same buffer solution was used to prepare the protein/peptide/polymer solutions, to obtain the initial baseline, and for the final washing step of an experiment.

The time-resolved frequency and dissipation changes of the crystals due to polymer-protein interaction and deposition were simultaneously recorded for the

overtones n = 1, 3, 5, 7, 9, 11, and 13 using Q Soft software (Biolin Scientific). Frequency and dissipation data were analyzed via viscoelastic or Sauerbrey modelling using DFind software (Biolin Scientific).

#### 4.2.2.2 Analysis of the frequency and dissipation data obtained from the QCM-D experiments

Quartz crystal microbalance with dissipation monitoring (QCM-D) is a highly sensitive technique which provides quantitative information about changes in thickness, mass, and the viscoelastic properties of the materials deposited on a quartz crystal. The resonance frequency (f) and dissipation characteristics (D) of a piezoelectric sensor change as adsorption/desorption or any other interactions or changes occur on the surface.[12] If the adsorbed layer on a crystal surface is thin and rigid and the energy dissipation due to the viscous loss is negligibly small, then the frequency is proportional to the added mass[13, 14] and the mass deposited on the crystal can be calculated via the Sauerbrey equation (eq. 4.1).[14]

$$\Delta m = -C\frac{1}{n}\Delta f \qquad (4.1)$$

The film thickness can be expressed as, $\delta = \frac{\Delta m}{\rho}$ (4.2)

In the equations 4.1 and 4.2, $\Delta m$ is the mass deposited per unit surface area of the crystal, $\Delta f$ is the frequency change, n is the vibrational mode number (overtone), $c$ is the instrument constant which is a function of the properties of the quartz crystal including its fundamental frequency ($f_0$), and $\rho$ is the density of the rigid layer. The negative sign in eq. 4.1 indicates that the frequency decreases when mass is deposited. The Sauerbrey model is simple and is widely used in the literature to calculate mass adsorption on a

QCM crystal surface.[15, 16] However, the Sauerbrey model cannot accurately interpret the frequency and dissipation changes for a system involving viscoelastic materials, and it underestimates the deposited mass.[17]

A very thin film (overlayer) can dissipate a significant amount of energy and is considered viscoelastic in nature.[13, 21] For a QCM crystal that is oscillating in a bulk Newtonian liquid, the energy dissipation at the solid-liquid interface and the resonance frequency shift of the crystal are functions of the elasticity, viscosity, and the density of the overlayers.[13]

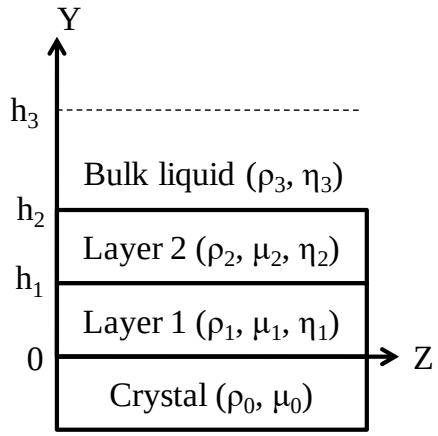


Figure 4.1 Schematic representation of a quartz crystal microbalance system. The quartz crystal remains covered with layers of viscoelastic films in a bulk liquid; h is the thickness, ρ is the density, η is the viscosity, μ is the elastic shear modulus.

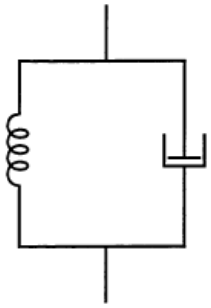

Figure 4.2 Schematic of a Voight viscoelastic model. Spring represents elastic and dashpot represents viscous elements of a polymer.

The shift in frequency (Δf) and the dissipation (ΔD) due to viscoelastic mass deposition on the crystal can be expressed by Voight-Voinova equations, eq (4.3) and eq (4.4).[13] The Voight-Voinova model assumes (a) uniform thickness and density of the overlayers (i.e. layer 1, layer 2 and bulk liquid in the Figure 4.1.), (b) viscosity of the overlayers are independent of the overtones, and (c) no-slip conditions.[13]

$$\Delta f \approx -\frac{1}{2\pi\rho_0 h_0}\left\{\frac{\eta_3}{\delta_3}+\sum_{j=1,2}\left[h_j\rho_j\omega-2h_j\left(\frac{\eta_3}{\delta_3}\right)^2\frac{\eta_j\omega^2}{\mu_j^2+\omega^2\eta_j^2}\right]\right\} \qquad (4.3)$$

$$\Delta D \approx \frac{1}{2\pi f\rho_0 h_0}\left\{\frac{\eta_3}{\delta_3}+\sum_{j=1,2}\left[2h_j\left(\frac{\eta_3}{\delta_3}\right)^2\frac{\mu_j\omega}{\mu_j^2+\omega^2\eta_j^2}\right]\right\} \qquad (4.4)$$

The viscous penetration depth, δ, can be expressed as

$$\delta=\sqrt{\frac{2\eta}{\rho\omega}} \qquad (4.5)$$

The change in frequency (Δf) and dissipation (ΔD) of a crystal at different overtones (n) are measured and the Voigt-Voinova equations (eq 4.3 and eq 4.4) are solved to estimate the thickness, shear elastic modulus, and the shear viscosity of the overlayers. In this model, for a single harmonic (n) four parameters are unknown and two parameters, frequency (Δf) and dissipation (ΔD), are known. Therefore, the system is undefined. However, it is possible to make a unique determination by using two or more harmonics since each harmonic provides two experimental values (frequency and dissipation).[17, 22] In the viscoelastic model, film thickness and density are frequency independent properties while the shear modulus and viscosity are assumed to be specific frequency dependent.[22]

In the modelling software, DFind, minimum and maximum estimates for the viscosity (η), thickness (h), and the shear elastic modulus (μ) are made. This minimum-maximum interval forms a grid of coordinates which are used to find the best fit of the data. From the best fit equation, the thicknesses, shear viscosity, and the shear elastic modulus were obtained. Surface mass density (mass/surface area) of the overlayers were calculated by multiplying the thickness with the density of the overlayers. The data of the frequency and dissipation changes of the crystals were collected via Q-Soft (Biolin Scientific) and the Sauerbrey and Voight-Voinova viscoelastic modelling was performed using DFind (Biolin Scientific) software. For this work, it was assumed that the density of the polymer layer (PGlcEAm or PGalEAm or the polymer brush) was 1050 kg/m$^3$, the density of the protein layer (RCA or Aβ) was 1100 kg/m$^3$, and the density of the buffer solution was 1000 kg/m$^3$. The viscoelastic modelling was performed utilizing frequency and dissipation changes for the overtones, n = 3, 5, 7, 9, 11, and 13. The ΔF and ΔD for the first overtone (n = 1) were ignored for the viscoelastic modelling, as is commonly done by others, due to the large amount of noise associated with the first overtone.[20, 23, 24]

#### 4.2.2.3 Fluorescence microscopy

Microscopic images of the fluorescein-labelled RCA deposited onto surfaces of neat and glycopolymer modified QCM crystals were captured via a Leica M165 FC microscope. The incident light intensity and the exposure time was kept constant for all the samples.

## 4.3 Results and discussion

### 4.3.1 Interaction of RCA 120 with galactose containing glycopolymer (PGalEAm350)

Upon the introduction of the PGalEAm350 solution to the QCM crystal, a decrease in the frequency ($\Delta F$ = 15 Hz for n = 3) and an increase in dissipation ($\Delta D$ = 4 ppm for n = 3) occurs [Figure 4.3 (A) and (B)]. The change in F and D are attributed to the polymer mass deposition on the sensor surface and the viscoelastic nature of the polymer, respectively. Using this method, glycopolymers were deposited on the crystal surface due to gravitational pull or by the electrostatic interaction between the crystal surface and the polymers, and polymers deposited in this method typically adopt a pancake like conformation.[25, 26] A decrease in the frequency of 170 Hz during the flow of RCA is attributed to the strong interaction between the RCA and the galactose containing polymer leading to a large amount of RCA deposition on the polymer. Interestingly, upon the introduction of RCA, the dissipation initially dropped and then increased monotonously as more RCA was introduced (Figure 4.3 B). The initial drop in dissipation suggests that the viscoelasticity decreased. i.e. rigidity of the overlayers (polymer-RCA) increased. This is attributed to the release of trapped water from the glycopolymer pancake, thus collapsing the pancake and compacting the glycopolymer chains.[27] The increase in dissipation, after the initial drop, was due to the deposition of more RCA and an overall increase in the viscoelasticity of the system. The final buffer wash did not significantly change the frequency or the dissipation, i.e. the washing did not significantly remove any of the layers or affect their viscoelasticity. Therefore, the polymer-RCA layers on the crystal were stable.

Figures 4.4 (A), (B), and (C) show the viscoelastic model of the change in thickness, shear viscosity, and shear elastic modulus of the overlayers (PGalEAm and RCA) due to the interaction and deposition of the PGalEAm350 and RCA. The thickness

of the PGalEAm layer initially increased to 55 nm with the introduction of the polymer solution (Figure 4.4 A) and then slightly decreased to 50 nm with the continued flow of polymer which we attribute to the compaction of the polymer layer. The mass of the deposited PGalEAm polymer was calculated to be 5250 ng/cm$^2$. With the introduction of the RCA, the thickness initially decreases which we attribute to the further compaction of the polymer layer and release of trapped water. The observed decrease of the dissipation during this time indicated the formation of a less viscoelastic or more rigid layer (Figure 4.3 B). After the initial period of RCA flow, the thickness of the overlayers continuously increased due to the deposition of more RCA on the polymer layer (Figure 4.4 A). The viscosity (Figure 4.4 B) and the shear elastic modulus (Figure 4.4 C) of the overlayers increased sharply with the deposition of RCA. It is clear from the modelling results that the RCA exhibited strong viscoelastic behavior. The mass deposition for RCA could not be determined via viscoelastic modelling, because it was not possible to correctly determine the thickness of the RCA layer due to the compaction of polymer layer during in the initial RCA deposition (20 to 24 min).

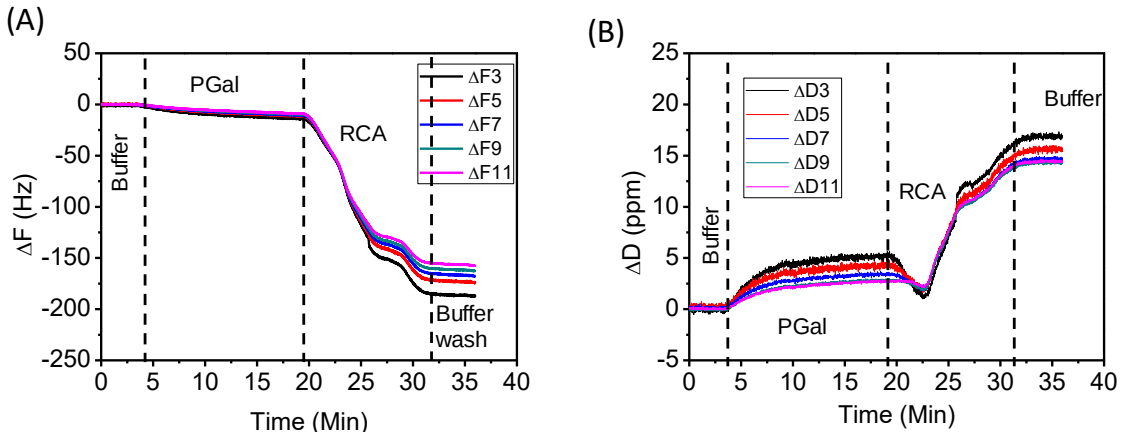


Figure 4.3 QCM-D frequency (A) and dissipation (B) change of the Au crystal during GalEAm350, RCA and buffer flow through the flow cell. The frequencies and

dissipations at different overtones (n = 3, 5, 7, 9, and 11) are shown. (flow rate = 50 µL/min, temperature = 25°C)

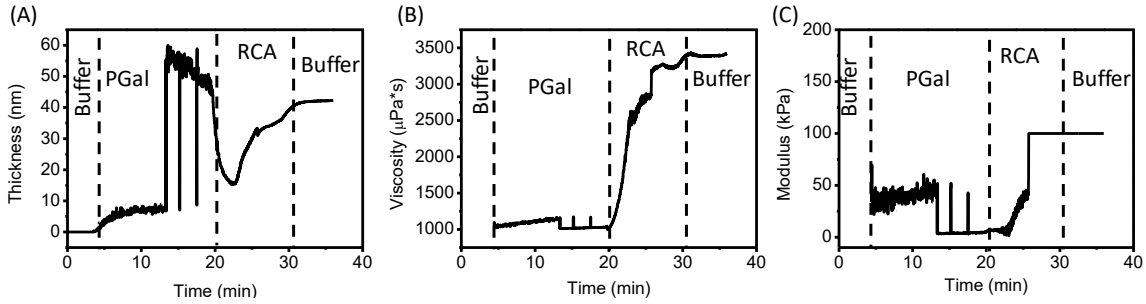


Figure 4.4 Thickness (A), shear viscosity (B), and elastic shear modulus (C) of the adsorbed layers with time estimated by Voight-Voinova viscoelastic modelling with n = 3, 5, 7, 9, and 11, $\rho_{polymer}$ = 1050 kg/m$^3$, $\rho_{RCA}$ = 1100 kg/m$^3$.

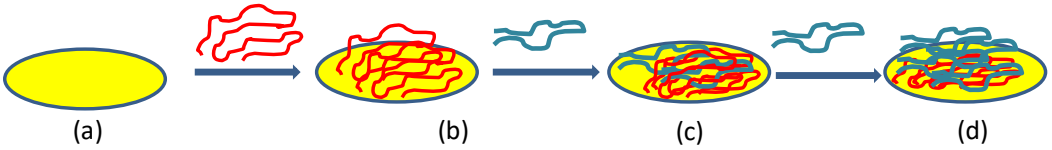


Figure 4.5 Schematic diagram of the deposition of PGalEAm350 polymer on Au crystal followed by RCA deposition. (a) clean gold crystal, (b) polymer deposited on crystal, and (c) RCA deposited on the galactose polymer (believed to be pancake shaped). Trapped water gets removed from the pancake and the polymer layers become more compact and rigid, (d) more RCA deposition on the surface and increased thickness and viscoelasticity.

### 4.3.2 Interaction of RCA 120 with glucose containing glycopolymer (PGlcEAm350)

PGlcEAm350 modified surfaces, on the other hand, showed no interaction with RCA. A 23 Hz drop in frequency (ΔF) (Figure 4.7 A) and 6 ppm increase in dissipation (ΔD) (Figure 4.7 B) occurs during the flow of the PGlcEAm solution which is attributed to mass deposition and the viscoelastic nature of the glycopolymer. Using viscoelastic modelling, the thickness of the polymer layer was found to be 30 nm (Figure 4.8 A) which corresponds to a mass deposition on 3150 ng/cm$^2$. On the injection of RCA, a drop of frequency by 45 Hz and dissipation by 4 ppm occurs, which is attributed to the deposition of RCA on the polymer layer and an increase in the overall rigidity of the

deposited layers. The overall thickness is decreased by 12 nm (Figure 4.8 A), attributed to the compaction of the polymer layer or the collapse of the pancake due to the release of the trapped water. The modulus (Figure 4.8 C) and the viscosity (Figure 4.8 B) of the overlayers (polymer and RCA) increase sharply with the deposition of RCA which also indicate the formation of rigid layers on the surface.

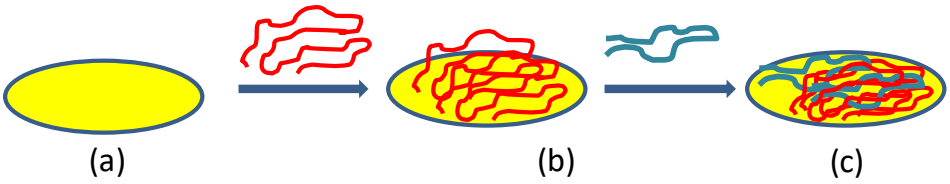


Figure 4.6 Schematic diagram of the deposition of GlcEAm350 polymer on Au crystal followed by RCA deposition. (a) clean gold crystal, (b) crystal with polymer deposited on it, and (c) RCA deposited on the glucose polymer after trapped water was removed from the pancake-like structures of the polymer and the polymer layer became compact and rigid.

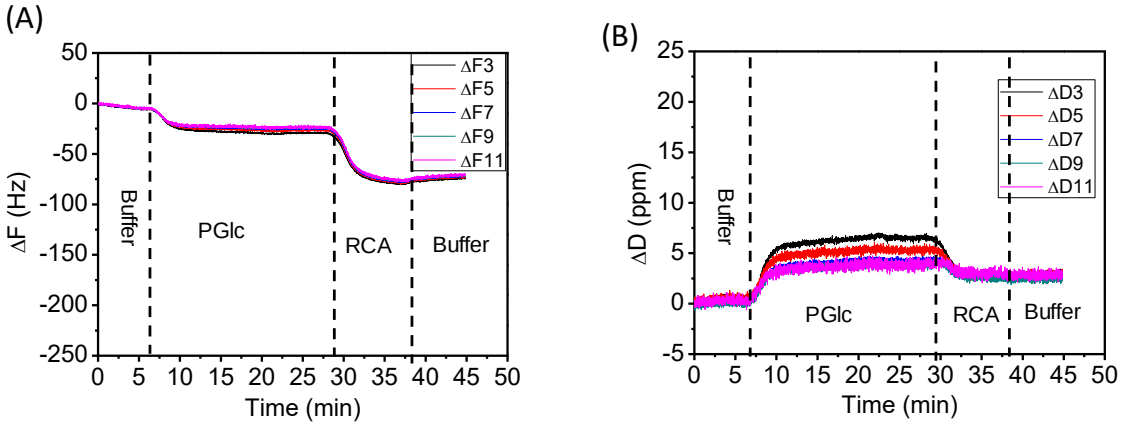


Figure 4.7 QCM-D frequency (A) and dissipation (B) change of the crystal during GlcEAm350, RCA, and buffer flow through the flow cell. The frequencies and dissipations at different overtones (n = 3, 5, 7, 9, and 11) are shown. (flow rate = 50 µL/min, temperature = 25°C)

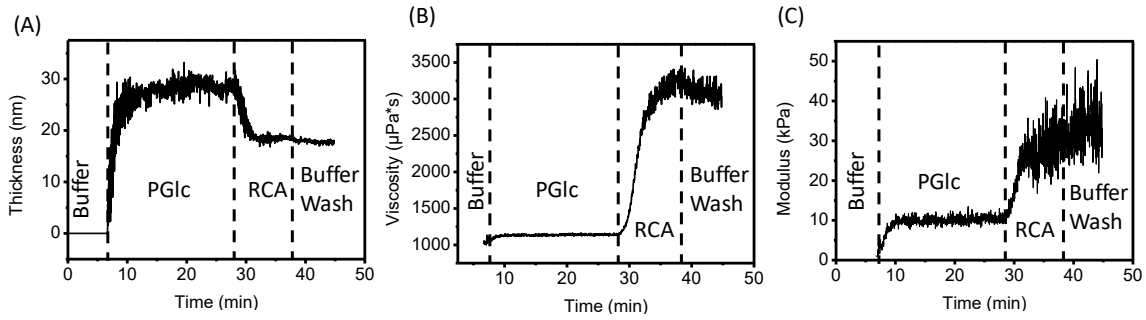


Figure 4.8 Thickness (A), shear viscosity (B) and elastic shear modulus (C) of the adsorbed layers with time, estimated by Voight-Voinova viscoelastic modelling with n = 3, 5, 7, 9, and 11, $\rho_{polymer}$ = 1050 kg/m$^3$, $\rho_{RCA}$ = 1100 kg/m$^3$

### 4.3.3 Negative control: interaction of RCA120 with gold coated quartz crystal

As a negative control experiment, RCA120 solution (0.2 mg/mL) was introduced over a gold coated quartz crystal and the change in frequency (ΔF) and dissipation (ΔD) of the crystal due to the RCA deposition were monitored. An initial frequency drop of 80 Hz (Figure 4.10 A) and dissipation increase of 3 ppm (Figure 4.10 B) are observed on RCA introduction. Subsequent buffer wash shows little change in the frequency, indicating no significant removal of RCA. The small increase in dissipation is attributed to the penetration of the water molecules into the RCA layer, making it more viscoelastic. From viscoelastic modelling, the thickness of the RCA layer was found to be 15 nm which corresponds to a mass deposition of 1650 ng/cm$^2$. The thickness was reduced by 2 nm after the buffer wash.


Figure 4.9 Schematic diagram of the deposition of lectin RCA120 on the Au crystal. (a) clean gold crystal and (b) crystal with RCA deposited on it.

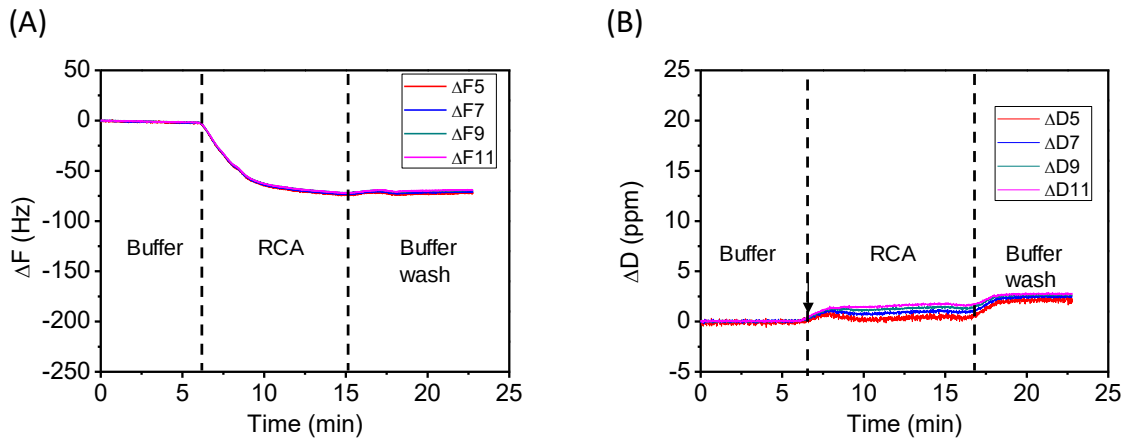


Figure 4.10 QCM-D frequency (A) and dissipation (B) change of the Au crystal during RCA and buffer flow through the flow cell. The frequencies and dissipations at different overtones (n = 5, 7, 9, and 11) are shown. (flow rate = 50 µL/min, temperature = 25°C)

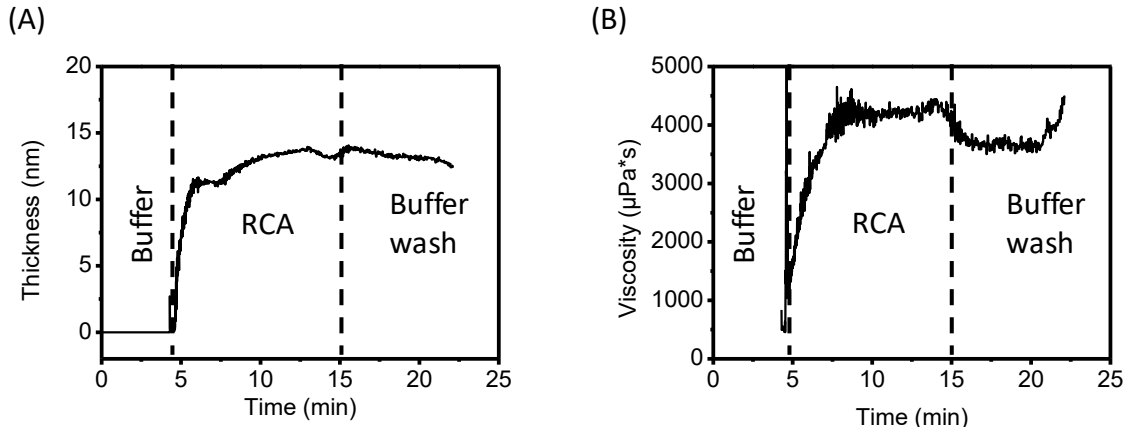


Figure 4.11 Thickness (A) and shear viscosity (B) of the adsorbed layers with time, estimated by Voight-Voinova viscoelastic modelling at n = 3, 5, 7, 9, and 11, $\rho_{RCA}$ = 1100 kg/m$^3$.

Using the Sauerbrey model (eq 4.1), mass deposition of RCA on the bare crystal (negative control), PGalEAm350, and PGlcEAm350 deposited crystals is estimated to be 1000, 3050, and 850 ng/cm$^2$ respectively. This confirms that the β-D- galactose containing glycopolymer exhibits strong affinity towards the RCA, as expected, while the glucose containing polymer and bare crystal show only non-specific absorption.

### 4.3.4 Fluorescence microscopic imaging

Microscopic images of fluorescein labelled RCA deposited onto surfaces of the neat and glycopolymer modified QCM crystals after the final buffer wash, are shown in Figure 4.12. RCA deposition is observed in all, as expected, but the intensity varies with the surface type. The highest fluorescein intensity is observed for the galactose-modified surface (Figure 4.12 C), followed by the clean Au crystal (Figure 4.12 A), and then the glucose polymer-modified surface (Figure 4.12 B). The fluorescence intensity mirrors the trends observed in QCM-D mass deposition experiments.

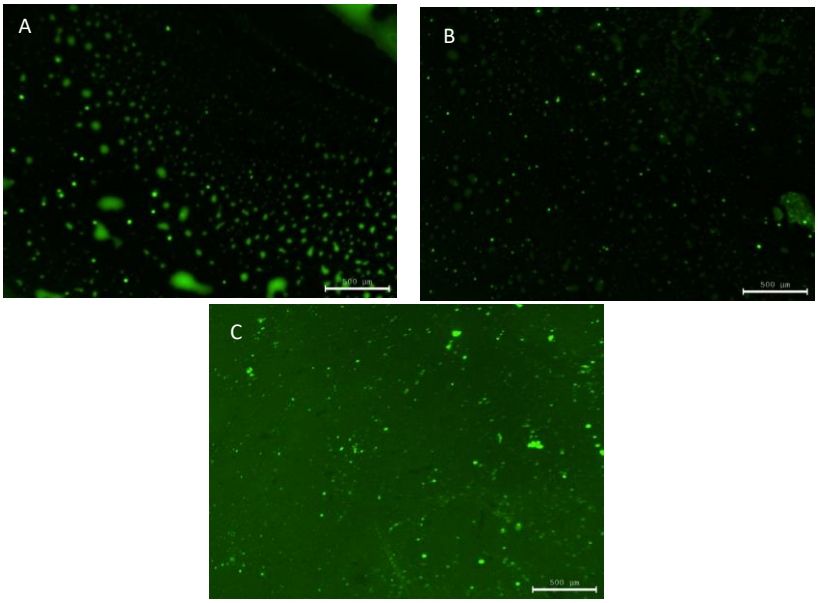


Figure 4.12 Dissecting microscopic images of the surfaces of fluorescein labelled RCA deposited on (A) Au crystal, (B) Glucose polymer modified Au crystal, and (C) galactose polymer modified Au crystal. Scale = 500 µm.

These model studies involving the glycopolymers and RCA established that the surface immobilized (deposited) β-galactose containing polymers exhibited a strong affinity, as anticipated, towards RCA. Therefore, QCM was confirmed as a reliable technique to determine the interaction and affinity of Aβ with the surface grafted glycopolymers.

### 4.3.5 Glycopolymer brush-Aβ interaction

Covalently attached glycopolymers of thickness 90 nm were synthesized on $SiO_2$ coated QCM crystal surfaces via photopolymerization as outlined in Chapter III. Frequency or dissipation of the glycopolymer grafted crystals did not change significantly as the Aβ was pumped through the QCM cells (Figure 4.13 A, inset). As the flow of the Aβ was stopped and held for 24h, the frequency increased, and the dissipation decreased slowly but steadily. The negative control experiments involving the neat brush and the buffer solution (without Aβ) showed similar change in frequency and dissipation with time (Supporting information, Appendix C, Figure C.3).

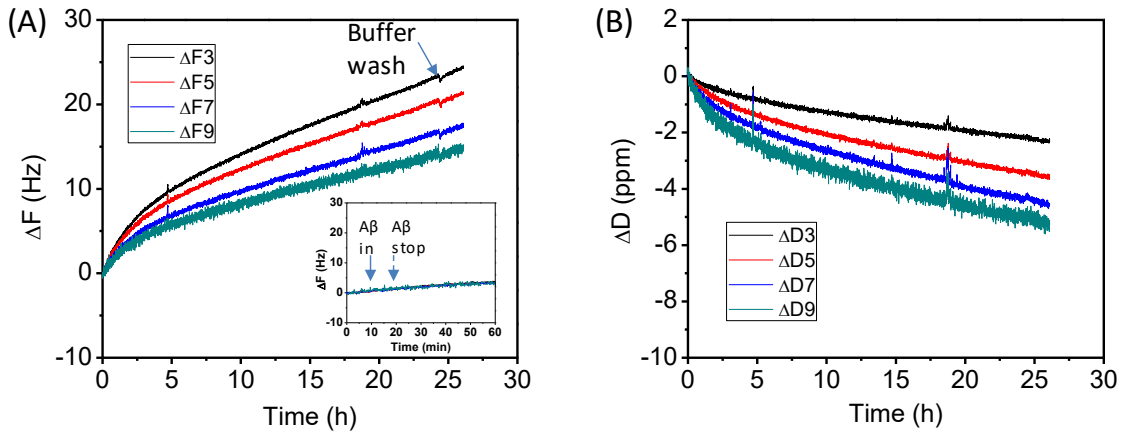


Figure 4.13 QCM-D frequency (A) and dissipation (B) change of PGlcEAm polymer immobilized QCM crystal during its interaction with Aβ. The frequencies and dissipations at different overtones (n = 3, 5, 7, 9, and 11) were plotted. (flow rate = 50 µL/min, temperature = 25°C)

It has been reported that QCM-D measured protein adsorption on polymer brushes decreases as the brush thickness, or polymer molecular weight, increases.[28-31] Luan et al.[28] investigated the effect of PHEMA brush thickness on QCM-D frequency and dissipation changes during the adsorption of the protein fibrinogen on the brush. They found that the change in frequency and dissipation was dependent on the thickness

of the brush, and as the thickness increased, the changes in F and D decreased. For the experiments using brush thicknesses of 20, 40, and 90 nm, the maximum F and D changes were observed for the 20 nm thick brush-protein system while almost no change in F and D was observed for the 90 nm thick brush-protein system. This observation led to the hypothesis of the existence of a critical brush thickness above which the QCM sensors cannot detect the events occurring on top of the brush and hence F and D do not change (referred as 'hearing loss').[28] To understand the phenomenon more clearly, Luan et al. considered the polymer brush layer as a system of many sub-layers which can slip with respect to one another when a stress is applied, such as shear stress in QCM-D. Slippage between the sub-layers is viscosity dependent, and when the viscosity is low, the friction between the layers is reduced and the slippage is increased and vice-versa. As the protein is adsorbed at the top of the polymer brush, the oscillation of the topmost layer is modulated first, and the effect is then transmitted through the layers and ultimately reaches the sensor crystal. The effect is gradually attenuated during the transmission, and if the viscosity of the adsorbed layer on the polymer brush is low enough, then the signal may be completely attenuated by the time it reaches the sensor. In this case, the sensor does not respond to the mass deposition by changing its frequency. We assume that a similar phenomenon is occurring in our system, and for that reason the Aβ interactions are not detected for the 90 nm thick glycopolymer brushes.

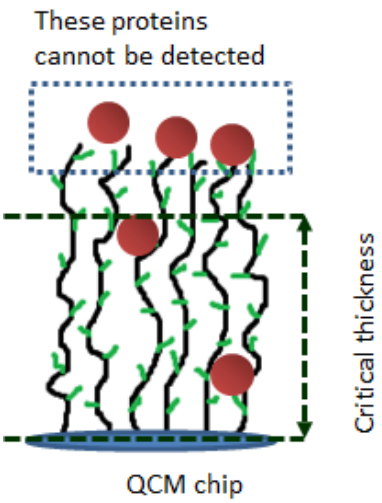


Figure 4.14 Schematic illustration of adsorption of small proteins on a polymer brush surface.

## 4.4 Conclusions

Deposition of lectin RCA on the quartz crystals modified by deposited and surface grafted glycopolymer layers was investigated via QCM-D and fluorescence microscopy. Selective interaction of RCA on the β-galactose containing polymer, PGalEAm, was established in thin glycopolymer films formed by solution deposition. No clear interaction was observed between the covalently attached glycopolymer brushes of 90 nm thickness and the Aβ, attributed to the attenuation effects of the long brush. Modified experiments with shorter brushes are described in Chapter V.

## 4.5 References

(1) Wang, Z.; Chen, G.; Lu, J.; Hong, L.; Ngai, T. Investigation of the factors affecting the carbohydrate–lectin interaction by ITC and QCM-D. Colloid and Polymer Science, **2014**, *292*(2), 391-398.

(2) Gou, Y.; Richards, S.-J.; Haddleton, D. M.; Gibson, M. I. Investigation of glycopolymer-lectin interactions using QCM-d: comparison of surface binding with inhibitory activity. Polymer Chemistry, **2012**, *3*(6), 1634-1640.

(3) Pedroso, M. M.; Watanabe, A. M.; Roque-Barreira, M. C.; Bueno, P. R.; Faria, R. C. Quartz Crystal Microbalance monitoring the real-time binding of lectin with carbohydrate with high and low molecular mass. Microchemical Journal, **2008**, *89*(2), 153-158.

(4) Pfaff, A.; Barner, L.; Müller, A. H. E.; Granville, A. M. Surface modification of polymeric microspheres using glycopolymers for biorecognition. European Polymer Journal, **2011**, *47*(4), 805-815.

(5) Wang, Y.; Narain, R.; Liu, Y. Study of Bacterial Adhesion on Different Glycopolymer Surfaces by Quartz Crystal Microbalance with Dissipation. Langmuir, **2014**, *30*(25), 7377-7387.

(6) Cao, Z.; Tsoufis, T.; Svaldo-Lanero, T.; Duwez, A.-S.; Rudolf, P.; Loos, K. The Dynamics of Complex Formation between Amylose Brushes on Gold and Fatty Acids by QCM-D. Biomacromolecules, **2013**, *14*(10), 3713-3722.

(7) Matsumoto, E.; Yamauchi, T.; Fukuda, T.; Miura, Y. Sugar microarray via click chemistry: molecular recognition with lectins and amyloid β (1–42). Science and Technology of Advanced Materials, **2009**, *10*(3), 034605.

(8) Matsuzaki, K. How Do Membranes Initiate Alzheimer's Disease? Formation of Toxic Amyloid Fibrils by the Amyloid β-Protein on Ganglioside Clusters. Accounts of Chemical Research, **2014**, *47*(8), 2397-2404.

(9) Das, P. K.; Dean, D. N.; Fogel, A. L.; Liu, F.; Abel, B. A.; McCormick, C. L.; Kharlampieva, E.; Rangachari, V.; Morgan, S. E. Aqueous RAFT Synthesis of

Glycopolymers for Determination of Saccharide Structure and Concentration Effects on Amyloid β Aggregation. Biomacromolecules, **2017**, *18*(10), 3359-3366.

(10) Fais, M.; Karamanska, R.; Allman, S.; Fairhurst, S. A.; Innocenti, P.; Fairbanks, A. J.; Donohoe, T. J.; Davis, B. G.; Russell, D. A.; Field, R. A. Surface plasmon resonance imaging of glycoarrays identifies novel and unnatural carbohydrate-based ligands for potential ricin sensor development. Chemical Science, **2011**, *2*(10), 1952-1959.

(11) Mokhtari, H.; Pelton, R.; Jin, L. Polyvinylamine-g-galactose is a route to bioactivated silica surfaces. Journal of Colloid and Interface Science, **2014**, *413*, 86-91.

(12) Sun, Y.; Lee, C.-C.; Chen, T.-H.; Huang, H. W. Kinetic Process of β-Amyloid Formation via Membrane Binding. Biophysical Journal, **2010**, *99*(2), 544-552.

(13) Voinova, M. V.; Rodahl, M.; Jonson, M.; Kasemo, B. Viscoelastic Acoustic Response of Layered Polymer Films at Fluid-Solid Interfaces: Continuum Mechanics Approach. Physica Scripta, **1999**, *59*(5), 391.

(14) Sauerbrey, G. Verwendung von Schwingquarzen zur Wägung dünner Schichten und zur Mikrowägung. Z. Physik, **1959**, *155*(2), 206-222.

(15) Kotarek, J. A.; Johnson, K. C.; Moss, M. A. Quartz crystal microbalance analysis of growth kinetics for aggregation intermediates of the amyloid-β protein. Analytical Biochemistry, **2008**, *378*(1), 15-24.

(16) Hovgaard, M. B.; Dong, M.; Otzen, D. E.; Besenbacher, F. Quartz Crystal Microbalance Studies of Multilayer Glucagon Fibrillation at the Solid-Liquid Interface. Biophysical Journal, **2007**, *93*(6), 2162-2169.

(17) Cho, N.-J.; Kanazawa, K. K.; Glenn, J. S.; Frank, C. W. Employing Two Different Quartz Crystal Microbalance Models To Study Changes in Viscoelastic Behavior upon

Transformation of Lipid Vesicles to a Bilayer on a Gold Surface. Analytical Chemistry, **2007**, *79*(18), 7027-7035.

(18) Höök, F.; Rodahl, M.; Brzezinski, P.; Kasemo, B. Energy Dissipation Kinetics for Protein and Antibody−Antigen Adsorption under Shear Oscillation on a Quartz Crystal Microbalance. Langmuir, **1998**, *14*(4), 729-734.

(19) Höök, F.; Rodahl, M.; Kasemo, B.; Brzezinski, P. Structural changes in hemoglobin during adsorption to solid surfaces: Effects of pH, ionic strength, and ligand binding. Proceedings of the National Academy of Sciences, **1998**, *95*(21), 12271-12276.

(20) Dutta, A. K.; Belfort, G. Adsorbed Gels versus Brushes: Viscoelastic Differences. Langmuir, **2007**, *23*(6), 3088-3094.

(21) Voinova, M. V.; Jonson, M.; Kasemo, B. Dynamics of viscous amphiphilic films supported by elastic solid substrates. Journal of Physics: Condensed Matter, **1997**, *9*(37), 7799.

(22) Munro, J. C.; Frank, C. W. Polyacrylamide Adsorption from Aqueous Solutions on Gold and Silver Surfaces Monitored by the Quartz Crystal Microbalance. Macromolecules, **2004**, *37*(3), 925-938.

(23) Vogt, B. D.; Lin, E. K.; Wu, W.-l.; White, C. C. Correction to "Effect of Film Thickness on the Validity of the Sauerbrey Equation for Hydrated Polyelectrolyte Films". The Journal of Physical Chemistry B, **2013**, *117*(28), 8647-8647.

(24) Irwin, E. F.; Ho, J. E.; Kane, S. R.; Healy, K. E. Analysis of Interpenetrating Polymer Networks via Quartz Crystal Microbalance with Dissipation Monitoring. Langmuir, **2005**, *21*(12), 5529-5536.

(25) Li, F.; Pincet, F. Confinement free energy of surfaces bearing end-grafted polymers in the mushroom regime and local measurement of the polymer density. Langmuir, **2007**, *23*(25), 12541-8.

(26) Taira, Y.; McNamee, C. E. Polysaccharide films at an air/liquid and a liquid/silicon interface: effect of the polysaccharide and liquid type on their physical properties. Soft Matter, **2014**, *10*(42), 8558-8572.

(27) Liu, G.; Zhang, G. Collapse and Swelling of Thermally Sensitive Poly(N-isopropylacrylamide) Brushes Monitored with a Quartz Crystal Microbalance. The Journal of Physical Chemistry B, **2005**, *109*(2), 743-747.

(28) Luan, Y.; Li, D.; Wei, T.; Wang, M.; Tang, Z.; Brash, J. L.; Chen, H. "Hearing Loss" in QCM Measurement of Protein Adsorption to Protein Resistant Polymer Brush Layers. Analytical Chemistry, **2017**, *89*(7), 4184-4191.

(29) Kim, M.; Schmitt, S. K.; Choi, J. W.; Krutty, J. D.; Gopalan, P. From Self-Assembled Monolayers to Coatings: Advances in the Synthesis and Nanobio Applications of Polymer Brushes. Polymers, **2015**, *7*(7), 1346.

(30) Zhao, C.; Li, L.; Zheng, J. Achieving Highly Effective Nonfouling Performance for Surface-Grafted Poly(HPMA) via Atom-Transfer Radical Polymerization. Langmuir, **2010**, *26*(22), 17375-17382.

(31) Zhao, C.; Li, L.; Wang, Q.; Yu, Q.; Zheng, J. Effect of Film Thickness on the Antifouling Performance of Poly(hydroxy-functional methacrylates) Grafted Surfaces. Langmuir, **2011**, *27*(8), 4906-4913.

# CHAPTER V – SYNTHESIS OF SHORT GLYCOPOLYMER BRUSHES VIA RAFT AND INVESTIGATION OF THEIR EFFECT ON Aβ AGGREGATION

## 5.1 Introduction

The thickness of polymer brushes restricts their use for protein sensing via the QCM-D technique. It has been reported that the detection of protein adsorption on polymer brushes decreases as the brush length increases,[1, 2] and, after a certain critical length, the QCM cannot detect deposition of a protein on a brush surface.[3] For a poly(hydroxyethyl methacrylate) (PHEMA) brush of thickness 90 nm, the QCM-D technique was unable to detect interactions between the brush and fibrinogen (protein) although the fibrinogen deposition was proven by surface plasmon resonance (SPR).[3] However, the QCM technique detected the mass deposition and interaction of the PHEMA brush and fibrinogen when the thickness of the brush was only 20 nm. This observation has led to the hypothesis of the existence of a critical thickness of the brush above which the QCM crystal does not respond to the mass deposition by changing its resonance frequency and dissipation.[3] Our surface photopolymerized glycopolymer brush of 90 nm thickness did not show any interaction with the Aβ peptide when investigated via QCM-D. Therefore, short brushes of 10 nm thickness were synthesized on silicon dioxide coated QCM crystal surfaces and were utilized to investigate the effect of saccharide structure on Aβ interaction and aggregation. We hypothesize that the QCM will be able to detect interactions, if any, between the glycopolymer brushes of 10 nm thickness and Aβ peptide at 20 μM concentration when allowed to interact at 37 °C. Short polymer brushes of a target thickness can be synthesized via controlled polymerization techniques such as surface-initiated atom transfer radical polymerization

(SI-ATRP) or reversible addition chain transfer (RAFT) polymerization. SI-ATRP has been widely used for the synthesis of glycopolymer brushes from the surface of silicon wafers.[4, 5] In this technique, an ATRP initiator is first immobilized on the surface, and then polymerization of monomers is carried out in the presence of a sacrificial initiator.[5-7] The polymers formed in the solution are characterized and are widely accepted as representative of the polymer formed on the surface.[5, 6, 8] One of the disadvantages of the SI-ATRP technique is the removal of the metal catalyst from the polymer; complete removal of the catalyst is a challenge.[9] Removal of metal catalyst is essential especially when the polymer is utilized for studies involving proteins, because the metal catalyst can affect the protein interaction; for example, $Cu^{++}$ has been reported to reduce the lag time and increase the rate of Aβ aggregation.[10-12]

In contrast to ATRP, the reversible addition-fragmentation chain transfer polymerization (RAFT) mechanism does not require the use of a metal catalyst. Therefore, a polymer synthesized via RAFT does not contain metal ions as impurities. RAFT polymerization has been used to synthesize well-controlled polymer brushes from a variety of surfaces made of polymeric materials,[13-15] gold,[16, 17] or silica/silicon.[18, 19] Most commonly the polymerization strategy in these cases involved immobilizing a RAFT agent (chain transfer agent, CTA) on the surface and addition of an initiator in the solution,[13, 17, 19, 20] but the opposite case has been reported.[15, 18] Surface-initiated RAFT polymerization by immobilizing an initiator (such as an azo initiator) on a surface and adding a free RAFT agent in the solution was successful only when an excess of free initiator was added to the solution.[18] A RAFT agent can be immobilized on a surface either by its R group (free radical leaving group) or by its Z group (non-leaving group

which controls the reactivity of the C=S bond). Attachment through the R group leads to the detachment of the RAFT agent during polymerization and a controlled growth of brushes can only be achieved for a very low conversion.[19] Additionally, the R-group attachment method allows for the termination of two macroradicals on the surface, resulting in the loss of RAFT agents.[20] In contrast, in the Z group approach, RAFT agents always remain covalently attached to the surface and no thiocarbonylthio group is lost during polymerization. However, in the Z-group approach, transfer of the macroradical to the RAFT agent takes place close to the surface (grafting onto method), and, with the increase in brush length, the RAFT agent might be less and less accessible due to steric reasons.[20] Consequently, the Z-group approach may lead to the termination of polymerization and limit the brush growth.[21] Stenzel et al. utilized a Z-group approach to synthesize well-controlled thermoresponsive glycopolymer brushes on silicon wafer surfaces.[20] One significant advantage of the Z group approach is that the polymer can be easily cleaved from the surface using a nucleophile, and the cleaved polymers can then be utilized for analytical characterization in solution.[22]

We utilized the Z-group approach to immobilize a RAFT agent on the surfaces of silicon wafers and silicon dioxide coated QCM crystals and synthesized glycopolymer brushes of target thickness (10 nm) following the procedure reported by Stenzel et al.[20] Polymers formed in the solution during the surface polymerization were assumed to be representative of the polymers formed on the surface and were characterized for their molecular weight.

## 5.2 Materials and methods

### 5.2.1 Materials

The galactose and glucose-containing glycomonomers were synthesized via the procedure reported in Chapter II. The RAFT chain transfer agent (CTA), 3-benzylsulfanylthiocarbonyl sulfanylpropionic acid (BSPA) and its acyl chloride derivative 3-benzylsulfanylthiocarbonyl sulfanylpropanoyl chloride (BSPC) were synthesized following the procedure reported by Stenzel et al.[23] The surface modifier 3-aminopropyl trimethoxysilane (APTMS), 4,4′-azobis(cyano-pentanoic acid) (V-501) and other chemicals and solvents were obtained from Sigma-Aldrich in their highest purity available.

### 5.2.2 Polymer grafting on surface

Silicon wafer surfaces (1 cm X 1 cm) were cleaned via sonicating in toluene, acetone, and ethanol (10 min each) and then dried with a stream of nitrogen. The clean wafers were treated with UV-ozone for 10 min and were immersed in a solution of APTMS (5 vol% in toluene) in test tubes. The test tubes were heated at 60 °C for 1 h in an oil bath, and the wafers were washed with toluene, acetone, and ethanol. The thickness of the modification layer was measured by ellipsometry and the water contact angle of the surfaces were measured. The same procedure was followed for the silicon dioxide coated QCM crystal surfaces except the initial washing was done with SDS solution (2 % v/v in water) and ethanol and sonicated for 30 s in each solution.

The APTMS-immobilized surfaces were immersed in a solution of 3-benzylsulfanylthiocarbonyl sulfanylpropanoyl chloride (5 % v/v) in chloroform. A few drops of triethyl amine (3-4 drops per 1 mL of solution) were added in the solution and

the reaction proceeded for overnight (16 h) at room temperature in the dark while shaking on a shaker plate. The RAFT agent immobilized surfaces were rinsed with chloroform and ethanol. The thickness of the RAFT agent layer and the water contact angle of the surfaces were measured by ellipsometry and goniometry respectively.

The grafting of the glucose or galactose containing glycopolymers on the surfaces was performed by immersing the RAFT agent immobilized surface (wafer or crystal) in a solution of a glycomonomer (1.0 M), initiator (V-501), RAFT agent, and an internal standard, benzene sulfonic acid (BSA). The monomer and the BSA were dissolved in an acetate buffer solution of pH 5.0, and the V-501 and RAFT agent were dissolved in ethanol. The small amount of ethanol present in the reaction medium was not expected to affect the RAFT polymerization reaction.[20] The ratio of the monomer to RAFT agent and the RAFT agent to initiator was 500:1 and 5:1, respectively. Five to six test tubes, each of which contained a CTA immobilized wafer surface and the polymerization mixture, were prepared and sealed with a rubber septum. Each test tube was purged with highly pure $N_2$ for 15 min, and then the polymerization was carried out at 70 °C for a predetermined time at which the polymerization reaction was stopped by opening the septum. The surfaces were washed well with DI water and then dried with nitrogen, and the thickness and the water contact angle of the glycopolymer films on the surfaces were measured by ellipsometry. The solution of each test tube was characterized via $^1$H NMR spectroscopy to determine the monomer conversion

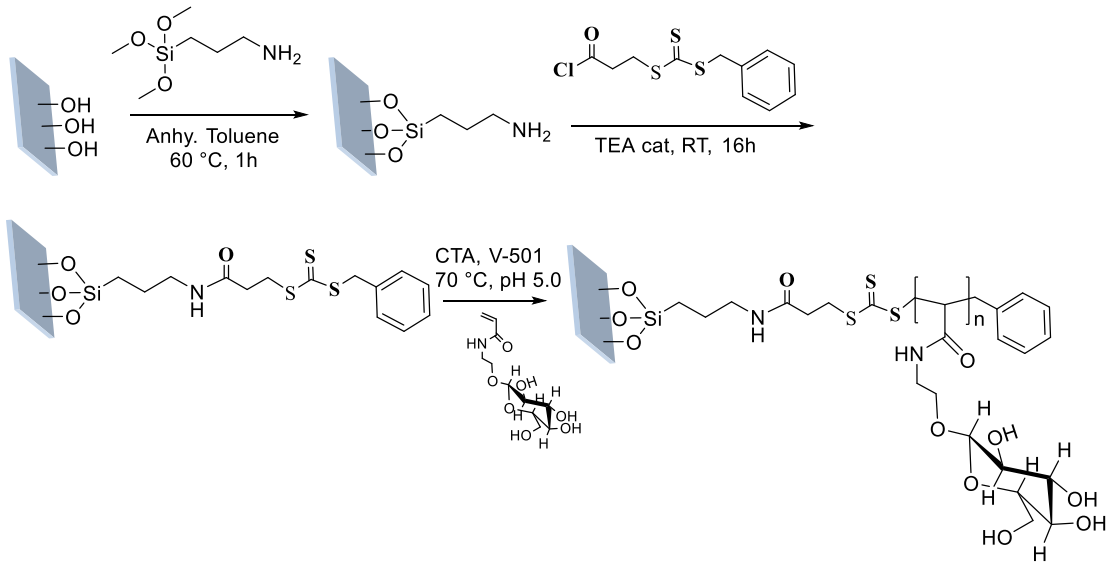


Scheme 5.1 Surface polymerization of a glycomonomer (GlcEAm) from a silicon wafer and SiO2 coated QCM quartz crystal surfaces via the Z-group approach of RAFT polymerization

From the kinetic studies, the time required to synthesize surface grafted glycopolymer films of 10 nm on silicon wafer surfaces was determined. The same reaction conditions were used for the synthesis of glycopolymer films on silicon dioxide coated QCM crystals. Glycopolymer films of ~10 nm thickness were prepared on the crystals by terminating the reactions at the predetermined time of 2 h.

### 5.2.3 Characterization

Nuclear magnetic resonance (NMR) spectroscopy was performed with a Varian MercuryPLUS (300 MHz) spectrometer by taking an average of 128 scans (delay 5 s) using appropriate solvents ($CDCl_3$ or $D_2O$).

Water contact angle on the surfaces of the unmodified and modified wafers and $SiO_2$ coated quartz crystals were measured after each step during the initiator immobilization and the glycopolymer synthesis. The contact angle was measured using a

Rame-Hart 200-00 Std. Tilting B goniometer. A 6 μL water droplet was added to the surface and the average of three measurements was reported.

Thickness was measured using a Gaertner Scientific Corporation LSE Stokes ellipsometer with a 632.8 nm laser at a 70° incident angle. The refractive index of 3.85 was used for wafers and silicon dioxide coated quartz surfaces and 1.46 was used for initiator and glycopolymer films.

X-ray photoelectron spectroscopy (XPS) analysis of the glycopolymer grafted surfaces was performed using a Thermo Scientific ESCALAB Xi+ X-Ray Photoelectron Spectrometer employing monochromatic Al-Kα radiation (1486.6 eV). A surface area of 650 μm × 600 μm was analyzed under ultra-high vacuum. For the XPS survey, 5 scans were taken at a pass energy of 215 eV, dwell time of 10 ms, and an energy step size of 1eV. High-resolution scans (3 scans) were performed using pass energy of 20 eV, 50 ms of dwell time, and 0.1 eV of energy step size. The XPS spectra were deconvoluted via non-linear Gaussian curve fitting using Origin Pro 8 software.

AFM imaging for the neat and modified silicon wafers and $SiO_2$ coated QCM crystals was performed with a Dimension Icon (Bruker) instrument in tapping mode following the procedure described in Chapter III.

### 5.2.4 Quartz crystal microbalance with dissipation monitoring (QCM-D)

Glycopolymer grafted QCM crystals were mounted on a flow cell of a QCM-D instrument and Tris buffer (10 mM, pH = 8.0, 0.01 % (w/v) of sodium azide) was pumped through the cell until a stable baseline was obtained. Aβ peptide solution of 20 μM concentration was allower to flow for a period of 20 min and a buffer wash was performed. A flow rate of 10 μL/min was maintained whenever a solvent/solution was

flowing through the QCM cell and a constant temperature of 37 °C was maintained throughout the experiment. The time-resolved frequency and dissipation changes were recorded using Q Soft software (Biolin Scientific). Mass deposition of Aβ was calculated using a Sauerbrey model[24] with DFind software (Biolin Scientific). The density of the Aβ monomer was assumed to be 1.1 g/cm$^3$.

## 5.3 Results and discussion

### 5.3.1 Grafting of APTMS and CTA on silicon wafer and $SiO_2$ coated crystal surfaces

The thickness of the APTMS layer on the silicon wafer surfaces is 12 ± 4 nm, which is higher than the previously reported value by Stenzel et al.[20] We believe this higher thickness is due to the presence of moisture/water in the solvent, glassware, and in the reaction medium which resulted in the formation of multilayers of crosslinked silane layers, rather than a monolayer.[26, 27] The CTA (RAFT agent) was immobilized by reacting BSPC with the APTMS modified surface. The thickness of the CTA immobilized layer is 4 ± 1 nm which is consistent with the previously reported CTA layer thickness by Stenzel et al. The water contact angle of the amino-functionalized surfaces is 47° ± 3° which increases to 77 ± 2° on CTA grafting due to the increased hydrophobicity of the surfaces (Figure 5.1). The contact angle values are consistent with the previously reported literature values.[20]

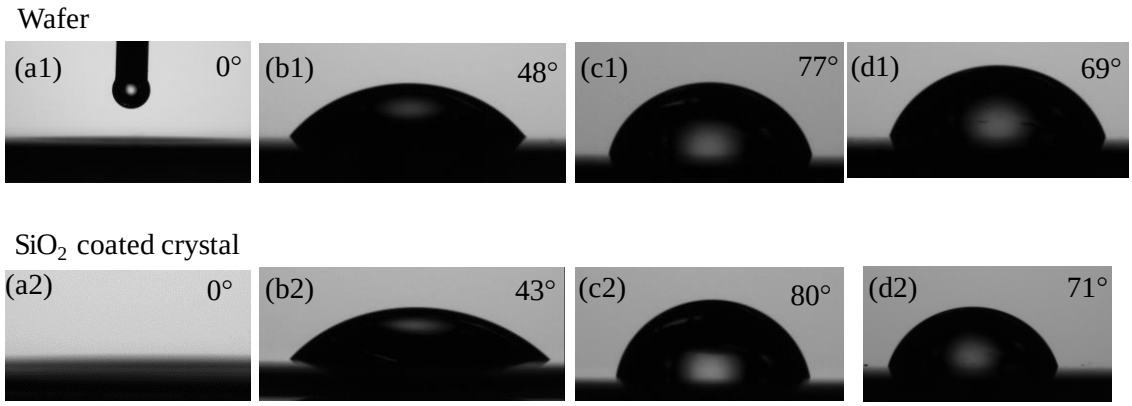


Figure 5.1 Water contact angles after different stages of surface modification. UV-ozone treated (a1, a2), APTMS (b1, b2), CTA (c1, c2), and PGlcEAm (d1, d2) grafted silicon wafer and $SiO_2$ coated QCM crystal surfaces.

The micro and nanoscale structures of the APTMS and CTA grafted on silicon wafer and silicon dioxide coated QCM crystal surfaces were investigated via atomic force microscopy (AFM). Figure 5.2 shows height images of bare, APTMS, and CTA grafted surfaces. The bare surfaces are smooth with low RMS roughness. The surfaces become non-uniform and rough after APTMS attachment which indicates the surfaces were not fully covered. AFM images of the CTA grafted surfaces are not significantly different from the APTMS grafted surfaces; therefore, we are unable to determine whether the CTA grafting was achieved on the surfaces using that technique. However, the contact angle measurement (Figure 5.1) indicates the presence of CTA on the surfaces due to the change from 45° ± 2° to 79° ± 2°.

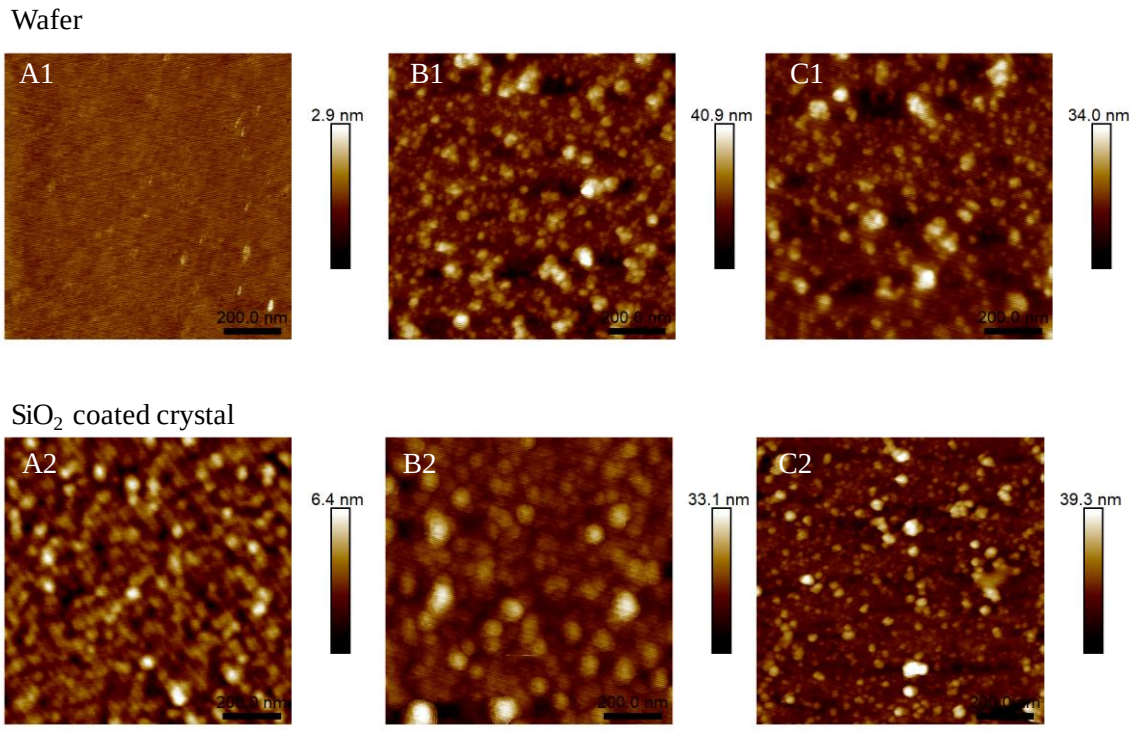


Figure 5.2 AFM height images of the bare (A1, A2), APTMS (B1, B2), and CTA (C1, C2) grafted silicon wafer and $SiO_2$ coated QCM crystal surfaces. A1: RMS roughness = 0.2 nm, B1: RMS roughness = 4.1 nm, thickness = 12 ± 4 nm, C1: RMS roughness = 3.2 nm, thickness = 4 ± 1 nm. A2: RMS roughness = 0.9 nm. B2: RMS roughness = 3.0 nm, thickness = 7 ± 2 nm. C2: RMS roughness = 3.6 nm, thickness = 5 ± 1 nm. RMS roughness was obtained from AFM height image and the thickness was determined via ellipsometry. Scan size = 1 µm, scale bar = 200 nm.

### 5.3.2 Glycopolymer synthesis on the silicon surfaces

The polymerization of both glycomonomers in solution and on the surfaces follows pseudo-first-order kinetics (Figure 5.3) which indicates the presence of a constant number of radicals on the surfaces and in the solution. The linear increase of the thickness of the glycopolymer films with monomer conversion (Figure 5.4) reveals the controlled nature of the polymerization from the surfaces. The glycopolymer film thickness varies from 10 to 25 nm, depending on the monomer conversion and the reaction time. It is commonly accepted in literature that the molecular weight and the

polydispersity of the polymers produced in solution during a surface polymerization are comparable to the polymers grown from the surface.[6, 8, 20] PGalEAm and PGlcEAm grafted films of 10.2 nm and 10.6 nm thickness, respectively, were obtained on silicon dioxide coated quartz crystals after a 2 h polymerization reaction during which the monomer conversion in solution was found to be 16.4 % and 10.3 %, respectively. This corresponds to a theoretical (NMR) molecular weight of 23000 g/mol and 14700 g/mol and degree of polymerization of 82 and 52 for PGalEAm and PGlcEAm polymers, respectively. Assuming the molecular weight of the polymers in solution is the same as the molecular weight of the polymers attached to the surface, the grafting density of the surface immobilized polymers, σ, can be calculated by using equation (1).[20, 28, 29]

$$\sigma = \frac{h\rho N_A}{M_n} \quad (1)$$

where h is the thickness of the glycopolymer film, ρ is the bulk density of the film (assumed to be 1.05 g/cm$^3$ for simplicity), $N_A$ is Avogadro's number, and Mn is the molecular weight of the grafted polymer which was assumed to be same as the molecular weight of the polymer formed in the solution. The glucose polymer grafted surface was estimated to have higher grafting density (0.45 chains/nm$^2$) than the galactose polymer grafted surface (0.28 chains/nm$^2$). We hypothesize that the difference in the grafting density is due to the participation of different numbers of CTA molecules in the polymerization reaction which we believe is due to the (i) difference in the total number of CTA molecules present on the surfaces, (ii) difference in the steric effect exerted by the glucose vs galactose containing glycomonomers making some of the CTA non-available for the reaction, and/or differences in intramolecular hydrogen bonding in the glucose and galactose monomers. More CTA is believed to have participated in the

surface polymerization involving glucose than that for galactose. Previously, Pfaff et al. reported a grafting density of 0.35 chains/nm$^2$ for galactose containing glycopolymers, poly(6-O-methacryloyl-1,2:3,4-di-O-isopropylidene-galactopyranose, (PMAIGal), grafted on the surfaces of poly(divinylbenezene) (PDVB) via RAFT polymerization.[30] The conformation of graft polymer chains on a surface depends on the grafting density.[31, 32] For the low-grafting density of the galactose polymers on surface, we believe the graft chains remain either as a single chain or a cluster of a few chains, thus forming a mushroom-like structure with coil dimensions.[31] The higher grafting density of the glucose polymers suggest that the chains are stretched away from the surface and are likely in brush-like conformation.[31, 32]

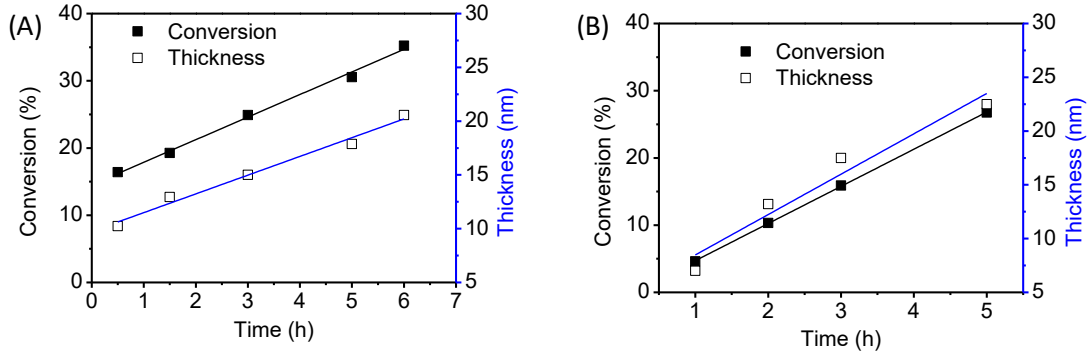


Figure 5.3 Monomer conversion in solution during the surface polymerization reaction and the corresponding thickness of the PGalEAm (A) and PGlcEAm (B) films on wafer surfaces.

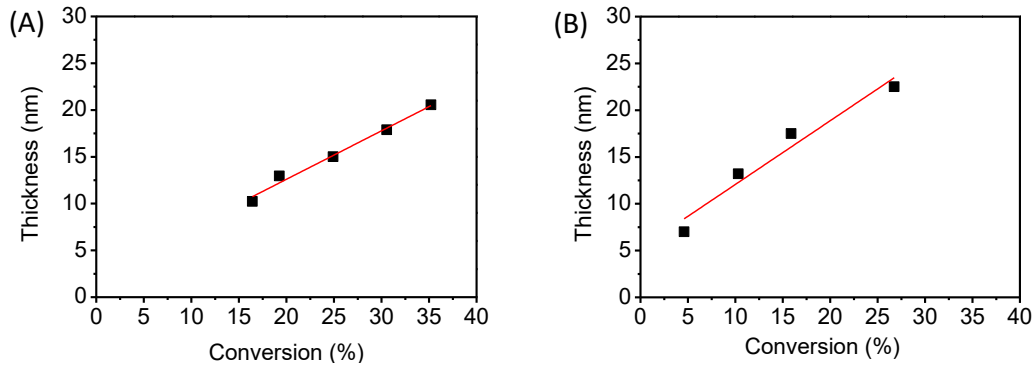

Figure 5.4 Monomer conversion vs thickness plots for PGalEAm (A) and PGlcEAm (B) films. A linear increase of film thickness with monomer conversion indicates the controlled nature of the surface polymerization.

The water contact angles of the PGlcEAm and PGalEAm- modified surfaces are 69 ± 2° and 72 ± 2°, respectively, which is slightly lower than that of the CTA immobilized surfaces (Figure 5.1). The galactose containing film, PGalEAm exhibits higher water contact angle than the glucose-containing film, PGlcEAm, which is attributed to the difference in the hydrogen bonding pattern of the pendant glucose and galactose of the glycopolymers. We hypothesize that the galactose forms stronger intra molecular H-bonds than the glucose. Therefore, the galactose containing film weakly binds with water and exhibits higher water contact angle.

### 5.3.3 XPS analysis of the polymer grafted surfaces

Figure 5.5 (A), (B), and (C) shows the XPS survey, O1s, and C1s spectra, respectively, of a 10 nm thick PGalEAm film on a silicon wafer. The C1s spectrum of the galactose film was resolved into four spectra which confirm the presence of carbon atoms corresponding to C=C (283.8 eV), C-C (284.9 eV), C-O-C (286.7 eV) and C=O/ O-C-O (288.0 eV) functional groups. The characteristic peak at 286.7 eV confirms the presence of the saccharide groups in the film.[33] As expected, peaks corresponding to other elements and functional groups of the silicon wafer surface, APTMS, CTA, and

glycopolymers appear at their appropriate binding energies.[33-36]

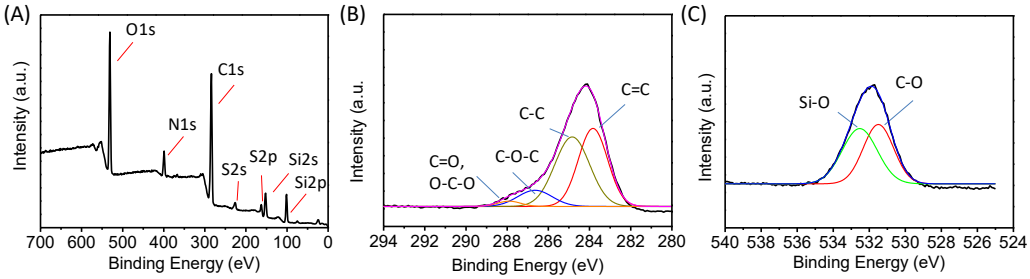


Figure 5.5 High-resolution XPS spectra of 10 nm thick glycopolymer (PGalEAm) film grown on silicon wafers. (A) XPS survey scan, (B) C1s spectra, and (C) O1s spectra with the corresponding fitting of different components.

### 5.3.4 AFM imaging of the glycopolymer grafted surfaces

Figures 5.6 (A), (B), and (C) show AFM tapping mode height images of bare silicon wafer and $SiO_2$ coated crystal surfaces (control surfaces), PGalEAm, and PGlcEAm grafted films on the surfaces. The bare surfaces are smooth with a very low rms roughness (0.2 nm for wafer and 0.9 nm for crystal). The surfaces became rough after the polymer was grafted on the surface. AFM height images of PGalEAm (Figure 5.6 B) and PGlcEAm grafted surfaces (Figure 5.6 C) do not show clear differences between the grafted surface. The grafting density calculations suggest that the galactose polymers adopt a collapsed (mushroom) conformation on the surface, but the glucose polymers adopt an extended (brush) conformation.

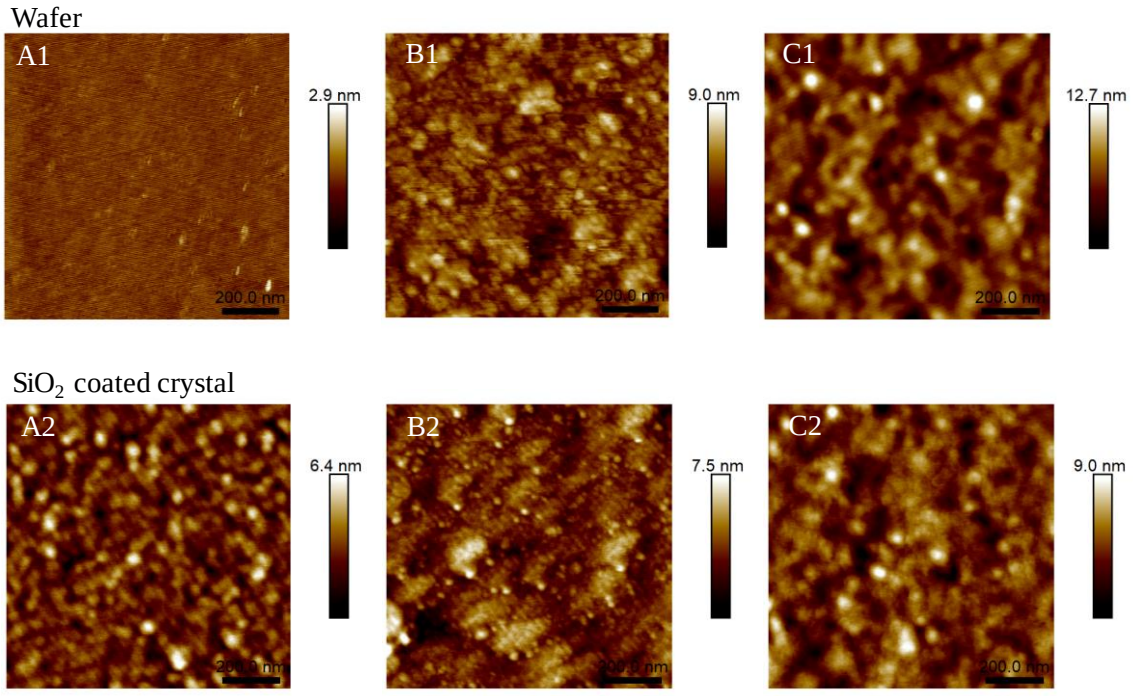


Figure 5.6 AFM height images of bare (A1, A2) , GalEAm grafted (B1, B2) (), and GlcEAm grafted (C1, C2) silicon wafer and $SiO_2$ coated QCM crystal surfaces. A1: RMS roughness = 0.2 nm, B1: thickness = 11.5 ± 0.5 nm, RMS roughness = 1.1 nm C1: thickness = 12.3 ± 1.2 nm, RMS roughness = 1.7 nm. A2: RMS roughness = 0.9 nm, B2: thickness = 10.4 ± 0.2 nm, RMS roughness = 1.0 nm, C2: thickness = 10.6 ± 1.2 nm, RMS roughness = 1.2 nm. RMS roughness was obtained from AFM height image and the thickness was measured via ellipsometry. AFM scan size = 1.0 µm and scale bar = 200 nm.

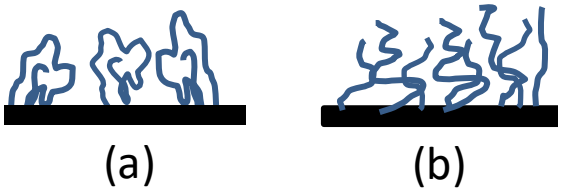


Figure 5.7 Schematic representation of PGalEAm mushroom (a) and PGlcEAm brush (b) on the surfaces of the silicon wafer and silicon dioxide coated crystals.

The thicker (90 nm) surface grafted glycopolymer brushes prepared via UV-photopolymerization (Chapter III) appear to be more uniform (AFM images, Figure 3.5 vs Figure 5.6) and have higher grafting density than the short (10 nm) brush prepared via

RAFT polymerization. This suggests that the initiator molecules of the surface-initiated UV-polymerization were more densely grafted and most of them participated in the polymerization versus the CTA in the RAFT polymerization reaction.

### 5.3.5 Aβ interaction with glycopolymer grafted surfaces investigated via QCM-D

Figure 5.8 shows the change in frequency and dissipation of control ($SiO_2$ coated crystal) and glycopolymer grafted QCM crystals during their interaction with Aβ monomers. A stable baseline was first obtained with tris buffer solution, followed by a solution of Aβ monomer, with a buffer wash at the end.

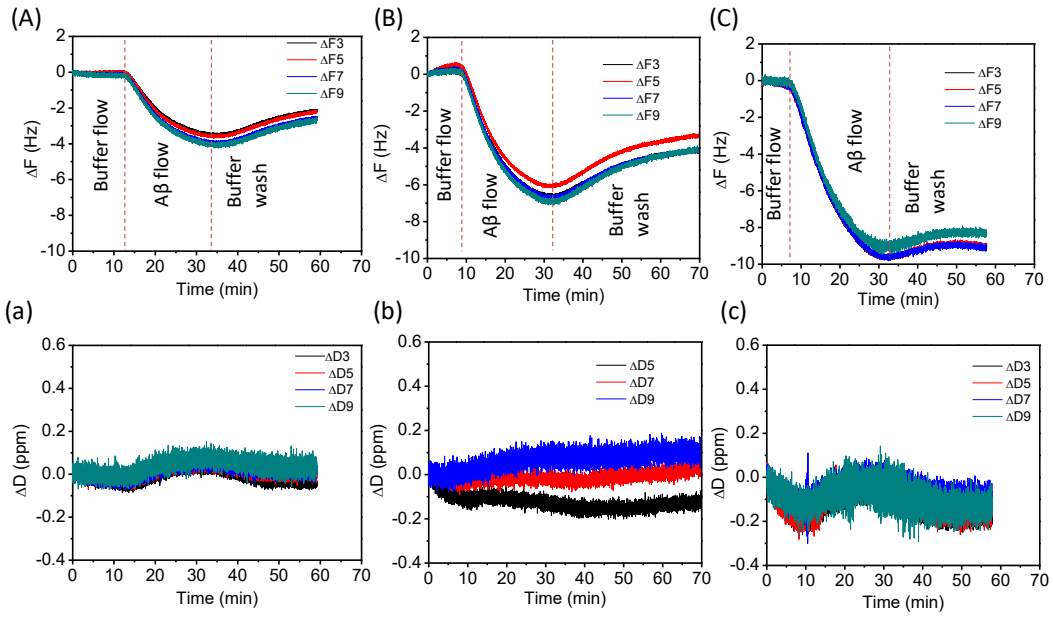


Figure 5.8 Frequency (A, B, and C) and dissipation (a, b, and c) shift due to the Aβ interaction with the bare $SiO_2$ crystal (control) (A, a), GalEAm film of 10.4 nm thickness (B, b), and GlcEAm film of 10.6 nm thickness (C, c). [Tris buffer pH 8.0, Aβ conc = 20 µM, temp = 37 °C, flow rate = 10 µL/min.]

The frequency decreases as the Aβ met with the pristine $SiO_2$ coated crystal (control) or the glycopolymer grafted crystals. The frequency drop is the highest for the glucose polymer grafted surface (9.5 Hz for n = 3) followed by the galactose polymer grafted surface (6 Hz) and the control surface (3.5 Hz). Using the Sauerbrey model, the

Aβ mass deposition on the control, PGalEAm, and PGlcEAm film surfaces was calculated to be 60, 120, and 180 ng/cm$^2$ respectively. The increased deposition of Aβ on the glycopolymer surfaces is attributed to the stronger interaction of glycopolymers with Aβ through their hydrophilic saccharide units and hydrophobic backbone. The mass of Aβ deposited on PGlcEAm grafted surface is 1.5 times higher than that on the PGalEAm surface. Because the PGlcEAm and PGalEAm surfaces have approximately the same number of saccharide units (glc/gal ratio = 1.02) (calculation: Supporting information, Appendix D), we attribute the higher amount of Aβ deposition on the PGlcEAm surface to the stronger interaction exerted by the glucose units.

On buffer wash, the frequency was increases by 0.5, 1.5, and 1.3 Hz for glucose, galactose grafted, and control surfaces respectively. The increase is attributed to removal of loosely bound Aβ washed from the surface. The smallest amount is removed from the glucose polymer grafted surface, indicating stronger Aβ interaction with the glucose-containing polymer. The dissipation changes during the Aβ flow and the buffer wash for all three cases is insignificant. This is attributed to the weak viscoelastic nature of the short-chain polymers.

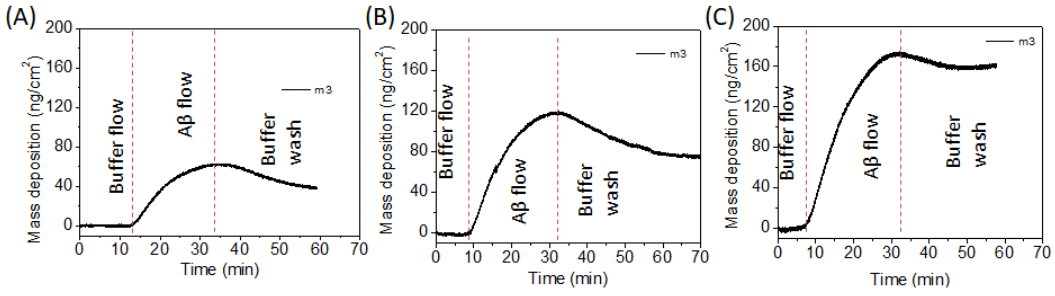


Figure 5.9 Surface mass density of Aβ determined via the Sauerbrey model for overtone n = 3. (A) Aβ deposition on bare silicon dioxide coated crystal, (B) Aβ deposition on PGalEAm grafted surface, and (C) Aβ deposition on PGlcAm grafted surface.

### 5.3.6 Aβ aggregation investigated via AFM

Morphology of aggregated structures formed by the Aβ in the presence of the glycopolymer grafted surfaces were evaluated via atomic force microscopy (AFM). $SiO_2$ coated surfaces without any polymer (control surface) and the glycopolymer grafted surfaces were incubated with Aβ monomer (20 μM in tris buffer, pH 8.0) at 37 °C for 72 h. The surfaces were then rinsed three times with 150 μL of buffer, dried with $N_2$, and imaged via AFM tapping mode. Figure 5.10 shows height and amplitude images of aggregated structures of Aβ on the control, galactose, and glucose polymer grafted surfaces. Fibrillar structures of Aβ are observed on all the three surfaces. This observation supports our findings reported in Chapter II involving Aβ aggregation in solutions of glycopolymers, where fibrils were formed in the presence of low molecular weight polymers containing both glucose and galactose. Only the high molecular weight glucose-containing polymer promoted formation of oligomers. It is possible that the short chain grafted polymers do not provide a great enough density of glucose monomers to promote the oligomer formation. It is also possible that in the grafted systems, the fibrils formed in the solution above the polymer brushes and simply deposited on the surface. It is also possible that fibrils formed in solution seeded the formation of more fibrils. Further studies are required to quantify the oligomer and fibril formation in the grafted systems.

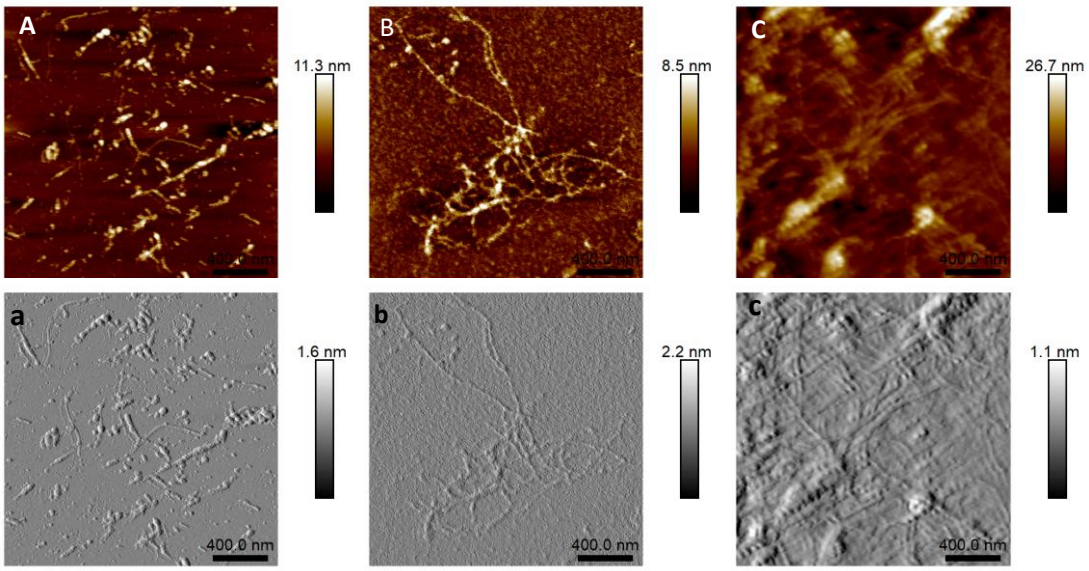


Figure 5.10 Tapping mode AFM height (A, B, and C) and amplitude (a, b, and c) images of Aβ aggregated structures formed on a silicon wafer (A, a), PGalEAm grafted (B, b), and PGlcEAm grafted (C, c) wafer surfaces. (scan size = 2 μm, scale = 400 nm)

## 5.4 Conclusions

The glycopolymer grafted films of 10 nm thickness were prepared on silicon surfaces via RAFT polymerization. The glucose polymer exhibited higher grafting density and adopted a brush conformation while the galactose polymer had lower grafting density and adopted a mushroom conformation. QCM-D studies indicated that Aβ bound more strongly with the glucose polymers than with the galactose polymers. However, it is not possible to fully and quantitatively compare the results because of the low grafting density with the RAFT synthesis. Incubation of Aβ solutions on silicon wafers grafted with glycopolymers showed formation of fibrils for both types of glycopolymers, however it was not possible to quantify the concentration of fibrils and soluble aggregates. It is not clear if fibril formation occurred because of the low molecular weight of the grafted polymers or if it was related to experimental conditions. A thermal free radical surface polymerization can be attempted to synthesize polymer brushes to

investigate the effect of grafting density, thickness, and saccharide structure on the Aβ aggregation.

**5.5 References**

(1) Zhao, C.; Li, L.; Wang, Q.; Yu, Q.; Zheng, J. Effect of Film Thickness on the Antifouling Performance of Poly(hydroxy-functional methacrylates) Grafted Surfaces. Langmuir, **2011**, *27*(8), 4906-4913.

(2) Zhao, C.; Li, L.; Zheng, J. Achieving Highly Effective Nonfouling Performance for Surface-Grafted Poly(HPMA) via Atom-Transfer Radical Polymerization. Langmuir, **2010**, *26*(22), 17375-17382.

(3) Luan, Y.; Li, D.; Wei, T.; Wang, M.; Tang, Z.; Brash, J. L.; Chen, H. "Hearing Loss" in QCM Measurement of Protein Adsorption to Protein Resistant Polymer Brush Layers. Analytical Chemistry, **2017**, *89*(7), 4184-4191.

(4) Barbey, R.; Lavanant, L.; Paripovic, D.; Schüwer, N.; Sugnaux, C.; Tugulu, S.; Klok, H.-A. Polymer Brushes via Surface-Initiated Controlled Radical Polymerization: Synthesis, Characterization, Properties, and Applications. Chemical Reviews, **2009**, *109*(11), 5437-5527.

(5) Xu, F. J.; Neoh, K. G.; Kang, E. T. Bioactive surfaces and biomaterials via atom transfer radical polymerization. Progress in Polymer Science, **2009**, *34*(8), 719-761.

(6) Ejaz, M.; Ohno, K.; Tsujii, Y.; Fukuda, T. Controlled Grafting of a Well-Defined Glycopolymer on a Solid Surface by Surface-Initiated Atom Transfer Radical Polymerization. Macromolecules, **2000**, *33*(8), 2870-2874.

(7) Mateescu, A.; Ye, J.; Narain, R.; Vamvakaki, M. Synthesis and characterization of novel glycosurfaces by ATRP. Soft Matter, **2009**, *5*(8), 1621-1629.

(8) Idota, N.; Ebara, M.; Kotsuchibashi, Y.; Narain, R.; Aoyagi, T. Novel temperature-responsive polymer brushes with carbohydrate residues facilitate selective adhesion and collection of hepatocytes. Science and Technology of Advanced Materials, **2012**, *13*(6), 064206.

(9) Chen, W.-L.; Cordero, R.; Tran, H.; Ober, C. K. 50th Anniversary Perspective: Polymer Brushes: Novel Surfaces for Future Materials. Macromolecules, **2017**, *50*(11), 4089-4113.

(10) Hane, F.; Tran, G.; Attwood, S. J.; Leonenko, Z. Cu(2+) Affects Amyloid-β (1–42) Aggregation by Increasing Peptide-Peptide Binding Forces. PLoS ONE, **2013**, *8*(3), e59005.

(11) Kim, A. C.; Lim, S.; Kim, Y. K. Metal Ion Effects on Aβ and Tau Aggregation. International Journal of Molecular Sciences, **2018**, *19*(1), 128.

(12) Bin, Y.; Li, X.; He, Y.; Chen, S.; Xiang, J. Amyloid-β peptide (1–42) aggregation induced by copper ions under acidic conditions. Acta Biochimica et Biophysica Sinica, **2013**, *45*(7), 570-577.

(13) Roy, D.; Guthrie, J. T.; Perrier, S. Graft Polymerization: Grafting Poly(styrene) from Cellulose via Reversible Addition−Fragmentation Chain Transfer (RAFT) Polymerization. Macromolecules, **2005**, *38*(25), 10363-10372.

(14) Wang, Z.; He, J.; Tao, Y.; Yang, L.; Jiang, H.; Yang, Y. Controlled Chain Branching by RAFT-Based Radical Polymerization. Macromolecules, **2003**, *36*(20), 7446-7452.

(15) Yoshikawa, C.; Goto, A.; Tsujii, Y.; Fukuda, T.; Yamamoto, K.; Kishida, A. Fabrication of High-Density Polymer Brush on Polymer Substrate by Surface-Initiated Living Radical Polymerization. Macromolecules, **2005**, *38*(11), 4604-4610.

(16) Sumerlin, B. S.; Lowe, A. B.; Stroud, P. A.; Zhang, P.; Urban, M. W.; McCormick, C. L. Modification of Gold Surfaces with Water-Soluble (Co)polymers Prepared via Aqueous Reversible Addition−Fragmentation Chain Transfer (RAFT) Polymerization. Langmuir, **2003**, *19*(14), 5559-5562.

(17) Raula, J.; Shan, J.; Nuopponen, M.; Niskanen, A.; Jiang, H.; Kauppinen, E. I.; Tenhu, H. Synthesis of Gold Nanoparticles Grafted with a Thermoresponsive Polymer by Surface-Induced Reversible-Addition-Fragmentation Chain-Transfer Polymerization. Langmuir, **2003**, *19*(8), 3499-3504.

(18) Baum, M.; Brittain, W. J. Synthesis of Polymer Brushes on Silicate Substrates via Reversible Addition Fragmentation Chain Transfer Technique. Macromolecules, **2002**, *35*(3), 610-615.

(19) Tsujii, Y.; Ejaz, M.; Sato, K.; Goto, A.; Fukuda, T. Mechanism and Kinetics of RAFT-Mediated Graft Polymerization of Styrene on a Solid Surface. 1. Experimental Evidence of Surface Radical Migration. Macromolecules, **2001**, *34*(26), 8872-8878.

(20) Stenzel, M. H.; Zhang, L.; Huck, W. T. S. Temperature-Responsive Glycopolymer Brushes Synthesized via RAFT Polymerization Using the Z-group Approach. Macromolecular Rapid Communications, **2006**, *27*(14), 1121-1126.

(21) Hernández-Guerrero, M.; Davis, T. P.; Barner-Kowollik, C.; Stenzel, M. H. Polystyrene comb polymers built on cellulose or poly(styrene-co-2-hydroxyethylmethacrylate) backbones as substrates for the preparation of structured honeycomb films. European Polymer Journal, **2005**, *41*(10), 2264-2277.

(22) von der Ehe, C.; Weber, C.; Gottschaldt, M.; Schubert, U. S. Immobilized glycopolymers: Synthesis, methods and applications. Progress in Polymer Science, **2016**, *57*, 64-102.

(23) Stenzel, M. H.; Davis, T. P.; Fane, A. G. Honeycomb structured porous films prepared from carbohydrate based polymers synthesized via the RAFT process. Journal of Materials Chemistry, **2003**, *13*(9), 2090-2097.

(24) Sauerbrey, G. Verwendung von Schwingquarzen zur Wägung dünner Schichten und zur Mikrowägung. Z. Physik, **1959**, *155*(2), 206-222.

(25) Harmon, M. E.; Jakob, T. A. M.; Knoll, W.; Frank, C. W. A Surface Plasmon Resonance Study of Volume Phase Transitions in N-Isopropylacrylamide Gel Films. Macromolecules, **2002**, *35*(15), 5999-6004.

(26) Arkles, B. (2014). Silane Coupling Agents: Connecting Across Boundaries.

(27) Arkles, B. (1977). Tailoring Surfaces with Silanes.

(28) Patil, R. R.; Turgman-Cohen, S.; Šrogl, J.; Kiserow, D.; Genzer, J. Direct Measurement of Molecular Weight and Grafting Density by Controlled and Quantitative Degrafting of Surface-Anchored Poly(methyl methacrylate). ACS Macro Letters, **2015**, *4*(2), 251-254.

(29) Cao, Z.; Tsoufis, T.; Svaldo-Lanero, T.; Duwez, A.-S.; Rudolf, P.; Loos, K. The Dynamics of Complex Formation between Amylose Brushes on Gold and Fatty Acids by QCM-D. Biomacromolecules, **2013**, *14*(10), 3713-3722.

(30) Pfaff, A.; Barner, L.; Müller, A. H. E.; Granville, A. M. Surface modification of polymeric microspheres using glycopolymers for biorecognition. European Polymer Journal, **2011**, *47*(4), 805-815.

(31) Kato, K.; Uchida, E.; Kang, E.-T.; Uyama, Y.; Ikada, Y. Polymer surface with graft chains. Progress in Polymer Science, **2003**, *28*(2), 209-259.

(32) Auroy, P.; Auvray, L.; Leger, L. Building of a grafted layer. 1. Role of the concentration of free polymers in the reaction bath. Macromolecules, **1991**, *24*(18), 5158-5166.

(33) Chernyy, S.; Jensen, B. E.; Shimizu, K.; Ceccato, M.; Pedersen, S. U.; Zelikin, A. N.; Daasbjerg, K.; Iruthayaraj, J. Surface grafted glycopolymer brushes to enhance selective adhesion of HepG2 cells. J Colloid Interface Sci, **2013**, *404*, 207-14.

(34) Huang, A.; Chen, L.-H.; Chen, C.-H.; Tsai, H.-Y.; Tung, K.-L. (2018). Carbon dioxide capture using an omniphobic membrane for a gas-liquid contacting process.

(35) Honkanen, M.; Hoikkanen, M.; Vippola, M.; Vuorinen, J.; Lepistö, T.; Jussila, P.; Ali-Löytty, H.; Lampimäki, M.; Valden, M. Characterization of silane layers on modified stainless steel surfaces and related stainless steel–plastic hybrids. Applied Surface Science, **2011**, *257*(22), 9335-9346.

(36) Jensen, D.; Kanyal, S.; Madaan, N.; A. Vail, M.; Dadson, A.; Engelhard, M.; Linford, M. Silicon (100)/SiO2 by XPS. Surface Science Spectra, **2013**, *20*, 36 -42.

# CHAPTER VI CONCLUSIONS AND FUTURE WORK

## 6.1 Conclusions

Glycopolymer mimics of the clustered saccharides of gangliosides were synthesized in solution and grafted from solid surfaces. The polymers were utilized as in vitro models to investigate the effect of saccharide structure and concentration on peptide Aβ aggregation. The kinetics of aggregation and the size and morphology of the aggregates were investigated via a series of biochemical and advanced analytical techniques.

The key accomplishments of the research are as follows:

1. Acrylamide based glycomonomers, 2-(β-D-glucosyloxy)ethyl acrylamide (GlcEAm) and 2-(β-D-galactosyloxy)ethyl acrylamide (GalEAm) containing β-D-glucose and β-D-galactose as pendent groups, respectively, were synthesized. The monomers exhibited high stereospecificity.
2. Glycopolymers, PGlcEAm and PGalEAm, and a control polymer, polydimethyl acrylamide (PDMA) of target molecular weights (degree of polymerization of 35 and 350) were synthesized in solution by aqueous reversible addition fragmentation chain transfer (RAFT) polymerization. Surface grafted glycopolymer films of high and low thickness were synthesized via photopolymerization and RAFT. Although identical polymerization conditions were employed, the glucose-containing graft polymer yielded a high grafting density and a brush-like architecture, while the galactose-containing graft polymer demonstrate a low grafting density and mushroom architecture. The glycopolymers mimic the glyco-clusters of

gangliosides in raft-like membranes of neuronal cells. Therefore, the model polymers possess high biological relevance.

3. The effect of the glycopolymers on the kinetics of Aβ aggregation and the size of the aggregates was investigated via ThT fluorescence spectroscopy and polyacrylamide gel electrophoresis (PAGE) techniques. The rate of aggregation of Aβ monomers was faster in the presence of high molecular weight glucose containing polymers (PGlcEAm350) and the ultimate aggregates were smaller in size (oligomers). Aβ aggregation was not affected by other polymers (PGalEAm350, PGalEAm35, PGalcEAm35, PDMA35, and PDMA350), and the final aggregated structures were large (fibrils). QCM studies showed significantly higher levels of Aβ deposition on the glucose polymer grafted surface (roughly 1.5 times that of the galactose polymer grafted surface), and the peptide remained tightly bound to the glucose containing polymer surface after extensive buffer washing. AFM imaging of silicon wafers incubated with Aβ solutions indicated formation of fibrils in the presence of neat, glucose polymer, and galactose polymer grafted surfaces.

The Aβ aggregation kinetics and the size, structure, and morphology of the aggregates in the presence of the glycopolymers in solution agree well with the results obtained using glycopolymer grafted surfaces. In brief, it is concluded that the high molecular weight glucose containing polymers which mimic glucose clusters of gangliosides promote the formation of highly toxic Aβ oligomers, and the high molecular weight galactose polymer resembling galactose ganglioside clusters promote the formation of less toxic

fibrils. Therefore, we believe that the ganglioside saccharide structure and stereochemistry may have influence on the progression of a Alzheimer's disease.

### 6.2 Recommendations for future work

1. Isolation of aggregates at different time points during the incubation of the Aβ monomers with glycopolymers would be an important next step in this project. This would allow for the determination of the stability and structural transition of the aggregates and whether one type of aggregate leads to the other (if oligomers lead to fibrils or vice-versa). This will determine if the aggregation process is "on" or "off" pathway. Additionally, aggregates can be analyzed for their secondary structures via circular dichroism (CD).
2. Investigation of Aβ aggregation in the presence of low (DP 35) and high (DP 350) molecular weight glycopolymers while keeping the total saccharide concentration the same in the reaction medium. To achieve this balance of saccharide groups, the molar concentration of 35 DP polymer needs to be 10 times higher than the molar concentration of 350 DP polymer. The results can be compared with the Aβ aggregation results we obtained (Chapter II) and will establish if the difference in Aβ aggregation and structure formation was due to the difference in the overall concentration of saccharides or due to the difference in molecular weight of the polymers (i.e. local concentration of saccharides).
3. The head group of gangliosides contain N-acetyl-D-galactosamine and sialic acid in addition to the glucose and galactose. The effect of sialic acid on Aβ aggregation has been studied, but there are very few reports on the effect of N-

acetyl-D-galactosamine on Aβ aggregation. An acrylamide based glycomonomer with N-acetyl-D-galactosamine as a pendant group can be synthesized via literature procedures.[1, 2] Controlled glycopolymers with target molecular weights can be synthesized via an aqueous RAFT polymerization technique as has been described for glycopolymer synthesis in our current research. This would complete the studies of the effects of the individual saccharides of a ganglioside head group on Aβ aggregation.

4. Further efforts to quantify fibril vs oligomer formation in the presence of polymer brushes should be undertaken, perhaps via SPR.

### 6.3 References

(1) Vázquez-Dorbatt, V.; Maynard, H. D. Biotinylated Glycopolymers Synthesized by Atom Transfer Radical Polymerization. Biomacromolecules, **2006**, *7*(8), 2297-2302.

(2) Takasu, A.; Niwa, T.; Itou, H.; Inai, Y.; Hirabayashi, T. Chemical modification of hydroxyl groups of poly(vinyl alcohol) by a glycosidation reaction. Macromolecular Rapid Communications, **2000**, *21*(11), 764-769.

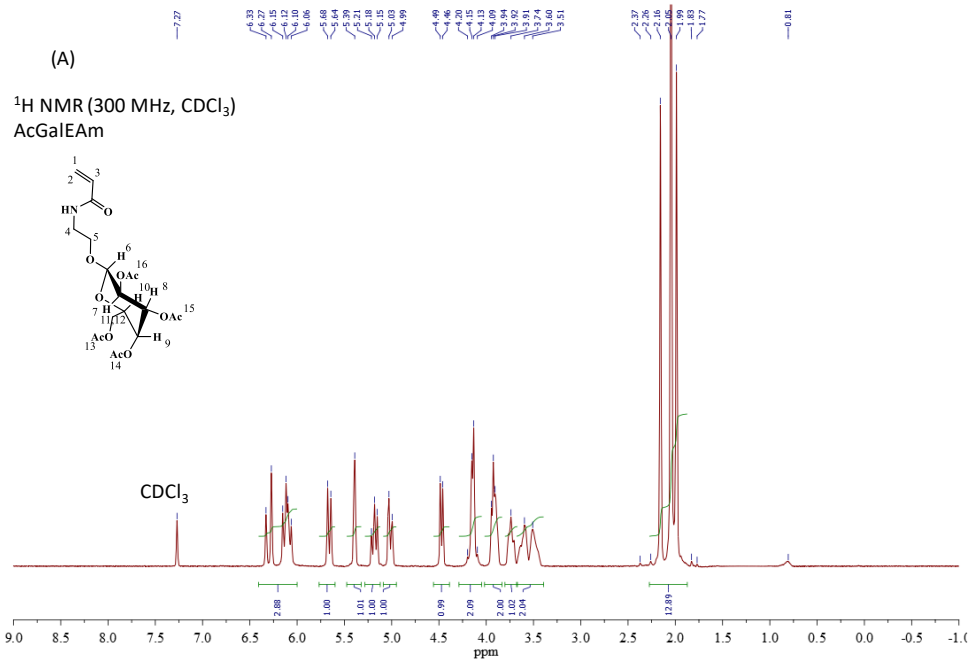


Figure A.1 $^1$H NMR spectrum of acetylated (protected) galactose containing glycomonomer, AcGalEAm.

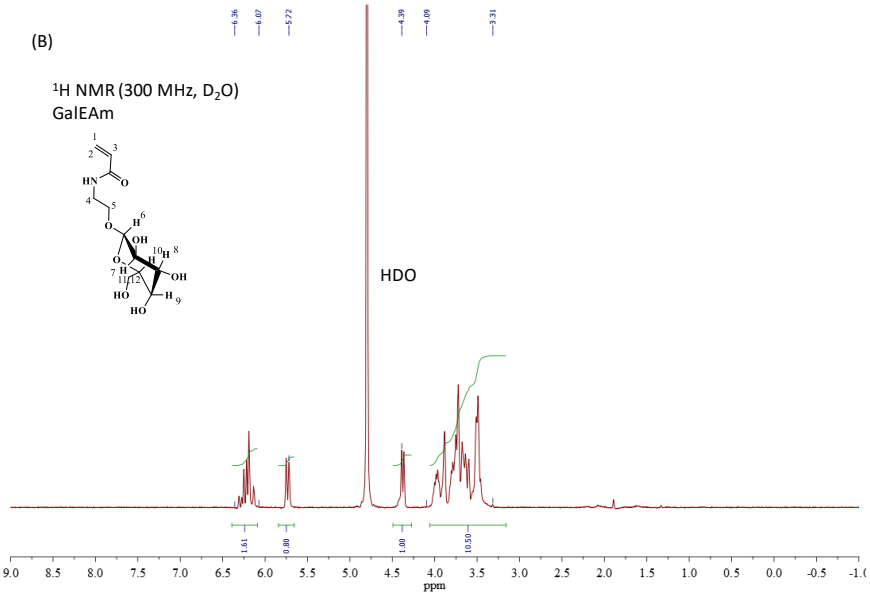


Figure A.2 $^1$H NMR spectrum of deacetylated (deprotected) galactose containing glycomonomer, GalEAm.

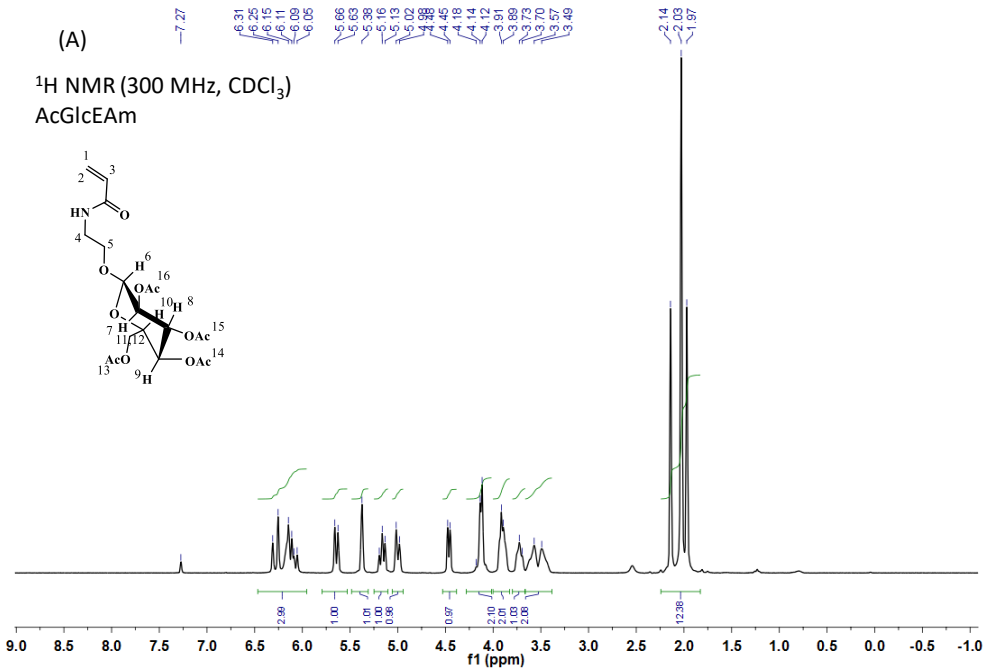


Figure A.3 $^1$H NMR spectrum of acetylated (protected) glucose containing glycomonomer, AcGlcEAm.

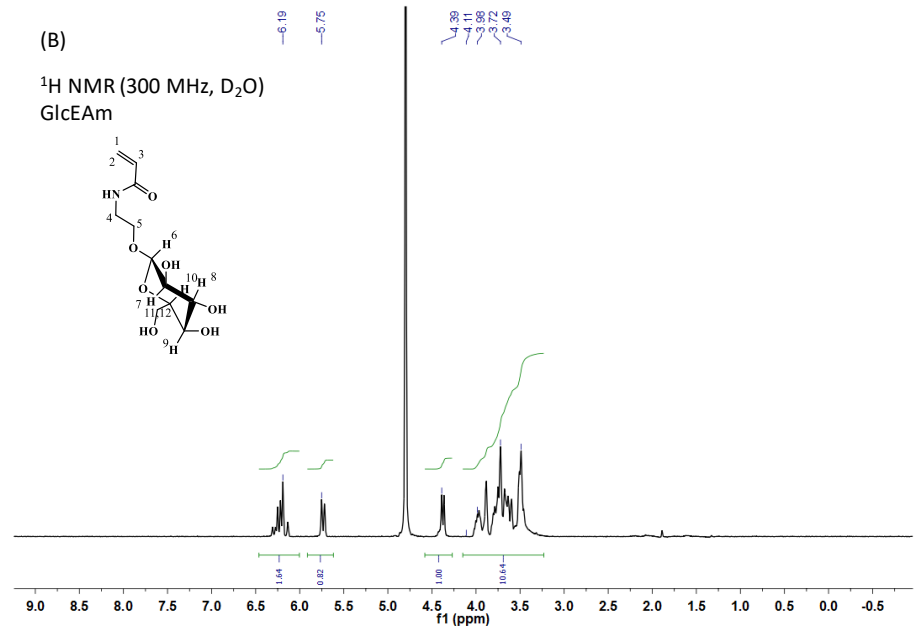


Figure A.4 $^1$H NMR spectrum of deacetylated (deprotected) glucose containing glycomonomer, GlcEAm.

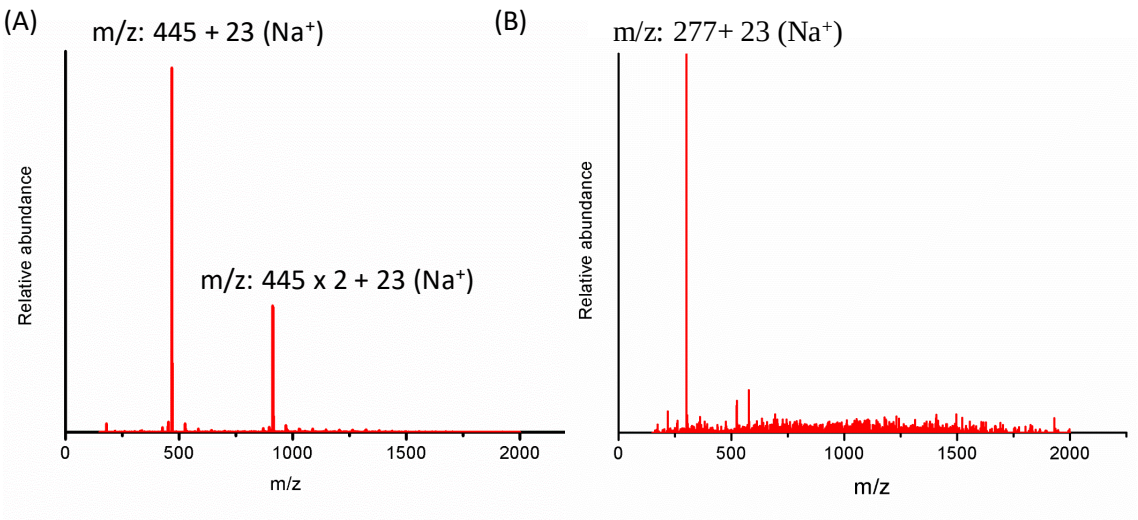


Figure A.5 ESI-MS spectra of (A) acetylated (protected) glucose containing glycomonomer, AcGlcEAm and (B) deacetylated (deprotected) glucose containing glycomonomer, GlcEAm.

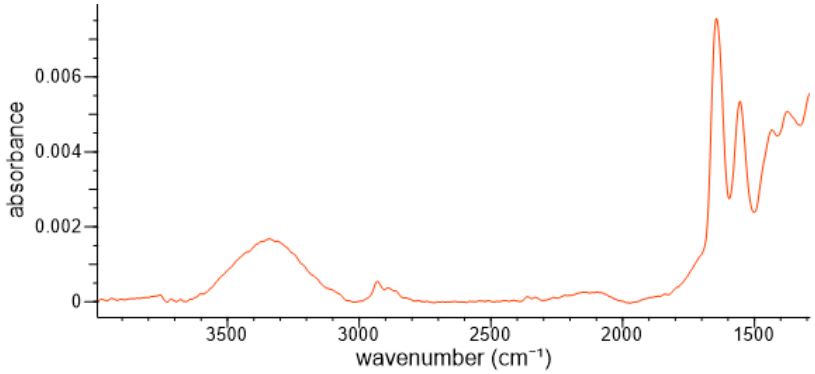


Figure A.6 FTIR spectra of GlcEAm.

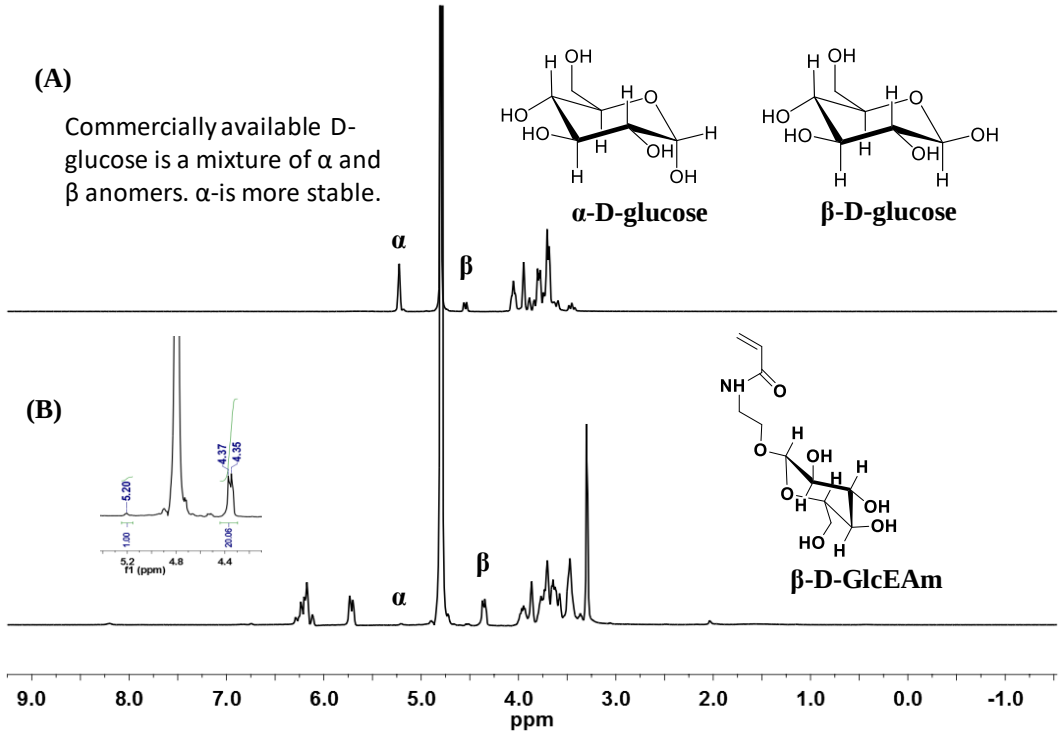


Figure A.7 $^{1}$H NMR spectra of (A) commercially available D-glucose and (B) glycomonomer, GlcEAm.

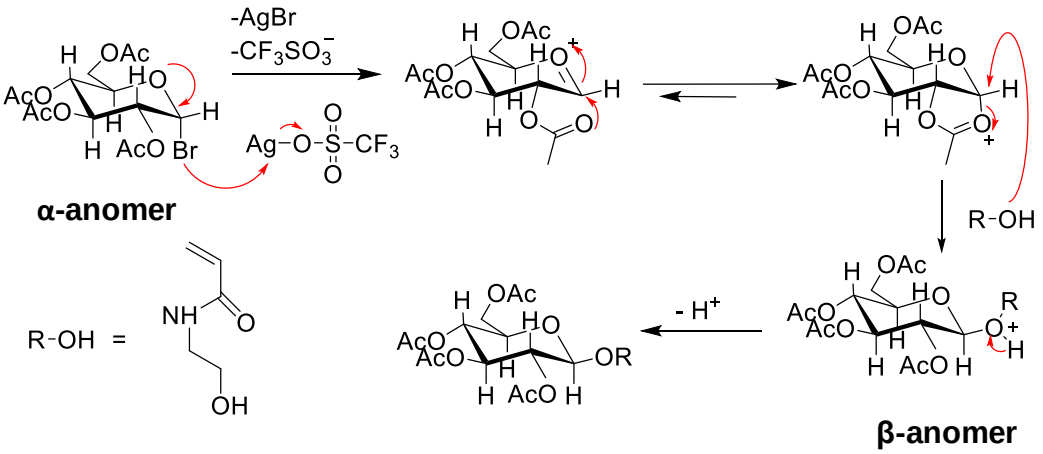


Figure A.8 A proposed reaction mechanism for the synthesis of stereospecific saccharide containing glycomonomers.

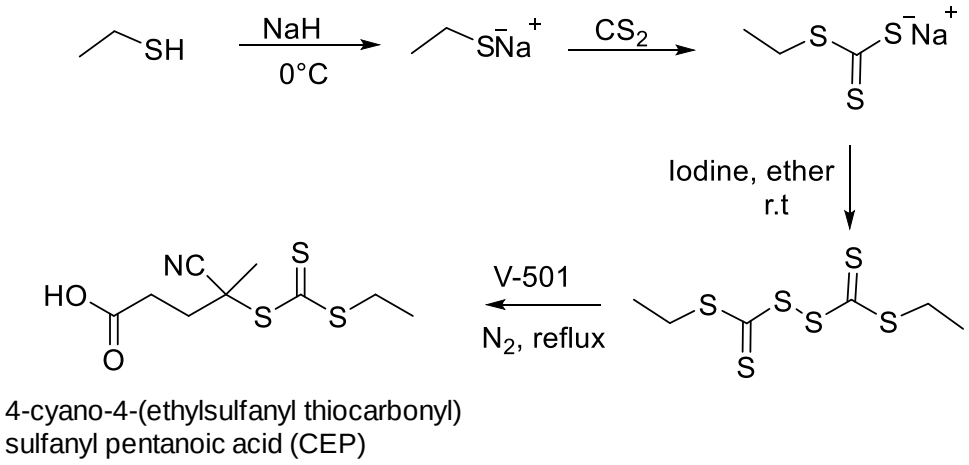


Figure A.9 Synthesis scheme of the RAFT chain transfer agent, 4-cyano-4-(ethylsulfanyl thiocarbonyl) sulfanyl pentanoic acid (CEP).

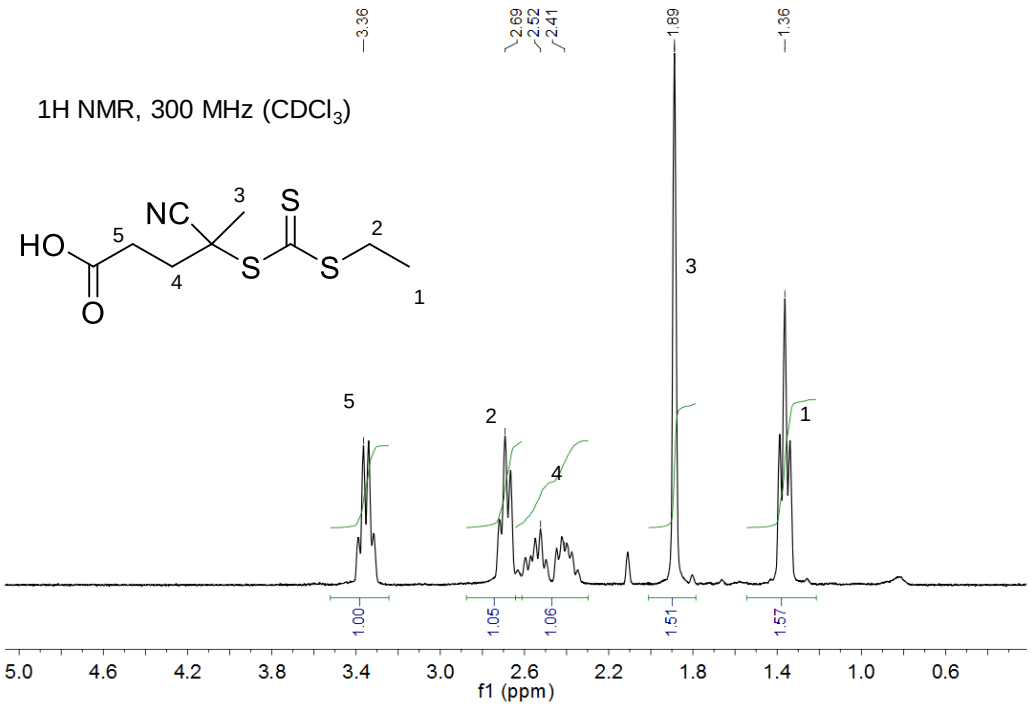


Figure A.10 $^{1}$H NMR spectrum of the chain transfer agent, CEP.

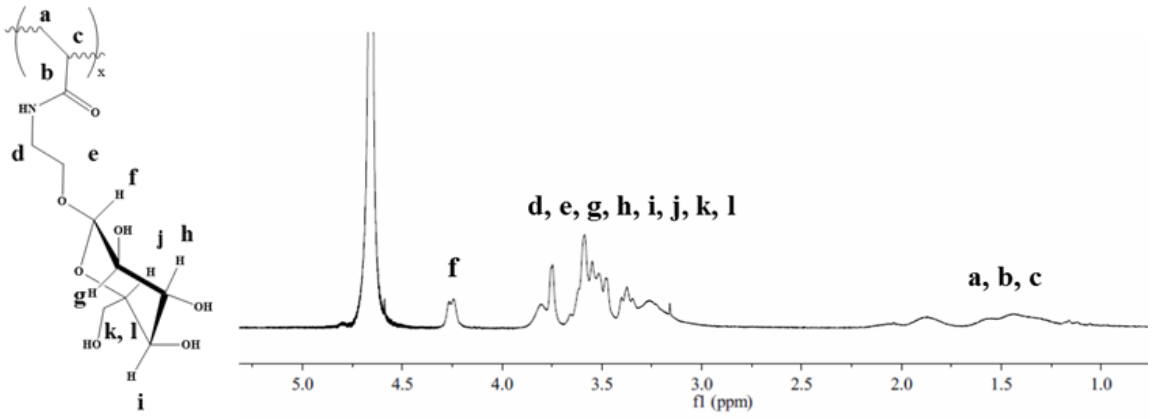


Figure A.11 $^{1}$H NMR spectrum of glycopolymer, PGlcEAm.

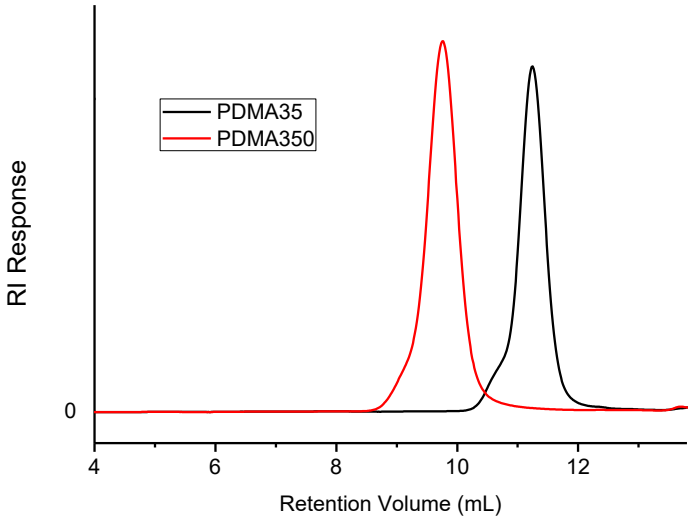


Figure A.12 GPC traces for poly(dimethyl acrylamide), (PDMA) of the degree of polymerization (DP) 35 and 350.

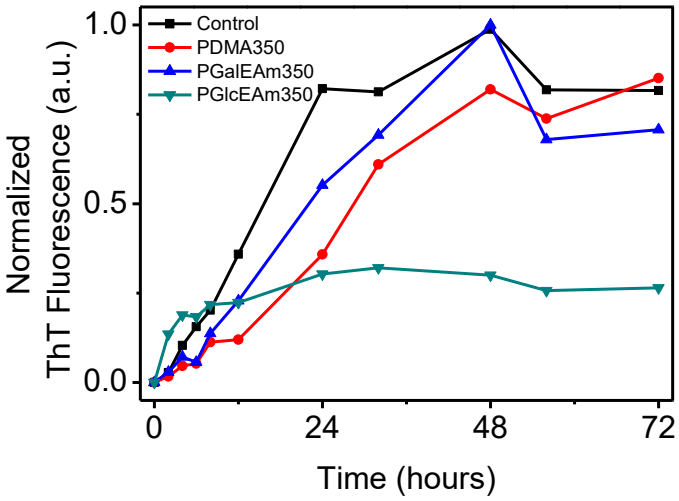


Figure A.13 ThT fluorescence intensity of Aβ aggregates with incubation time. Aβ incubated with polymers of DP 350. Control = neat Aβ.

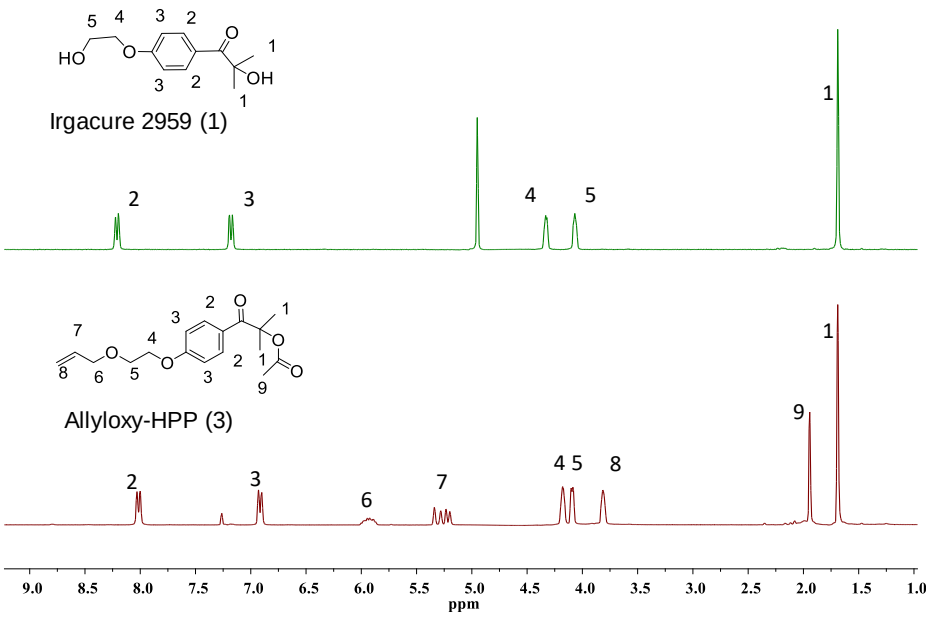


Figure B.1 $^{1}$H NMR spectra of UV photoinitiator, Irgacure 2959 and allyloxy -HPP.

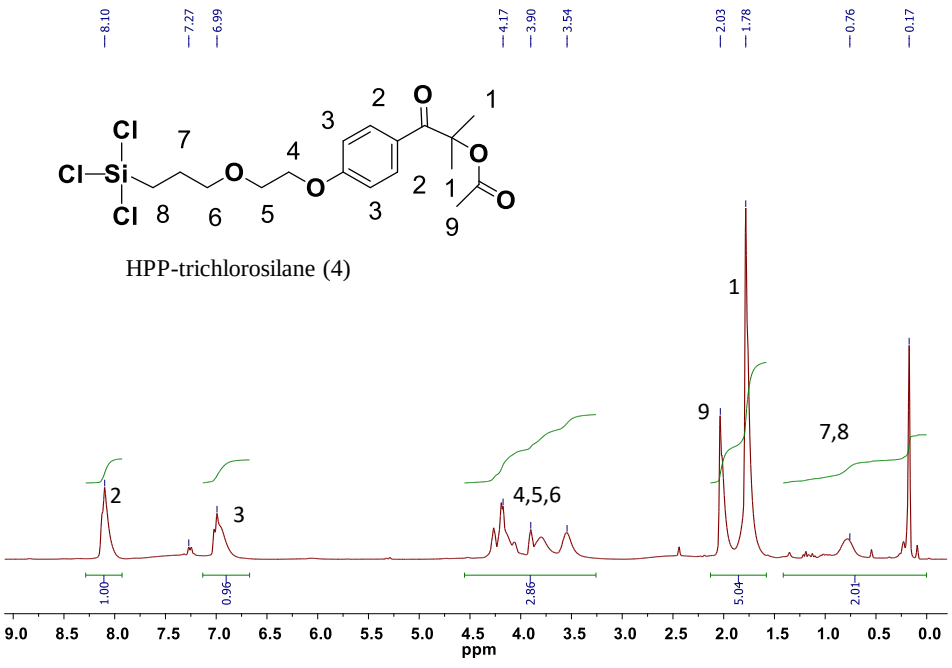


Figure B.2 $^{1}$H NMR spectra of HPP-trichlorosilane.

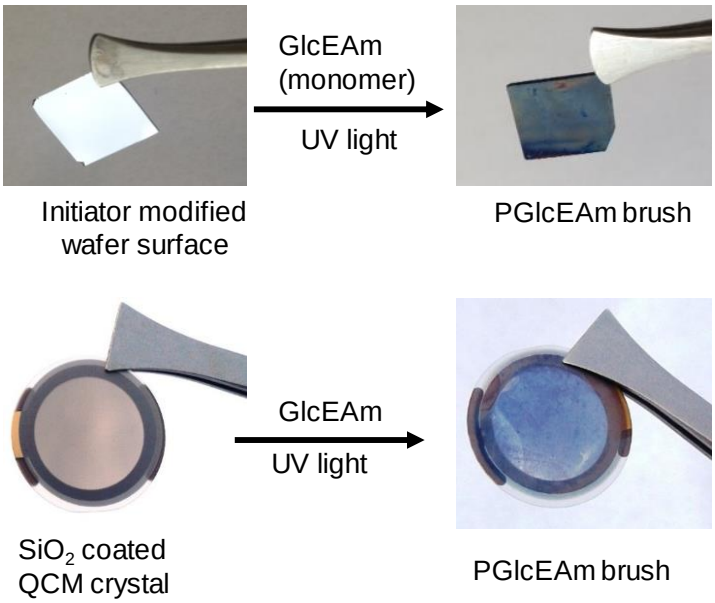


Figure B.3 Silicon wafer and $SiO_2$ coated QCM quartz crystal before and after glycopolymer grafting.

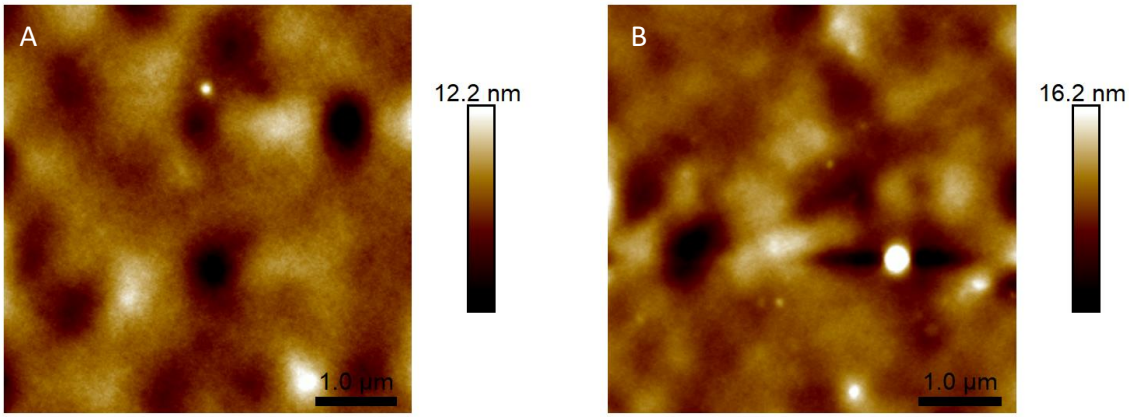


Figure B.4 AFM height images of (A) GlcEAm brush (RMS roughness 1.49 nm) and (B) GalEAm brush (RMS roughness = 2.15 nm) on silicon dioxide coated quartz crystal surfaces. Scan size = 5.0 µm and scale = 1.0 µm

Table B.1 IR absorption bands for initiator and polymer grafted on the silicon wafer

| Description | Absorption ($cm^{-1}$) | Peak assignment (signal strength) |
|---|---|---|
| Irgacure immobilized wafer | 2927 | C-H stretching, alkane (s) |
| | 2854 | C-H stretching, alkane (s) |
| | 1733 | C=O stretching (s) |
| | 1216 | C-O, alkyl-aryl ether (s) |
| | 1112 | C-O stretching, aliphatic ether (s) |
| PGlcEAm brush | 3700-3000 | N-H stretching (m), O-H stretching (s, broad, intermolecular H bonded) |
| | 2925 | C-H stretching, alkane (s) |
| | 2854 | C-H stretching, alkane (s) |
| | 1714 | C=O stretching (s) |
| | 1649 | C=O stretching (s), 2˚ amide |
| | 1556 | N-H bending (m) |
| | 1218 | C-O, alkyl-aryl ether (s) |
| | 1076 | C-O stretching, aliphatic ether (s) |

**Calculation: Degree of polymerization of glycopolymer brush**

A= 109.5°, B= C= 35.25°
b = c = 0.154 nm, a= ?

$$\frac{a}{sinA} = \frac{b}{sinB} = \frac{c}{sinC}$$

**a = 0.251 nm**

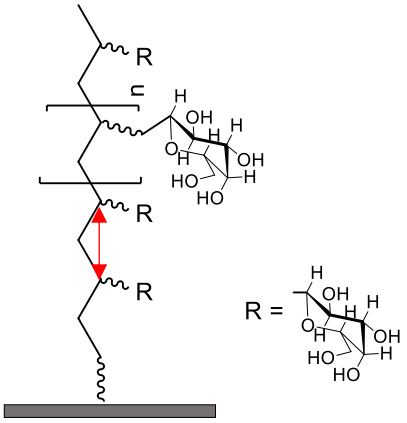


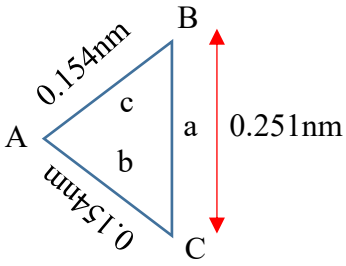


Bond length, C ($sp^3$)- C ($sp^3$) = 1.54Å
= 0.154 nm
1 repeat unit = 0.251 nm
For a brush thickness of 90 nm,
Degree of polymerization = 90/0.251 = 358

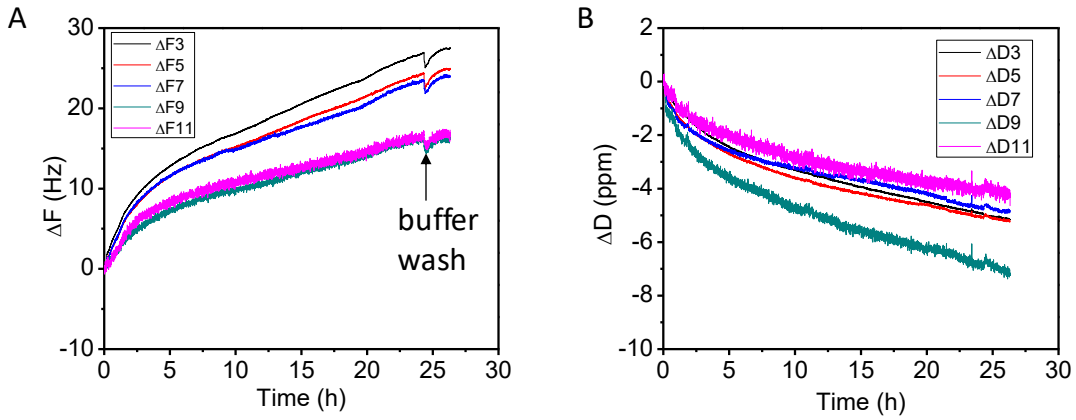


Figure C.1 Frequency (A) and Dissipation (B) change of galactose polymer (PGalEAm) of 90 nm grafted crystals during its interaction with Aβ. Baseline with buffer = 10 min, Aβ flow = 10 min, Aβ hold 24 h, final buffer wash = 2 h, flow rate = 50 µL/min, temp = 25 °C.

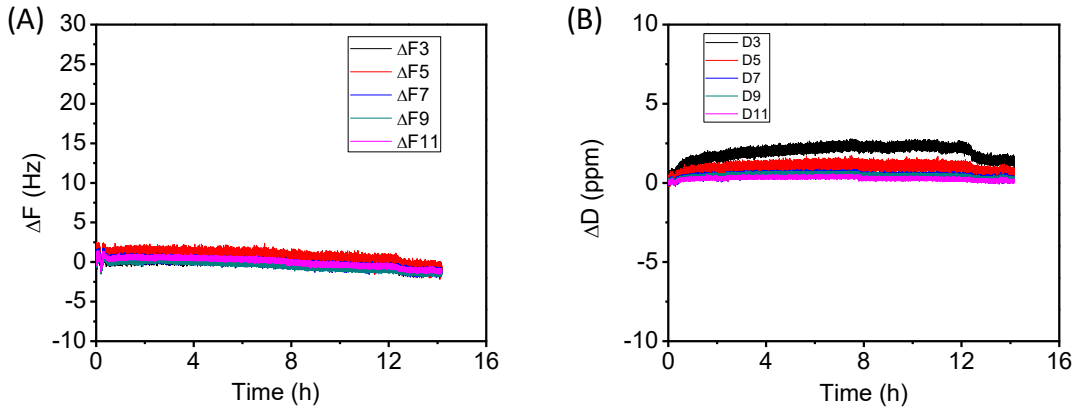


Figure C.2 Frequency (A) and Dissipation (B) change of a pristine $SiO_2$ coated crystal during its interaction with Aβ. Baseline with buffer = 10 min, Aβ flow = 10 min, Aβ hold 14 h, flow rate = 50 µL/min, temp = 25 °C. Final buffer wash was not performed.

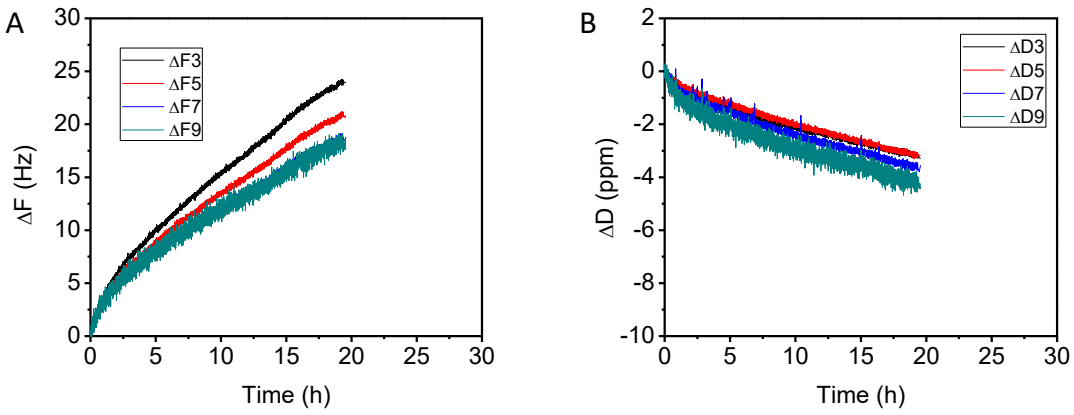


Figure C.3 Negative control experiment: frequency (A) and Dissipation (B) change of glucose polymer (PGlcEAm, 90 nm) grafted crystals during its interaction with buffer. Baseline with buffer = 10 min, buffer hold 24 h, final buffer flow = 1 h, flow rate = 50 µL/min, temp = 25 °C.

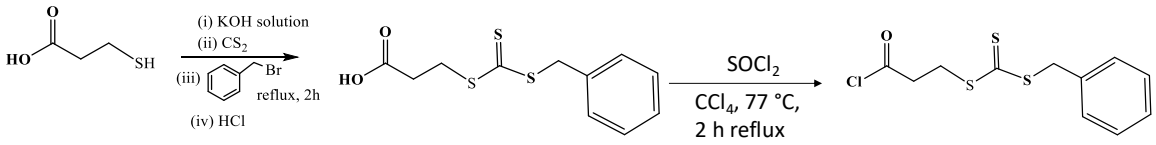


Figure D.1 Reaction scheme for the synthesis of the chain transfer agent, 3-benzylsulfanylthiocarbonyl sulfanylpropionic acid and its acid chloride derivative, 3-benzylsulfanylthiocarbonyl sulfanylpropanoyl chloride.

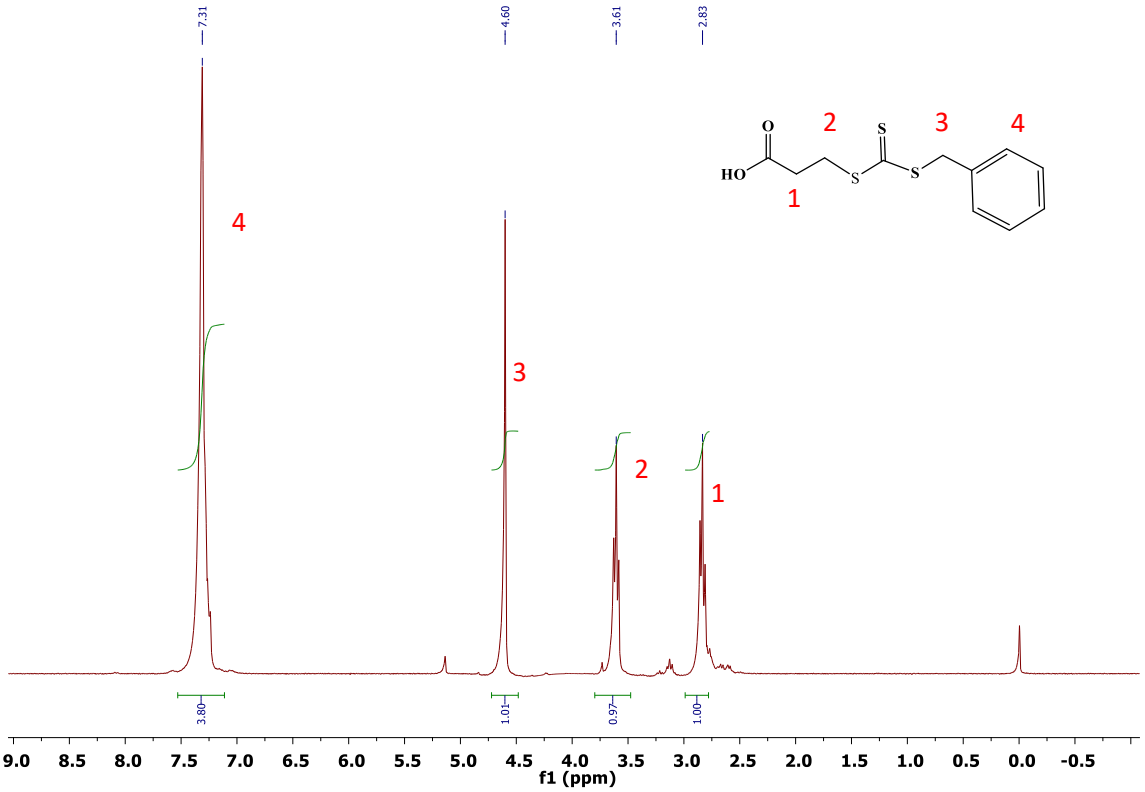


Figure D.2 $^{1}$H NMR spectrum of the chain transfer agent, 3-benzylsulfanylthiocarbonyl sulfanylpropanoyl chloride.

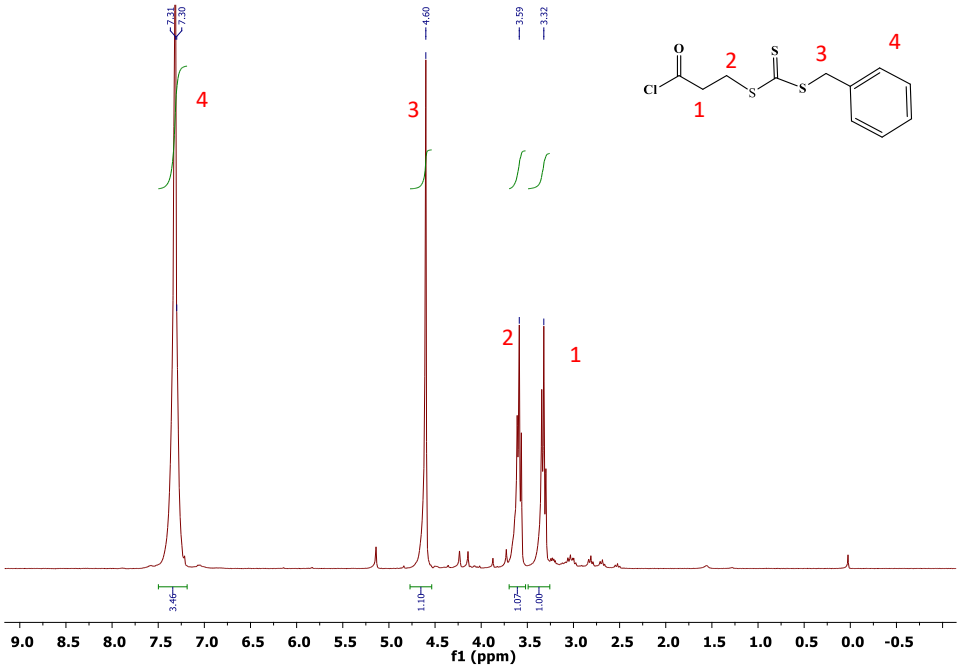


Figure D.3 $^{1}$H NMR spectrum of the 3-benzylsulfanylthiocarbonyl sulfanylpropanoyl chloride.

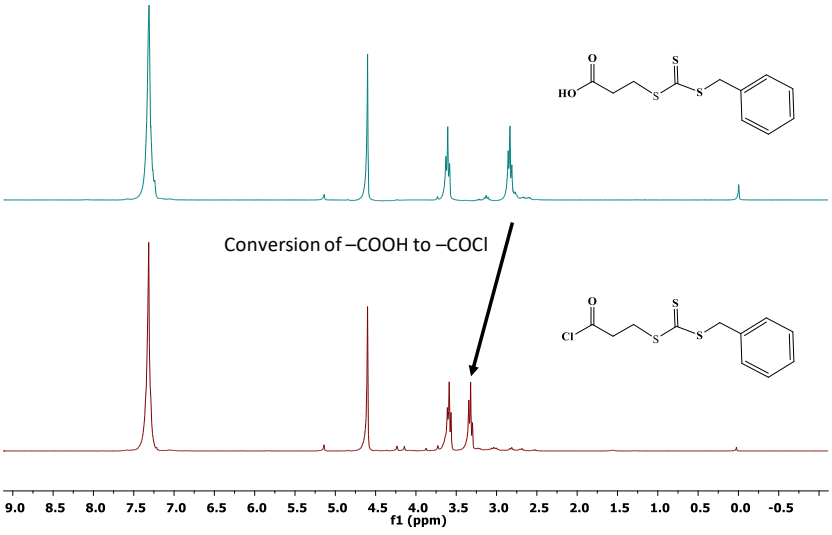


Figure D.4 Comparison of the $^{1}$H NMR spectra of the CTA and its acid chloride derivative shows the complete conversion of the carboxylic acid group to the acid chloride.

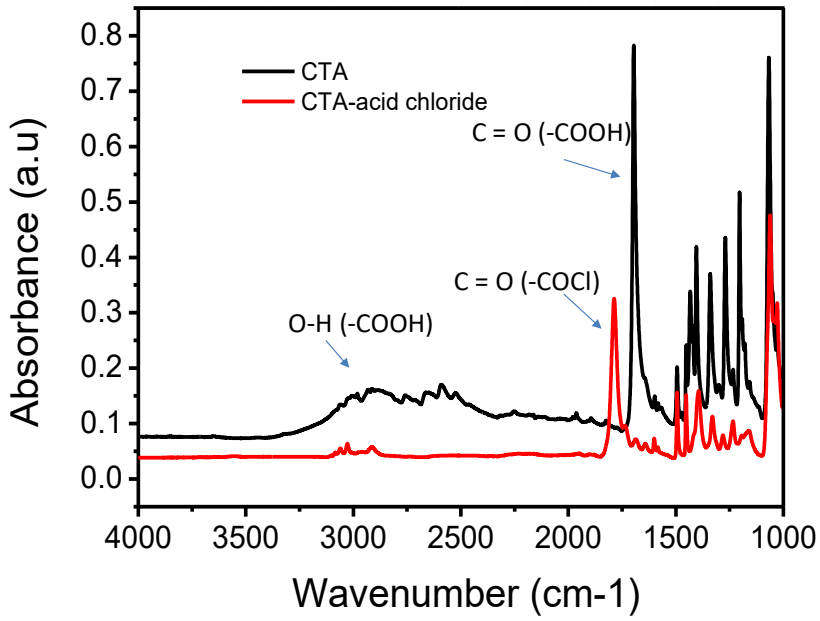


Figure D.5 ATR FTIR of the CTA and acid chloride derivative of the CTA.

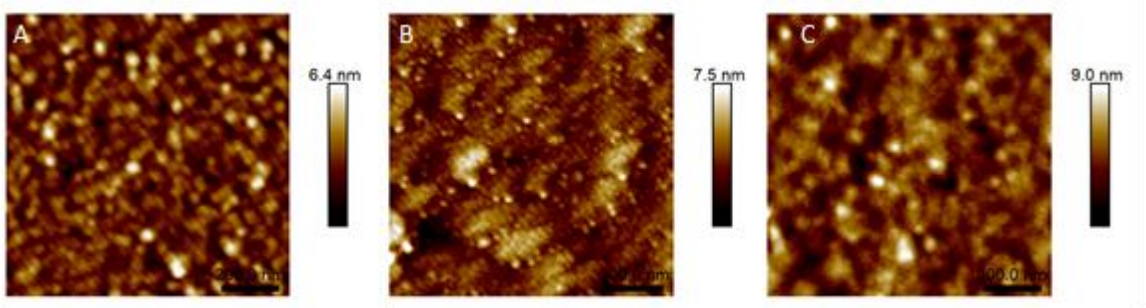


Figure D.6 AFM height images of (A) silicon dioxide coated crystal (rms roughness = 0.9 nm), (B) GalEAm grafted wafer (thickness = 10.4 ± 0.2 nm, RMS roughness = 1.0 nm), and (C) GlcEAm grafted wafer (thickness = 10.6 ± 1.2 nm, RMS roughness = 1.2 nm). Scan size = 1.0 µm and scale bar = 200 nm

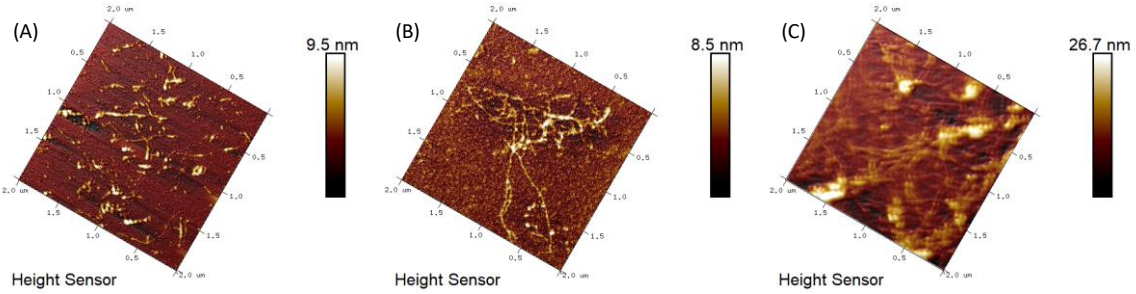


Figure D.7 AFM tapping images (3 dimensional) of the Ab aggregates formed/deposited on the surfaces of (A) clean crystal, (B) galactose, and (C) glucose film of 10 nm thickness.

**Calculation: Number of saccharide units on a grafted surface**

Glucose or galactose units/unit area of polymer grafted crystal surface is calculated

PGalEAm brush: film thickness = 10.4 nm, Mol wt =23000 g/mol, DP = 82, grafting density = 0.28 chains/$nm^2$

No. of galactose unit = (0.28 chains/$nm^2$) × (82 gal units/chain)

= 22.96 gal units/$nm^2$

PGlcEAm brush: film thickness = 10.6 nm, Mol wt = 14700 g/mol, DP = 52, grafting density = 0.45 chains/$nm^2$

No. of glucose units = (0.45 chains/$nm^2$) × (52 glc units/chain)

= 23.40 glc units/$nm^2$